

Steinar Fjelldal

Energy modelling and optimization for low- and zero-emission high speed passenger ferries

Master's thesis in Marine Technology

Supervisor: Roger Skjetne

Co-supervisor: John Martin Kleven Godø and Samieh Najjaran

June 2022

Steinar Fjelldal

Energy modelling and optimization for low- and zero-emission high speed passenger ferries

Master's thesis in Marine Technology

Supervisor: Roger Skjetne

Co-supervisor: John Martin Kleven Godø and Samieh Najjaran

June 2022

Norwegian University of Science and Technology

Faculty of Engineering

Department of Marine Technology



Norwegian University of
Science and Technology



MASTER OF TECHNOLOGY THESIS DEFINITION (30 SP)

| | |
|----------------------------------|---|
| Name of the candidate: | Steinar Fjellidal |
| Field of study: | Marine cybernetics |
| Thesis title (Norwegian): | Energimodellering og -optimering for lav- og nullutslipp hurtigbåter |
| Thesis title (English): | Energy modelling and optimization for low- and zero-emission high speed passenger ferries |

Background

Due to the reliability, power-to-weight and power-to-volume ratios, and the fast response to load changes of the diesel-engine, this has been a dominating power producer in ships. During the last decade, however, enabling technologies in energy storage, especially battery-based systems, have resulted in new hybrid-electric and battery-electric solutions to reduce and possibly eliminate fuel consumption and emissions. Unfortunately, the advantageous characteristics of the diesel engine cannot be matched easily by alternative zero-emission (ZE) power producers alone, such as fuel cells (FCs) or gas-driven engines. Hence, such solutions must be carefully designed, both in system design and in energy and emission management with online optimization algorithms commanding the power plant operation in order to satisfy required properties such as minimal fuel/energy consumption and emissions to air, at the same time as stability of the power plant is maintained.

In this project, we will be concerned with the feasibility of battery-electric or ZE hybrid-electric propulsion of fast speed ferries. Hence, the objectives will be to collect and pre-process available data for high-speed ferry operations in Norway (AIS, SeaWeb,...), specify a case study, establish a simplified resistance model that can be parametrized by available data for relevant vessels, perform segmentation of given vessel tracks into path segments and set up a corresponding data-structure for each segment, and then use this to calculate total propulsion power for a vessel along a track. This shall next be considered used for onboard energy optimization in proposed hybrid-electric ship power/propulsion plant, energy/emission calculations over route connections and schedules, and possibly route optimization.

This thesis will cover a miniature scope of the objectives of the project: *"enabling Zero Emission passenger Vessel Services"* (ZEVS). The thesis will be a deliverable to ZEVS.

Scope of Work

1. Perform a background and literature review to provide information and relevant references on:
 - High-speed passenger ferry applications and technologies, also for ZE operation, particularly typical propulsion systems.
 - Reports and articles on low- and zero-emission high speed boats and passenger ferries.
 - Projections on technological and economical evolution of energy carriers and ZE technology.
 - Relevant optimization methods under the categories of numerical optimization and AI methods.
 - Methods for optimal design and energy management of shipboard power and propulsion.
 - Route scheduling and logistic optimization.Write a list with abbreviations and definitions of terms and symbols, relevant to the literature study and project report.
2. Provide knowledge on relevant zero emission (ZE) technologies, such fuel cell solutions, ammonia and hydrogen engines, ammonia turbines, and battery energy storage systems. This should also report high-speed propulsion solutions from relevant vendors such as MTU and Servogear. Both economical aspects, such as CAPEX and OPEX, and technological specifications including dimensions, weight, volumetric and gravimetric capacities, functionality, efficiency, etc., should be discussed. Consider how will this technology fit the purpose compared to conventional machinery.
3. Get an overview of relevant high speed vessels. Collect and organize data on some relevant vessels, and ferry connections using SeaWeb, AIS, etc. Structure, categorize, and process AIS data for some relevant high-speed ferries, to provide route information such as duration at ports, average speed profiles, and other route logistics. Perform a case study of a relevant vessel, including hull



characteristics and machinery configuration, and discuss its compliance with retrofitting to zero emission propulsion.

4. Discuss relevant models for power, energy, and emission estimation of high-speed ferries. Establish a transparent model that can be parameterized by available data on existing vessels. The model should be used to calculate the mechanical (shaft) power needed to maintain a given speed of the vessel along a given track, exposed to relevant loads. Inputting this power into a proposed onboard power system should facilitate energy and emission calculations for the vessel.
5. We define a track to be a path from port A to B, and a route to be all tracks for a given periodic operation in a fast ferry schedule. For each track and route of tracks, perform a (vessel-specific) segmentation of the tracks into path segments, where each segment can be associated with data such as length, speed, weather parameters, vessel mechanical propulsion load, etc. Propose a data-structure that can be used to represent this data for each path segment, track/route as a whole, and relevant vessel data. Fill in data for your study cases.
6. Develop an energy optimization algorithm that ensures optimal power loadsharing between e.g. a battery and a fuel cell, for a given propulsion load profile and a proposed electric power/propulsion solution. The algorithm should be able to optimize over an entire periodic ferry route, including stops taken, to ensure sufficient capacities. The energy optimization should be used to calculate energy (and emissions) needed along a track and result in a “loadsharing reference profile” for the vessel. The data should be inserted into the data-structure.
7. Discuss (optimal) design of onboard ZE electric power/propulsion system to fulfill the mechanical power and energy demand for the vessel along a given route. This should consider weight and volume of the electric components in context of passenger capacity and needed vessel dimensions.

Specifications

Every weekend throughout the project period, the candidate shall send a status email to the supervisor and co-advisors, providing two brief bulleted lists: 1) work done recent week, and 2) work planned to be done next week.

The scope of work may prove to be larger than initially anticipated. By the approval from the supervisor, described topics may be deleted or reduced in extent without consequences with regard to grading.

The candidate shall present personal contribution to the resolution of problems within the scope of work. Theories and conclusions should be based on mathematical derivations and logic reasoning identifying the steps in the deduction.

The report shall be organized in a logical structure to give a clear exposition of background, problem/research statement, design/method, analysis, and results. The text should be brief and to the point, with a clear language. Rigorous mathematical deductions and illustrating figures are preferred over lengthy textual descriptions. The report shall have font size 11 pts., and it is not expected to be longer than 70 A4-pages, 100 B5-pages, from introduction to conclusion, unless otherwise agreed. It shall be written in English (preferably US) and contain the elements: Title page, project definition, preface (incl. description of help, resources, and internal and external factors that have affected the project process), acknowledgement, abstract, list of symbols and acronyms, table of contents, introduction (project background/motivation, objectives, scope and delimitations, and contributions), technical background and literature review, problem formulation or research question(s), method/design/development, results and analysis, conclusions with recommendations for further work, references, and optional appendices. Figures, tables, and equations shall be numerated. The contribute-on of the candidate shall be clearly and explicitly described, and material taken from other sources shall be clearly identified. Work from other sources shall be properly acknowledged using quotations and a Harvard citation style (e.g. natbib Latex package). The work is expected to be conducted in an honest and ethical manner, without any sort of plagiarism and misconduct, which is taken very seriously by the university and will result in consequences. NTNU can use the results freely in research and teaching by proper referencing, unless otherwise agreed.

The thesis shall be submitted with an electronic copy to the main supervisor and department according to NTNU administrative procedures. The final revised version of this thesis definition shall be included after the title page. Computer code, pictures, videos, data, etc., shall be included electronically with the report.

Start date: 15 January, 2022

Due date: 11th June, 2022

Supervisor: Roger Skjetne

Co-advisor(s): John Martin Kleven Godø and Samieh Najjaran

Signatures:

Digitally signed by rskjetne

Date: 2022.06.02 18:40:40


+02'00'

Preface

This thesis constitutes the concluding submission of my master's degree in Marine Cybernetics, written at the Norwegian University of Science and Technology (NTNU), in the spring of 2022. The workload of this thesis corresponds to 30 ECTS. The work is a continuation of my project thesis from the fall of 2021.

This thesis is motivated by the need to reduce the environmental footprint of the fast ferry industry. Fast ferries are in the upper layer of emissions per passenger in the transportation sector. With this in mind and a personal interest in new uprising technology, I was inspired to write a thesis on finding solutions and addressing challenges for the design problem of zero-emission fast ferries. The main focus of this thesis is to generate valuable information in order to find an optimal design for a zero-emission fast ferry.

The work direction and ambition of the thesis have been shaped together by Professor Roger Skjetne, my supervisor. The objectives of the thesis were inspired by the research project, ZEVS (Zero emission passenger Vessel Services), which the Institute of Transport Economics leads with a corporation with the Institute for Energy Technology, NTNU, and Katholieke Universiteit Leuven (Belgia).



Steinar Fjelldal
Trondheim, June 10 2022

Acknowledgments

I want to thank Professor Roger Skjetne, my supervisor, and John Martin Kleven Godø, my co-advisor, for valuable insight and guidance throughout the project. Professor Skjetne has triggered my interest in the introduction of low- and zero-emission ferries and inspired me to get into the material.

I would also thank, Westcon and LMG Marin for providing valuable insight into the zero-emission fast ferry industry, Ballard Europe for sharing information on their fuel cell technology, and Corvus energy for sharing information on their battery technology.

Abstract

With its long coastline and deep fjords, Norway has over 130 ferry connections. Both governmental restrictions and international goals propel the ferry industry to supply these ferry connections with low- and zero-emission ferries. To compete with cheap, lightweight diesel machinery, zero-emission vessels need to be custom-made not to sacrifice performance to reduce emissions. It is challenging to obtain all the relevant information to optimize the zero-emission vessel design. Therefore, finding methods for generating this information is the key to success.

This thesis aims to find methods for generating relevant information related to the optimal design problem. This problem includes generating route information from AIS data, finding an energy model that can be parameterized by available information, and providing technical information such as equipment efficiency, weight, and volume. All this, in combination, provides the background for finding a custom-made design of a zero-emission fast ferry.

In this thesis, two sets of AIS data have been studied. The first one, from 2018, was characterized by inconsistent sampling time and wild-points in position and speed. The second set of AIS data, from 2021, had significantly higher quality with 1000 times higher resolution. From this data, an implementation of a DBSCAN clustering algorithm was able to detect ports, which further led to the generation of the tracks of the route. Furthermore, the average speed profile from the route processing provided a good foundation for energy modeling along the route. This provided valuable information to the optimal design problem. In this thesis, the zero-emission technology of interest for short-distance operations of fast ferries are batteries and fuel cells. The gravimetric density of batteries is much higher than for hydrogen, but due to the weight of the fuel cell stack, the choice of equipment should be made with care.

This thesis conducts a case study of MS Tyrhaug, operating the ferry connection between Trondheim and Kristiansund. AIS data for this ferry was investigated, and the results show that AIS data is mature for providing route information. Evaluation of efficiency, weight, and volume of a battery configuration and a fuel cell configuration shows that a fuel cell configuration is the most suitable for longer distances, without charging opportuni-

ties, and battery configuration for shorter distances. The limit is found to be around 200 nm. A battery configuration for the case vessel, MS Tyrhaug, will be the most appropriate if the battery can be fully charged at both end ports. The battery's capacity should be at least 2660 kWh, with a weight and volume of 19,000 kg and 17.6 m^3 , respectively.

A hybrid-electric configuration has also been investigated, consisting of a fuel cell and a battery. An implementation of a dynamic programming (DP) algorithm has been applied to find a global solution to the optimal load-sharing problem. The DP implementation is simulated with different cost functions emphasizing various parameters to enlighten the importance of tuning. For example, when emphasizing 100% with the fuel consumption, the fuel consumption was reduced by 10 kg compared to a simulation emphasizing all parameters of interest. This illustrates the importance of a well-functioning loadsharing system.

Sammendrag

Norge med sin lange kystlinje og dype fjorder har totalt over 130 fergeforbindelser. Både statlige restriksjoner og internasjonale mål motiverer fergeindustrien til å forsyne disse fergeforbindelsene med lav- og nullutslippsferger. For å kunne konkurrere med billige, lette dieselmaskiner, må nullutslippsfartøyer spesiallages for ikke å ofre ytelse i prosessen med å redusere utslipp. Det er utfordrende å få tak i all relevant informasjon for å optimalisere nullutslippsfartøyets design. Derfor er det å finne metoder for å generere denne informasjonen nøkkelen til suksess.

Denne oppgaven har som mål å finne metoder for å generere relevant informasjon knyttet til det optimale designproblemet. Dette inkluderer generering av ruteinformasjon fra AIS-data, finne en energimodell som kan parameteriseres av tilgjengelig informasjon, og gi teknisk informasjon som utstyrseffektivitet, vekt og volum. Alt dette i kombinasjon er bakgrunnen for prosessen med å finne et skreddersydd design av en nullutslipp hurtigferge.

I dette prosjektet har to sett med AIS-data blitt studert. Det første, fra 2018, var preget av inkonsekvente tidssteg og feilmålinger i posisjon og hastighet. Det andre settet med AIS-data, fra 2021, hadde betydelig høyere kvalitet med 1000 ganger høyere oppløsning. Fra dette datasettet var en implementasjon av en DBSCAN-klyngealgoritme i stand til å oppdage havner, noe som videre førte til generering av delinstansene av ruten. Gjennomsnittshastighetsprofilen fra bearbeidingen av ruten ga et godt grunnlag for energimodellering langs ruten. Dette gav verdigfull informasjon for å løse design problemet. I denne oppgaven er nullutslippsteknologien av interesse for kortdistanseoperasjoner av hurtigferger batterier og brenselceller. Den gravimetrisk tettheten til batterier er mye høyere enn for hydrogen, men på grunn av vekten av brenselcellestabelen, bør valg av utstyr gjøres med forsiktighet.

I denne oppgaven gjennomføres en casestudie av MS Tyrhaug, som opererer fergeforbindelsen mellom Trondheim og Kristiansund. AIS-data for denne fergen ble undersøkt og resultatene viser at AIS-data er modent for å generere ruteinformasjon. Evaluering av effektivitet, vekt og volum til en batterikonfigurasjon og en brenselcellekonfigurasjon viser at en brenselcellekonfigurasjon er best egnet for lengre avstander, uten lademuligheter,

og batterikonfigurasjoner for kortere avstander. Grensen er funnet å være rundt 200 nm. For casefartøyet, MS Tyrhaug, vil en batterikonfigurasjon være den mest hensiktsmessige dersom batteriet er fulladet i begge ende havnene. Kapasiteten til batteriet bør være minst 2660 kWh, med en vekt og volum på henholdsvis 19 000 kg og 17,6 m³.

En hybrid-elektrisk konfigurasjon er også undersøkt, bestående av en brenselcelle og et batteri. En implementering av en dynamisk programmeringsalgoritme (DP) er brukt for å finne en global løsning på det optimale lastdelingsproblemet. DP-implementeringen er simulert med ulike kostnadsfunksjoner som legger vekt på ulike parametere for å belyse viktigheten av tuning. Når man kun legger vekt på drivstofforbruket, ble drivstofforbruket redusert med 10 kg sammenlignet med en simulering som vektlegger alle parametere av interesse. Dette illustrerer viktigheten av a velfungerende lastdeling.

Table of Contents

| | |
|--|------------|
| Preface | i |
| Acknowledgments | i |
| Abstract | ii |
| Sammendrag | iv |
| Table of Contents | x |
| List of Tables | xi |
| List of Figures | xv |
| Abbreviations | xvi |
| 1 Introduction | 1 |
| 1.1 Background and motivation | 1 |
| 1.2 Objectives | 2 |
| 1.3 Scope and delimitations | 2 |
| 1.4 Contributions | 3 |
| 2 Background and literature review | 5 |
| 2.1 Shipping towards zero-emission | 5 |
| 2.1.1 EU and IMO initiatives | 5 |
| 2.1.2 National initiatives and support schemes | 6 |
| 2.2 Historical hull technology | 6 |

| | | |
|----------|---|-----------|
| 2.3 | Hull technology for high speed operation | 7 |
| 2.3.1 | Hull-supported vessels | 7 |
| 2.3.2 | Foil-supported vessels | 8 |
| 2.3.3 | Air-cushion-supported vessels | 8 |
| 2.3.4 | Industrial application of different hull structures . . . | 9 |
| 2.4 | Conventional machinery | 10 |
| 2.4.1 | Emerging combustion engine technology | 10 |
| 2.5 | Hull and machinery in the Norwegian fast ferry fleet | 11 |
| 2.5.1 | Machinery | 11 |
| 2.5.2 | Hull | 12 |
| 2.6 | Propulsion systems for high speed operation | 12 |
| 2.7 | Energy management system | 13 |
| 2.7.1 | Numerical optimization methods | 14 |
| 2.7.2 | Artificial intelligence based optimization methods . . . | 16 |
| 2.7.3 | Machine learning for prediction of loads | 17 |
| 2.8 | Clustering | 17 |
| 2.8.1 | Density-based spatial clustering | 18 |
| 2.8.2 | K-means | 18 |
| 2.8.3 | Agglomerative hierarchical clustering | 18 |
| 2.9 | Existing low- and zero-emission concepts | 18 |
| 2.9.1 | Zero-emission high-speed ferry projects | 21 |
| 2.10 | Automatic identification system | 23 |
| 3 | Technology: State-of-the-art | 25 |
| 3.1 | Energy carriers and storage technology | 25 |
| 3.1.1 | Hydrogen and ammonia | 25 |
| 3.1.2 | Fuel cell technology | 28 |
| 3.2 | Battery energy storage systems | 29 |
| 3.2.1 | Battery technology | 30 |
| 3.2.2 | Battery energy storage systems for marine applications | 30 |
| 3.2.3 | Battery for high-speed passenger ferries | 32 |
| 4 | Theory | 33 |
| 4.1 | Hull resistance models | 33 |
| 4.1.1 | Total coefficient method | 33 |
| 4.1.2 | Top-down approach for energy modeling | 34 |
| 4.1.3 | Mathematical representation for energy modeling . . . | 35 |
| 4.1.4 | New approach: Energy modeling for practical appli- cations | 36 |
| 4.1.5 | Energy modeling with varying mass | 37 |

| | | |
|----------|---|-----------|
| 4.2 | Battery working principle and efficiency | 39 |
| 4.2.1 | Battery efficiency | 40 |
| 4.3 | Fuel cell working principle | 42 |
| 4.3.1 | Fuel cell efficiency | 43 |
| 4.4 | ZE-vessel system configuration | 45 |
| 4.4.1 | System efficiency | 45 |
| 4.4.2 | System weight and volume | 46 |
| 5 | Design: Optimal zero-emission vessel structure | 49 |
| 5.1 | Design overview | 49 |
| 5.2 | Module 0: Data pre-processing | 50 |
| 5.2.1 | Pre-processing of raw AIS-data | 50 |
| 5.2.2 | Port detection | 51 |
| 5.2.3 | Track generation | 52 |
| 5.2.4 | Waypoint generation | 52 |
| 5.3 | Route data-structure | 53 |
| 5.4 | Module 2: Power and energy model | 55 |
| 5.5 | Module 3: Energy-optimal electric loadsharing system | 55 |
| 5.6 | Module 4: Iterative ZE vessel redesign | 58 |
| 5.6.1 | Component dimensioning | 58 |
| 5.6.2 | Iterative process | 58 |
| 6 | Case study | 61 |
| 6.1 | Case study: MS Tyrhaug | 62 |
| 6.1.1 | Machinery | 62 |
| 6.1.2 | The ferry connection: Trondheim - Kristiansund | 63 |
| 6.1.3 | Retrofit of MS Tyrhaug | 64 |
| 7 | Results | 67 |
| 7.1 | Module 0: Data processing | 67 |
| 7.1.1 | Pre-processing | 67 |
| 7.1.2 | Port detection | 69 |
| 7.1.3 | Track detection | 71 |
| 7.1.4 | Route data-structure | 74 |
| 7.1.5 | AIS data versus timetable | 74 |
| 7.1.6 | Summary of route characteristics | 76 |
| 7.2 | Module 2: Energy modeling | 76 |
| 7.2.1 | Energy modeling | 76 |
| 7.2.2 | Total load profile | 78 |
| 7.3 | Module 3: Energy-optimal electric load sharing system | 79 |
| 7.3.1 | Parameters for the dynamic programming algorithm | 80 |

| | | |
|----------|---|------------|
| 7.3.2 | Load sharing: Trondheim - Kristiansund (all ports) . . | 80 |
| 7.3.3 | Load sharing: Trondheim - Kristiansund (round trip) | 82 |
| 7.3.4 | Load sharing: Trondheim - Hitra (with wind) | 83 |
| 7.4 | Module 4: Iterative ZE vessel design | 83 |
| 7.4.1 | System dimensioning | 83 |
| 7.4.2 | System dimensioning by the iterative approach | 84 |
| 8 | Discussion | 87 |
| 8.1 | AIS data | 87 |
| 8.2 | Generation of route-specific data | 87 |
| 8.3 | Energy modeling | 88 |
| 8.4 | Optimal loadsharing | 89 |
| 8.5 | Optimal design problem | 89 |
| 9 | Conclusion and Further Work | 91 |
| 9.1 | Conclusion | 91 |
| 9.2 | Recommendations for further work | 92 |
| | Bibliography | 93 |
| | Appendix | I |
| A | High-Speed Vessels | III |
| A.1 | Relevant high-speed vessels (from SeaWeb) | III |
| B | DP algoirthm verification | VII |
| B.1 | Respect to alpha (fuel) | VII |
| B.2 | Respect to beta (stable SOC) | IX |
| B.3 | Respect to gamma (low variation of fuel cell power) | IX |

List of Tables

| | | |
|-----|--|----|
| 2.1 | AIS data published every 2-10 seconds | 23 |
| 3.1 | Electrolyser technology evolution, now vs. 2030 vs. long term. (Agency-IEA, 2019). | 26 |
| 3.2 | Fuel cell summary table (Winter and Brodd, 2004) | 29 |
| 3.3 | Summary: Battery technology | 32 |
| 3.4 | Battery technology overview | 32 |
| 4.1 | Efficiency of system components | 46 |
| 4.2 | Weight of system components | 47 |
| 5.1 | Parameters for DP implementation | 57 |
| 6.1 | Design parameters of MS Tyrhaug (Maritimt-Magasin, 2015; Sea-web, 2014) | 62 |
| 6.2 | Engine specific parameters: MTU 16V200 M72 (MTU, 2020) | 63 |
| 6.3 | Timetable: Trondheim - Kristiansund | 64 |
| 6.4 | Weight of system configurations | 66 |
| 7.1 | Summary: Track information | 76 |
| 7.2 | Summary: Port information | 76 |
| 7.3 | Steps of iteration for finding battery capacity, weight, and volume | 85 |

List of Figures

| | | |
|------|--|----|
| 2.1 | Hull-supported vessels. Image courtesy of: Heyman-Yachts (2018) | 8 |
| 2.2 | Hydrofoil ferry (Boundary Layer Technologies) | 8 |
| 2.3 | Surface Effect Ship: Concept figure. Courtesy of Wavecraft (2018) | 9 |
| 2.4 | AiriEL; Photo: BB green | 10 |
| 2.5 | Propulsion efficiency curves, Courtesy of Servogear (2017) . . | 12 |
| 2.6 | Control architecture of the ship. Courtesy of NTNU | 14 |
| 2.7 | Shortest path problem solved with dynamic programming. Courtesy of Wikipedia contributors (2021) | 15 |
| 2.8 | MS Color Hybrid, photo: Skipsrevyen (2021) | 19 |
| 2.9 | MS Ampere, photo: Skipsrevyen (2014) | 19 |
| 2.10 | MS Hydra, photo: Skipsrevyen (2021) | 20 |
| 2.11 | Future of the Fjords, photo: Brodrene Aa | 20 |
| 2.12 | MS Bard, image courtesy of Brim Explorer | 21 |
| 2.13 | AREO40, image courtesy of Brodrene Aa. | 21 |
| 2.14 | MS Medstraum, image courtesy of TrAM. | 22 |
| 3.1 | The energy density of fuels. (Energy.gov) | 27 |
| 3.2 | Hydrogen price prediction. Courtesy of The International Renewable Energy Agency (2021) | 28 |
| 4.1 | Suggestion for simplified waterline area of catamaran hull . . | 38 |
| 4.2 | Schematic of a battery cell | 40 |
| 4.3 | Contour plots of the efficiency of a Li-ion battery being charged and discharged | 42 |
| 4.4 | Schematic of PEM fuel cell | 43 |

| | | |
|------|---|----|
| 4.5 | Efficiency curve for a PEMFC | 44 |
| 4.6 | Single line diagram of a zero-emission powertrain | 45 |
| 5.1 | Flowchart of the optimal design process for zero-emission fast ferry | 50 |
| 5.2 | Workflow of data processing | 51 |
| 5.3 | Illustration of DP algorithm finding the optimal path | 56 |
| 6.1 | MS Tyrhaug: Image courtesy of: Maritimt-Magasin (2015) | 61 |
| 6.2 | Route tracking: MS Tyrhaug (2021) | 64 |
| 7.1 | Raw data with wild points | 68 |
| 7.2 | Raw data with wild points zoomed in | 68 |
| 7.3 | Data evaluation: Sampling time vs. sog | 69 |
| 7.4 | Result from clustering process of ports | 70 |
| 7.5 | Data points in a port cluster | 70 |
| 7.6 | Trondheim - Lensvik: Track path and speed profile | 71 |
| 7.7 | Trondheim - Hasselvika: Track path and speed profile | 71 |
| 7.8 | Trondheim - Brekstad: Track path and speed profile | 71 |
| 7.9 | Brekstad - Hitra: Track path and speed profile | 71 |
| 7.10 | Hitra - Kjørvikbugen: Track path and speed profile | 72 |
| 7.11 | Hasselvika - Brekstad: Track path and speed profile | 72 |
| 7.12 | Lensvik - Hasselvika: Track path and speed profile | 72 |
| 7.13 | Kjørvikbugen - Edøy: Track path and speed profile | 72 |
| 7.14 | Edøy - Kristiansund: Track path and speed profile | 73 |
| 7.15 | Edøy - Kristiansund: Average speed profile | 73 |
| 7.16 | Speed profile: Trondheim - Kristiansund | 74 |
| 7.17 | Route tracking: MS Tyrhaug | 74 |
| 7.18 | AIS vs Timetable: Trondheim - Kristiansund | 75 |
| 7.19 | AIS vs Timetable: Kristiansund - Trondheim | 75 |
| 7.20 | Energy modeling: Edøy - Kristiansund | 77 |
| 7.21 | Component loads: Edøy - Kristiansund | 78 |
| 7.22 | Energy modeling with varying mass: Edøy - Kristiansund | 78 |
| 7.23 | Total load profile of components: Trondheim - Kristiansund | 79 |
| 7.24 | Optimal loadsharing concerning all parameters | 81 |
| 7.25 | Optimal loadsharing concerning all parameters: Trondheim - Kristiansund | 81 |
| 7.26 | Optimal loadsharing concerning all parameters | 82 |
| 7.27 | Optimal loadsharing concerning all fuel consumption | 82 |
| 7.28 | Optimal loadsharing concerning all parameters, with fluctu- ating wind component | 83 |

| | | |
|------|---|------|
| 7.29 | Energy, weight, and volume of battery and fuel cell configuration: Trondheim - Kristiansund - Trondheim | 84 |
| 7.30 | The iterative process of finding the total weight, volume, and capacity of a battery | 85 |
| B.2 | Optimizing the fuel consumption | VII |
| B.1 | Fuel cell efficiency for verification | VIII |
| B.3 | Optimizing the stable SOC | IX |
| B.4 | Optimizing the stable fuel cell power | IX |

Abbreviations

| | | |
|---------|---|---|
| ACO | = | Ant Colony Optimization |
| AI | = | Artificial Intelligence |
| AIS | = | Automatic Identification System |
| AM | = | Alkaline Membrane |
| BESS | = | Battery Energy Storage System |
| CCS | = | Carbon Capture and Storage |
| CII | = | Carbon Intensity Index |
| COG | = | Course over ground |
| CP | = | Controllable pitch |
| DBSCAN | = | Density-Based Spatial Clustering |
| DP | = | Dynamic Programming |
| EEXI | = | Energy Efficiency Design Index for existing ships |
| EMS | = | Energy Management System |
| ESS | = | Energy Storage System |
| GA | = | Genereic Algorithm |
| GHG | = | Green House Gasses |
| HFO | = | Heavy Fuel Oil |
| HHV | = | Higher Heating Value |
| HSC | = | High-Speed Craft |
| ICE | = | Internal Combustion Engine |
| IMO | = | International Maritime Organization |
| LGIM | = | Liquid Gas Injection Methanol |
| LHV | = | Lower Heating Value |
| LP | = | Linear Programming |
| MCFC | = | Molten Carbonate Fuel Cell |
| MDO | = | Marine Diesel Oil |
| MMSI | = | Maritime Mobile Service Identity |
| PEM(FC) | = | Polymer Emitting Membrane (Fuel Cell) |
| PEMS | = | Power and Energy Management system |
| PMS | = | Power Management System |
| PSO | = | Particle Swarm Optimization |
| QP | = | Quadratic Programming |
| Ro-Ro | = | Roll on Roll off |
| SES | = | Surface Effect Ship |
| SMR | = | Steam Methane Reforming |
| SOEC | = | Solid Oxide Electrolysis Cells |
| SOG | = | Speed over ground |
| ZE | = | Zero-Emission |

Introduction

1.1 Background and motivation

The objective of the Paris Agreement is to keep the increase in temperature well below 2°C and pursue efforts to keep it below 1.5°C. Therefore, the EU and the IMO have put down some goals for meeting this agreement. By 2030 the EU aims to reduce the emission of greenhouse gasses (GHG) by 30%, and by 2050 Europe shall be climate neutral. The International Maritime Organization (IMO) has also put down some specific targets for the maritime industry. An average across international shipping shall at least cut the emissions by 40% by 2030, pursuing efforts towards 70% by 2050, compared to 2008 values.

To achieve the climate goals, every market segment emitting GHG has to reduce its emissions. The shipping industry is responsible for 1.7% of the total global emission every year, and the high-speed ferry industry is responsible for over 1% of the total oil consumption in Norway. To reduce emissions in the maritime sector, various strategies have been suggested. This includes several climate-friendly propulsion systems such as hybrid propulsion, hybrid-electric propulsion, and electric propulsion.

The marine industry is being more and more digitized as new technology enters the market. This facilitates opportunities within the field of data mining of big data to obtain operational information. Furthermore, in the strive to lower emissions and design new low- and zero-emission vessels, this operational information provides valuable information to optimize the

operation and design of custom-made vessels.

1.2 Objectives

In the strive to reduce GHG emissions and become net-zero (carbon neutral) within 2050, several ZE concepts have entered the market, and several are in development. Diesel machinery has dominated the market over the last decades due to its low cost and reliable systems. To achieve a paradigm change in the maritime industry, from diesel to zero-emission, the zero-emission vessels need to have a custom-made design for their application. This thesis will address some of the challenges to achieving this. The objectives of this thesis are listed below.

- Review of literature providing information about characteristics of existing fast ferry, ZE fast ferries, ZE technology, sources of data providing route information, and data mining strategies.
- Evaluate and discuss existing energy models applied in the industry and suggest a new, transparent model that can be parameterized by available information (SeaWeb, etc.).
- Evaluate if AIS data is of high enough quality to provide route information effectively
- Generate route-specific information for a case vessel
- Find optimal structure for a zero-emission case vessel

1.3 Scope and delimitations

The scope of this work involves performing a literature review, providing relevant information, and similar work to the research question. This includes initiatives forcing the ferry industry towards zero-emission, characteristics of existing fast ferries, emerging low- and zero-emission technology, and different optimization methods. This will set the ground for comparing existing fast ferries with zero-emission solutions.

The components of a zero-emission configuration are determined by taking an existing fast ferry as a starting point, with its hull characteristics, machinery, route of operation, speed profile, etc. Then, an energy model is suggested to calculate component dimensions and capacities. This model provides accurate estimates of energy consumption around the service speed.

This is considered the essential property of the energy model because the vessel operates at service speed the majority of the time.

A case study is conducted for MS Tyrhaug, a fast ferry operating the ferry connection between Trondheim and Kristiansund. This case vessel is considered a good representative of most of the fast ferries in Norway. A zero-emission configuration is suggested by analyzing its AIS data, hull characteristics, power demand, etc.

The delimitations of this project are listed below:

- Hydrogen fuel cells and batteries are only studied in-depth as energy sources for zero-emission configurations.
- The power plants considered in the case study are simplified and do not concern low-level power management details.
- This thesis takes on the global optimal load sharing, providing a foundation for online power and energy management, but does not go into details in that field.
- The structure of the power plants, other than system components and their dimensions, is not studied in depth. The increase in weight is considered the most decisive parameter in the evaluation of zero-emission retrofitting.
- A comprehensive review of the infrastructure at ports is relevant to the problem, but it is not carried out in this thesis.

1.4 Contributions

The contributions of this project are:

- Provide insight into relevant technology, new zero-emission ferry concepts, and existing vessels of the Norwegian fast ferry fleet.
- Suggestion of a new transparent energy model parameterized by available data on existing vessels. The model can also take care of different dead weights.
- A method for processing raw AIS data. This method returns a structured JSON file of route information.
- A method for finding the resulting component dimensions, based on an iterative process.

- My own implementation of a dynamic programming algorithm solving the optimal load sharing problem.

Background and literature review

2.1 Shipping towards zero-emission

Parts of this literature review were done in the pre-project study in Fjelldal (2021) and are here reproduced for this thesis.

The objective of the Paris Agreement is to keep the increase in temperature well below 2°C and pursue efforts to keep it below 1.5°C (UNFCCC, 2015). The shipping industry is responsible for 1.7% of the total global emission every year and is under constant pressure to find more climate-friendly solutions. This Section provides some factors driving the shipping toward zero-emission.

2.1.1 EU and IMO initiatives

By 2030 the EU aims to reduce the emission of greenhouse gasses (GHG) by 30%, and by 2050, Europe shall be climate neutral. The International Maritime Organization (IMO) has also put down some targets. An average across international shipping shall at least cut the emissions by 40% by 2030, pursuing efforts towards 70% by 2050, compared to 2008 values (IMO). To achieve these goals, the EU and the IMO have introduced different types of sanctions/rules but also financial funding for ZE projects. In January 2021, the IMO introduced an Energy Efficiency Design Index for existing ships (EEXI), a measure of ship efficiency comparable to what the EEDI does for new buildings. The EEXI will be put to action in 2023, and it will force energy ineffective ships out of the seas. The IMO has also introduced

a Carbon Intensity Indicator (CII), which gives ships an annual rating from A to F, causing different measures (DNV).

The EU has earmarked €540bn to fund climate-related measures (within 2030). In addition, the EU has a variety of funds, such as the "Innovation Fund" for funding especially low-carbon innovative solutions (EU-Commission) and Horizon 2020, which was an EU funding scheme for innovation and development. Horizon 2020 supported projects with nearly €80 bn between 2014 and 2020.

2.1.2 National initiatives and support schemes

The Norwegian government plays a crucial role in Norway reaching the goals of the Paris Agreement. In 2018, the Norwegian parliament decided there shall be no emission from cruises and ferries in Norwegian fjords within 2026.

Similar to the EU support schemes, several Norwegian funding schemes exist, such as Enova, Innovation Norway, and the Norwegian Research council. The three mentioned have established PILOT-E, which provides funding for climate-friendly initiatives (Enova). In 2018, PILOT-E received 107 MNOK of governmental support, of which 71 MNOK was awarded to five maritime projects. One of them was the ferry concept of NCE Maritime CleanTech: ZeFF (Zero Emission Fast Ferry), which was awarded 10.5MNOK (Marine-Clean-Tech). Projects may also directly receive funding from Enova, Innovation Norway, and the Norwegian Research council. For example, Wärtsilä received a 20 MNOK grant from the Norwegian Research Council for testing their ammonia combustion engine (Wärtsilä), and Future of the fjords was awarded 22 MNOKs from Enova (Enova, 2018).

2.2 Historical hull technology

High speed crafts (HSC) have constantly changed design and concept during the last century. The first HSCs were built as hydrofoils. The usage of hydrofoils in marine applications was introduced in 1906, only three years after the first motorized airplane. Due to the lack of computer technology, the first hydrofoil vessels were passive stabilized by slanted foils. The usage of hydrofoils reduced the ship resistance in high-speed operations, but also reduced the performance in rough seas. When modern computers were introduced, active-controlled hydrofoils followed by, which improved the performance significantly. Hydrofoil passenger ferries dominated the

market in the 70s, but when catamarans were introduced in the 80s, hydro-foil vessels got wiped out of the market (Kleven Godø and Vinje Kramer (2019)). Today, high-speed ferries are typically built as catamarans, but also monohull crafts exist in the market. Monohull configurations provide a compact design and light hulls relative to the payload.

In 1956, Christopher Cockerell started developing the jet hovercraft, and in June 1959, the SR.N1 was ready for trials. The SR.N1 was successfully hovering 20cm over the ground. The prosecution proved the concept with success, but in practical aspects, the SR.N1 was only suitable for smooth surfaces, and the lifting force was very power demanding. Therefore, this technology was never commercialized in the ferry market. However, the concept of using pressurized air to lift the hull out of the water has led to another idea relevant for this project; Surface Effect Ship (SES) (Yun and Bliault, 2012).

2.3 Hull technology for high speed operation

There are, in general, three categories of high-speed vessels: Hull-supported vessels, foil-supported vessels, and air-cushion-supported vessels. These three types of hulls are based on three entirely different concepts, which will be briefly discussed in the following sections.

2.3.1 Hull-supported vessels

Hull-supported vessels are separated into displacement hull, semi-displacement hull, and planing hull. Displacement hulls are most common for low-speed vessels, where the buoyancy of the hull is carrying the weight of the vessel. Planing hulls are constructed such that dynamic pressure is induced at high speed, lifting the hull out of the water. This reduces the resistance significantly and is the most common technology for smaller high-speed crafts. Semi-displacement hull is something in between a planing hull and a displacement hull. The most popular hull designs for high-speed ferries are V-shaped hulls and multi-hull, such as catamarans. The catamaran was introduced for high-speed applications in the 80's with great panache. Catamarans have dominated the high-speed ferry market since, with slender bodies and high stability, but V-shaped monohulls are also represented.

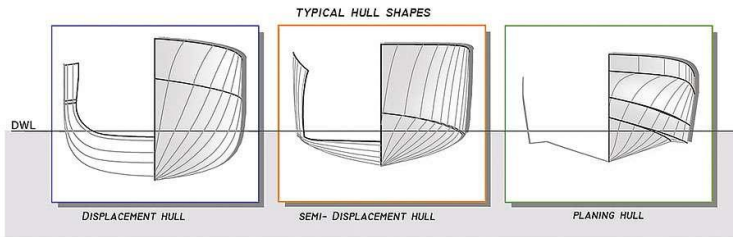


Figure 2.1: Hull-supported vessels. Image courtesy of: Heyman-Yachts (2018)

2.3.2 Foil-supported vessels

Foil-supported vessels are most commonly known as hydrofoils. Hydrofoils are based on wing technology from aerodynamics. When the speed is sufficiently high, the foils create enough lift to carry the vessel out of the water. Once the hull is out of the water, the resistance drops in proportion to the wet surface being lifted out of the water.



Figure 2.2: Hydrofoil ferry (Boundary Layer Technologies)

2.3.3 Air-cushion-supported vessels

Air-cushion-supported vessels are based on a mechanical air-cushion lifting the hull out of the water. This hull technology is usually referred to as surface effect ships (SES).

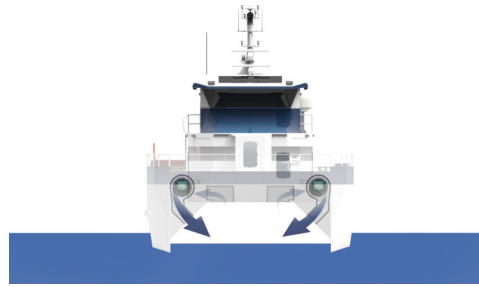


Figure 2.3: Surface Effect Ship: Concept figure. Courtesy of Wavecraft (2018)

2.3.4 Industrial application of different hull structures

Most high speed ferries are built with catamaran hulls in today's industry. In the 80's, hydrofoils were expensive and heavy, and compared to other technologies, they had the same resistance. When the catamaran entered the market with low resistant, slender bodies, it took over the market and has dominated since. There are several reasons for this. One is that the premium with hydrofoils is low resistance for very high speed surveys (50 knots), while most ferry connections only require 20-30 knots. Another reason is that catamarans have been under constant development ever since their introduction. Modern catamaran structures are based on lightweight materials, such as carbon fiber, while hydrofoil structures are based on steel and aluminum (Kleven Godø and Vinje Kramer, 2019). Carbon fiber hulls are said to reduce the total weight by 10% compared to aluminum (TU, 2015). However, aluminum is recyclable and brings other environmental aspects to the table.

Regardless of the theoretically high efficiency, SES technology is not notably represented in the ferry industry. This is because SES technology has been sensitive to rough seas and bullied with wear and tear of the propulsion system caused by ventilation and cavitation of the propellers. However, a new technology taking care of these problems is in development. SES ferries are therefore expected to enter the industry. The EU awarded project "BB Green" of SES-X resulted in a demo vessel called "AiriEL". AiriEL is a battery-driven ferry running using air-cushion technology. The ferry is said to be 40% more energy-efficient than a traditional high-speed catamaran (Wavecraft, 2018).



Figure 2.4: AiriEL; Photo: BB green

Hybrids between the different technologies have also been introduced to the market, such as the air lubrication system, which combines air-cushion support and hull-support.

2.4 Conventional machinery

In general, a vessel's machinery is based on a prime mover and a power transmission system. The prime mover converts chemical energy to mechanical and/or electrical energy. In the traditional marine industry, the prime mover has typically been an internal combustion engine (ICE) running on heavy fuel oil (HFO), diesel, or gasoline. Other prime movers in the marine industry is: steam engines (reciprocating and turbine), nuclear-powered steam engines, gas turbines, stirling engines (primarily used for submarines), fuel cells, and dual-fuel ICEs. During the last years, new technologies have been investigated for application in low- and zero-emission concepts, further discussed in the following section.

2.4.1 Emerging combustion engine technology

Due to the rising demand for climate-friendly solutions, ICEs are developed for running on dual-fuel. Dual-fuel ICEs are combustion engines that can run on, e.g., ammonia, natural gas, and marine diesel oil (MDO), (Karim, 1987). Wärtsilä delivers dual-fuel engines that can be run on natural gas, marine diesel oil (MDO), or heavy fuel oil (HFO) (Wärtsilä, 2017). *MAN energy solution* is also delivering dual-fuel engines and is in the development of a "fuel-flexible, two-stroke ammonia engine" (Lindstrand), causing no GHG emissions, no SO_x and low NO_x emission. The Japanese shipping major Mitsui O.S.K. Lines (MOL) has signed a memorandum of understanding (MoU) with Mitsui E&S Machinery and MAN Energy Solutions

to target a purchase contract for an ammonia-fuelled main engine for ships (Bahtić, 2021b).

Methanol is another emerging climate-friendly fuel alternative. Methanol synthesized from green hydrogen (see Section 3.1.1), and CO_2 is considered net carbon neutral. Methanol dissolves in water and is biodegraded rapidly, which means the environmental effects of large spills is harmless. Due to the chemical composition of methanol, CH_3OH , methanol provides no SO_x emission, low NO_x when operating efficiently, and very low particulate matter (PM) (Soni and Gupta, 2016). Several ships have converted their fuel to methanol by retrofitting existing machinery in recent years. For example, in 2015, the machinery of the ro-pax ferry Stena Germanica was converted to be run on methanol (Andersson and Salazar, 2015) as a part of the SPIRETH project of The Danish Maritime Fond (Ellis et al., 2014). New technology has also provided methanol-optimized engines with higher efficiency than the retrofitted concepts. The shipping giant Maersk has ordered eight MAN's B&W 8G95ME liquid gas injection methanol (LGIM) engines for their new boxship concept (Bahtić, 2021a).

The high-speed ferry Francisco Papa was launched in November 2012 as the world's first dual-fuelled high-speed Ro-Ro ferry. The ferry is installed with two 22MW GE Energy LM2500 gas turbines specially designed to burn both LNG and MDO (Ship-Technology). Early 2021, Mitsubishi Power announced they were in the development of the world's first ammonia-fired 40MW class gas turbine system. Mitsubishi is targeting commercialization in or around 2025 (Mitsubishi, 2021)

2.5 Hull and machinery in the Norwegian fast ferry fleet

2.5.1 Machinery

In the Norwegian fleet of fast ferries, one dominant supplier with respect to market share is MTU Friedrichshafen, owned by Rolls-Royce. A study of the Norwegian fast ferry fleet (Appendix A) shows that 17 of the 21 vessels studied are installed with either 2 or 4 MTU engines delivering between 1500 and 3600 kW.

2.5.2 Hull

The hulls of the fleet are heavily dominated by catamarans. 21 out of the 21 vessels studied are catamaran hulls, delivered by either Brødrene AA AS or Oma Båtbyggeri AS. The two shipyards share the Norwegian fast ferry market approximately 50/50. Brødrene AA started with constructions of fiberglass composites in 1970 but has over the years become a world leader in lightweight structures of carbon fiber composites (TU, 2014). On the other hand, Oma base their construction on recyclable aluminum hulls.

2.6 Propulsion systems for high speed operation

High speed vessels are, in most cases, configured with controllable pitch (CP) propellers or water jets. CP propulsion has a variety of advantages such as reduced level of noise and vibrations, high efficiency in high speed as well as good acceleration, and wide operational range. Servogear, one of the market leaders, offers package solutions for fast ferries, including propeller tunnel, effect rudder, controllable pitch propeller, shaft brackets, and reduction gearbox. Servogear has over 1800 installations in a variety of ships world wide and claims their CP propeller system for fast ferries has the highest efficiency known in the market (Servogear, 2017).

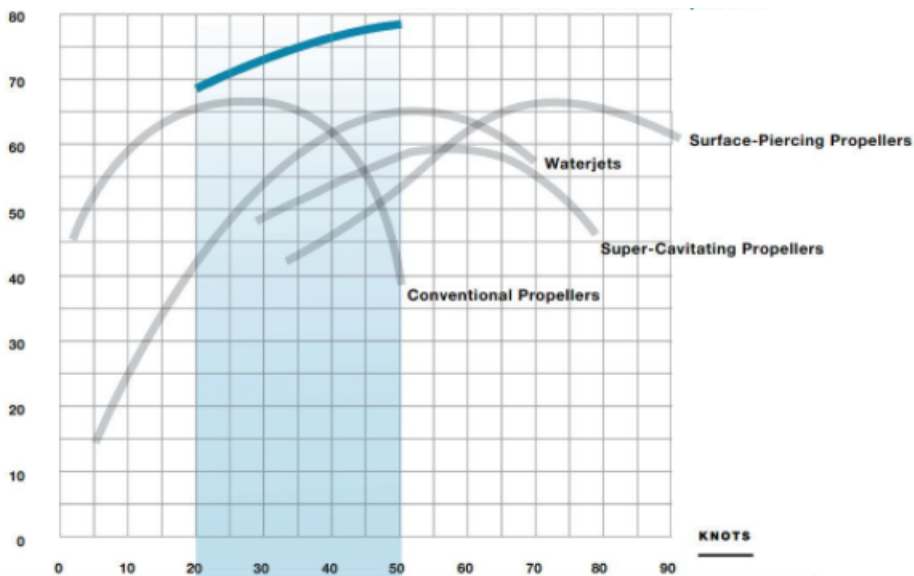


Figure 2.5: Propulsion efficiency curves, Courtesy of Servogear (2017)

From Figure 2.5, we see that water jets also provide high efficiency for high speed applications and fast throttle response. *Wärtsilä* delivers water jet systems along with their "Propulsion Control System". This system comes with lever controls, joystick, and touch screens for ease of use and ultimate vessel and water jet control. This configuration assists the crew with challenging maneuvering such as harbor entering, docking, etc. (Wärtsilä, 2021).

Based on research on high speed passenger ferries in Norway (see Appendix A), it appears as half on half of the ferries are installed with CP propellers and water jets.

In Section 2.9, different ZE high-speed ferries will be presented along with their propulsion system.

2.7 Energy management system

An energy management system (EMS) is a computer-based tool used for the high-level control of the energy flow in the vessel. The EMS is based on optimization algorithms trying to minimize/maximize some parameters of interest. A typical EMS issue is minimizing the cost during operation. The parameter of interest would then be the fuel consumption, which again depends on the prime movers' power and efficiency. Other optimization objectives are reducing NO_x and SO_x , and increasing the lifetime of components (minimize wear and tear). A weighted combination of the objectives mentioned should be considered for a good EMS.

In the topology of autonomous marine systems, the EMS is within the online optimization layer. Because the vessel does not know what will happen in the future, it is impossible to assure that the energy management is perfectly optimal. A fictional scenario is derived to enlighten the issue: Given a certain condition, the EMS thinks it is favorable to run the batteries hard to obtain the lowest fuel consumption. Later on, the vessel runs into a forceful headwind which causes a sudden increase in the load. The power of the battery is maxed out, and the dynamic response of the fuel cell is too slow to react to the change of load. This enlightens why the EMS should be developed carefully with good strategies. Further on, a couple of optimization methods will be discussed.

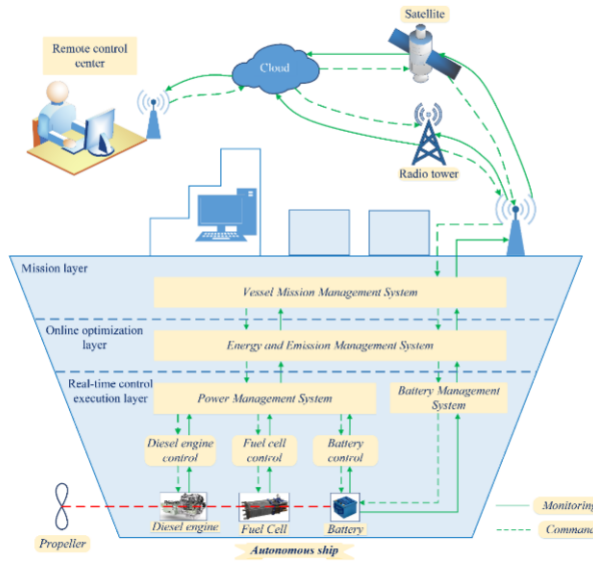


Figure 2.6: Control architecture of the ship. Courtesy of NTNU

2.7.1 Numerical optimization methods

Optimization problems are based on finding the minimum/maximum of a function of interest. This can be of economic motivation, environmental motivation, or time-saving motivation, among others. Based on the characteristics of the optimization problem, different techniques are more suitable than others. Here, some numerical optimization algorithms will be discussed.

Linear programming

Linear programming (LP) is an optimization technique used for systems with linear constraints and linear objective functions. A typical application of LP optimization is the maximization of profit for a factory producing different products, each with specific constraints. The result is typically a volume of product x_1 , product x_2 , etc. An extension of LP is mixed integer linear programming (MILP), which adds one more condition; at least one variable must take on integer values. MILP has been used for several optimization problems in the literature, such as: energy management of microgrids (Tenfen and Finardi, 2015), Optimization of Multi-Scale Material, Energy Integration (Kantor et al., 2020), and (Thorat et al., 2021).

Quadratic programming

Quadratic programming (QP) is the process of solving optimization problems in quadratic form. QP seeks to find minimum/maximum values of a multivariate quadratic function subject to linear constraints. Several methods exist for solving this kind of problems, such as Interior point, active set, augmented Lagrangian, and Newton's method (Wikipedia contributors, 2021b). In the literature, QP is commonly used in various optimization problems, such as for reactive power optimization (Grudin, 1998).

Dynamic programming

Dynamic programming (DP) is a powerful tool for finding a global optimal solution. The algorithm breaks down a problem into instances of base problems and solves each one separately. After computing the cost of each sub-problem, the algorithm tracks back the nodes with the lowest cost (or highest award) and finds the optimal path. DP is an offline method. This means the algorithm needs to know the entire environment to find the optimal solution. The algorithm starts at the goal node and investigates all nodes connected to the goal node (see Figure 2.7). Each solution (node) is added to the possible set of solutions with the associated cost (20, 25, 17) and their predecessor (goal). The new set of solutions is then investigated along with the connections to the new layer of nodes (here: start node). The cost of each node is the sum of all its predecessors. When the algorithm reaches the start of the structure, it evaluates which node has the lowest total cost. Then it backtracks to find the optimal path (start - upper node - goal, cost = 25).

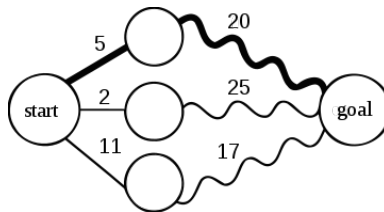


Figure 2.7: Shortest path problem solved with dynamic programming. Courtesy of Wikipedia contributors (2021)

DP guarantees a globally optimal solution. This makes the results from DP a good tool for evaluating the performance of other algorithms. Furthermore, the solution of the DP sets a benchmark that other online optimization methods can compare with. DP is used in various optimization

problems and is applicable for global optimal loadsharing problems (Zhang and Xiong, 2015; Scordia et al., 2005; Chen et al., 2014).

2.7.2 Artificial intelligence based optimization methods

Many real-life optimization problems are complex and cannot be solved by step-by-step methods to find the optimal solution. There are various artificial intelligence(AI) algorithms that easily find good solutions to solve such problems. Artificial intelligence is often defined as the study of "intelligent agents". Each agent represents a possible solution, and the fitness of each solution is evaluated concerning the objective function to be optimized. In this section, some AI-based optimization methods will be briefly explained (information based on Swarnkar and Swarnkar (2020)).

Genetic algorithm

The genetic algorithm (GA) is based on natural selection and evolutionary processes and was first introduced in 1975. GA was first applied to find a solution to "the knapsack problem". It creates a random population of general solutions. Each solution is encoded as a chromosome (ones and zeros), and each solution gets a measure of fitness. Then, the GA manipulates the solution by either crossovers or mutations. Crossovers are swapping parts of two "healthy" solutions, hoping to create even better solutions. A mutation is changing one or several bits of the chromosome.

Particle swarm optimization

The particle swarm optimization (PSO) algorithm was introduced in 1995. PSO is inspired by bird flocking and fish schooling. The algorithm is based on a number of agents with a position, velocity, and a personal best position. The population of agents is also constantly aware of the best global position of the population. By evaluating the current position, velocity, personal best position, and global best position, the agents have a great chance of finding the optimal solution, but it is not for sure. In the literature, PSO is used for, e.g., load balancing and loss reduction in power grids (Sivanagaraju et al., 2008).

Ant colony optimization

Ant colony optimization (ACO) is a method inspired by the strategy ants use to find a path between the nest and a food source. The method is based on ants laying down pheromones to direct other ants to resources

while investing in the environment. In addition, the ants "record" their position and solution quality, so in later events, more ants locate better solutions. ACO was first implemented to find a solution to the traveling salesman problem (TSP) and is well suited for finding an optimal path/route scheduling (Deng et al., 2019).

2.7.3 Machine learning for prediction of loads

As described in Section 2.7, it is hard to find the perfect energy management due to uncertainties in the future. The environmental loads on the vessel will vary from survey to survey due to different environmental conditions. However, high-speed ferries are typically operating the same route every day, and environmental forecasts are available. Knowledge of the speed profile provides a basis for generating the expected load profile for a survey, where the weather forecast works as a correction. This can be fed to a predictive machine learning (ML) algorithm that calculates the most likely load profile for the survey. ML is based on better and better algorithms the more it is used (trained). Broadly, there are three types of ML algorithms: Supervised Learning, Unsupervised Learning, and Reinforcement Learning. Supervised learning is well suited for time-series prediction, which is the objective for load prediction; therefore, the ML technique of scope in this Section. Supervised learning algorithms try to model relationships and dependencies between the target prediction output (load) and the input (weather data, passengers, etc.). The prediction of the new data is based on those relationships that it learned from in previous datasets (Fumo, 2017). In the literature, supervised learning is used on various prediction problems: Building thermal load prediction (Wang et al., 2020), coastal zone significant wave height prediction (Demetriou et al., 2021), and prediction of movement direction in crude oil prices (Shin et al., 2013).

2.8 Clustering

Clustering is a type of unsupervised learning where a machine acts, without any guidance, on data without any form for labeling. Clustering is used to find patterns, structures, and groups in a data set. A cluster (group) of a data set shares some characteristic or quality, separating the cluster from the rest of the data. Clustering algorithms provide a powerful tool for classifying data. In the literature, different clustering algorithms are commonly discussed for various objectives. The following sections will briefly explain some algorithms along with industrial applications.

2.8.1 Density-based spatial clustering

Density-based clustering is commonly known as DBSCAN. The method groups every data point in a cluster with a minimum number of neighbors (MinPts) within a predefined radius (eps). In the literature, DBSCAN is used to analyze vessel movements (Yan et al., 2016), shipping route characterization (Rong et al., 2020), and modeling vessel behavior (Han et al., 2021).

2.8.2 K-means

K-means clustering is a simple ML algorithm trying to allocate all the data in a data set to a predefined number of clusters. The algorithm takes the expected amount of clusters as input parameter. First, randomly located in the data set, one centroid is created for each cluster. The data points are then distributed to the closest centroid, creating a first iteration cluster. The new location of the centroid is then moved to the mean location of each cluster; then, the data points are reallocated to the closest centroid. This goes on until there are no more movement of the centroids.

For marine applications, K-means are commonly discussed in the literature. Marta and Ireneusz (2021) suggests a clustering-based approach, using K-means to avoid AIS package collision, Wu and Neilsen (2021) utilizes a K-mean algorithm to identify seabed types, and Lin et al. (2021) presents a method for identifying marine water pollution based on K-means clustering.

2.8.3 Agglomerative hierarchical clustering

The agglomerative hierarchical clustering (AHC) is within the family of hierarchical clustering. The AHC algorithm starts by treating each data point as a cluster. Then it starts to pair up clusters with comparable characteristics creating new clusters.

AHC also provides a good tool for marine applications. For example, in the literature, AHC is applied to AIS data for long-term trajectory prediction (R. Praveen and Adil, 2022), and port classification (Vicente-Cera et al., 2020), to mention some.

2.9 Existing low- and zero-emission concepts

As discussed in Section 2.1, significant forces are driving the ferry industry towards low- and zero-emission concepts. In this section, some new low-

and zero-emission concepts are presented.

MS Color Hybrid

MS Color Hybrid is the world's largest plug-in hybrid-electric ship. The ship is a 160m ferry operating between Sandefjord and Strømstad with a capacity of transporting 2,000 passengers and 500 vehicles. In 2017, Color Line and Ulstein shipyard started building the world's largest plug-in hybrid ship, and in 2019 MS Color Hybrid was put in operation (ColorLine). Color Hybrid is equipped with a hybrid-electric propulsion system consisting of a 5MWh battery and a diesel generator set. The ferry has four diesel-electric gensets from Rolls-Royce Engines, connected to 2 electric motors, driving 2 CP propellers, with a total capacity of 16,800kW (data from SeaWeb). The ferry can navigate at ports for 60 minutes, only running on batteries, which reduces noise and local emissions.



Figure 2.8: MS Color Hybrid, photo: Skipsrevyen (2021)

MS Ampere

MF Ampere was in 2014 awarded ship of the year by *Skipsrevyen*. M/S Ampere is the world's first large electric car ferry. The ship was built by Fjellstrand AS shipyard and is owned by Norled. Ampere operates between Lavik and Oppedal and has a capacity of 120 cars and 360 passengers. The hull is a catamaran made of aluminum with one azipull thruster of 450kW, from Siemens, at each side of one of the hulls. Ampere starts every morning with full batteries. However, due to a thigh schedule, it can only charge 10 minutes at the time at the quay (Puchalski, 2015). Therefore, the ferry is installed with a large lithium polymer battery system based on 224 Corvus Energy AT6500 modules with a total capacity of 1,46 MWh (Skipsrevyen, 2014).



Figure 2.9: MS Ampere, photo: Skipsrevyen (2014)

MF Hydra

MF Hydra is the world's first hydrogen passenger ferry. MF Hydra was awarded ship of the year 2021 from *Skipsrevyen* and is the second ferry owned by Norled to win the prestigious award. The ferry was built by Westcon shipyard and is to be operated between Hjelmeland and Nesvik with a total capacity of 299 passengers and 80 cars. Hydra is installed with PEM fuel cells from Ballard with a capacity of 400kW and a battery energy storage system. In addition, the ferry is configured with e-SEAMatic BLUE EMS system delivered by Westcon Power & Automation AS (Johannessen, 2016) for peak shaving and optimal control. The liquid hydrogen is stored in an $80m^3$ tank provided by Linde (Skipsrevyen, 2021). The fuel cells will be able to power two schottel thrusters and reach a speed of 9kt.



Figure 2.10: MS Hydra, photo: Skipsrevyen (2021)

Future of the Fjords

Future of the Fjords is an all-electric catamaran in carbon fiber composite, designed by Brodrene Aa. Brodrene Aa delivered the ferry in 2018 to the owners: The Fjords. It is in operation for sightseeing purposes between Flaam and Gudvangen. The ferry has a capacity of 400 passengers. Future of the Fjords has a loa of 42.5 m and is installed with fully electric propulsion, based on two electric 450kW motors. A battery package of 1800kWh can deliver power to the motors for sailing at 16 knots for 2.5 hours. The ship is also designed for a future hydrogen-based propulsion configuration (Strømgren et al., 2019).



Figure 2.11: Future of the Fjords, photo: Brodrene Aa

MS Bard

MS Bard is a hybrid-electric arctic cruise operating in northern Norway and Svalbard. The ship was delivered from Maritime Partner Shipyard to Brim Explorer in 2020. The ferry has a capacity of 146 passengers and is sailing on a cruise speed of 8-12 knots. Only running on batteries, the ferry can be operated for 10 hours without charging. Bard has a maximum speed of 20 knots when running the batteries in combination with a diesel motor. The hull of Bard was designed by Wave Propulsion and is a 25.2 meter long catamaran of aluminum. The hybrid-electric propulsion system is based on two Scania D113 ICEs from Nogva of 368kW and two gear integrated electric motors from Servogear of 80kW (Skipsrevyen, 2020). The propulsion is based on Servogear Ecoflow Propulsor CP propeller system (Servogear, 2017).



Figure 2.12: MS Bard, image courtesy of Brim Explorer

2.9.1 Zero-emission high-speed ferry projects

AERO40 H2 Fast Ferry

AERO40 is a ZE fast ferry project by Brodrene Aa. The ferry is designed for high speed ZE surveys of longer distances, where battery power does not have the capacity required. The Aero-design was first presented in Trondheim 2019 by Brødrene Aa and the industry partners Westcon, Boreal, and Ocean Hyway Cluster (Brodrene-Aa, 2019). The ferry is designed to carry 300 passengers.

The hull of AREO40 is a catamaran of carbon fiber. The ferry is designed to carry up to 600 kg of hydrogen, which allows the ferry to run up to 100 nm at 32 knots without refueling. Fuel cells are running two electrical motors with a total capacity of 2,600 kW. The propulsion system is separated into two parts, one for each hull, with its own fuel cell, motor, battery, and control system. This provides redundancy, segregation, and safe operation (The-Explorer, 2019).



Figure 2.13: AERO40, image courtesy of Brodrene Aa.

MS Medstraum

MS Medstraum is the name of TrAM's demonstrator vessel. TrAM is an EU-funded (Horizon 2020) project aiming to develop a zero-emission high speed ferry. Medstraum is a 30m long fully electric ferry with a capacity of 150 passengers. The ferry is to be operated on the route between Stavanger and Hommersaak. It is built by Fjellstrand shipyard with expected delivery in Mars 2022 to its owner, Kolumbus (Corvus, 2021). The ferry has an all-electric propulsion system with an energy storage system (ESS) capacity of 1524kWh, delivered by Corvus. The ferry is designed with a service speed of 23 knots running on two electric motors with a Servogear CP propulsion system.



Figure 2.14: MS Medstraum, image courtesy of TrAM.

2.10 Automatic identification system

Automatic Identification System is commonly known by its abbreviation, AIS. AIS information supplements marine radar, which is used for collision avoidance. The IMO's international convention for the safety of life at sea requires AIS to be fitted aboard international voyaging ships with 300 or more gross tonnage and all passenger ships regardless of size. An AIS transceiver is programmed to send data every 2 to 10 seconds, depending on the vessel's speed, and every 3 minutes while anchored (IMO, 2015). This data is shown in Table 2.1

| Data | Resolution |
|--|---------------------|
| Vessel Maritime Mobile Service Identity (MMSI) | - |
| Navigation Status | - |
| Rate of turn (rotations per minute) | - |
| Speed over ground (sog) | 0.1 knot (0.19km/h) |
| Position | 0.0001 arcminutes |
| Course over ground (cog) | 0.1 deg |
| True heading | 1 deg |
| True bearing | 1 deg |
| UTC seconds | 1 second |

Table 2.1: AIS data published every 2-10 seconds

In addition, more data are broadcast every 6 minutes, including IMO ship identification number, radio call sign, name of the vessel, type of ship, along with other ship-specific information (IMO, 2015).

Both real-time and historical AIS data are available online from various sources. In Norway, The Norwegian Coastal Administration is responsible for the AIS network. This data is free and universally accessible at Bar-entsWatch (Kystverket, 2022).

Over the years, the quality of the AIS data in Norway has improved. This is because of upgraded equipment and more base stations, with better coverage of the coastline (Conversation by phone with *Kystverket*, 2022).

AIS data is commonly used for a variety of purposes in the industry. Pallotta et al. (2013) suggests a methodology called TREAD (Traffic Route Extraction and Anomaly Detection) for automatically detecting anomalies and projecting current trajectories and patterns into the future, based on AIS data. In the literature, several methods have been suggested for this

purpose (Hu et al., 2006; Mascaro et al., 2014; Lane and Copsey, 2012). AIS data is also commonly discussed concerning Maritime Situation Awareness (Bomberger et al., 2006; Rhodes et al., 2005; Graziano et al., 2019).

Chapter 3

Technology: State-of-the-art

In this chapter, state-of-the-art technology relevant for zero-emission fast ferries will be presented. Parts of the content in this section were done in the preproject study in Fjelldal (2021) and are here reproduced for this thesis.

3.1 Energy carriers and storage technology

To achieve the EU's goal of being CO₂ neutral within 2050, gas and oil will be phased out and replaced by clean energy. Wind parks and solar PV farms will be installed on a big scale in the coming years. The prediction of the IEA says the total wind and solar PV capacity will expand to 1,123 GW by 2025 (IEA (2020)), which is almost 75 times the annual power consumption of Norway. Solar PV and wind power are non-dispatchable power sources. This causes a surplus of power on sunny and windy days and a lack of power on calm days with poor solar radiation. This leads to a demand for storing technology for capturing surplus power and/or flexible consumption. This demand will drive new technology and market segments forward.

3.1.1 Hydrogen and ammonia

Hydrogen plays a crucial role in several industrial segments, such as in oil refining, in the production of ammonia (through the Haber process) and methanol (through reduction of carbon monoxide), and also as a fuel in transportation (Wikipedia contributors, 2021a). Historically, hydrogen has

been produced from fossil fuels; today called grey hydrogen. In the process of producing grey hydrogen, GHG is emitted. A new technology of storing the CO_2 from the production is introduced to reduce the total emission. This technology is called CCS (carbon capture and storage), and the hydrogen produced in this manner is called blue hydrogen. CCS technology can reduce the CO_2 emission by 90%. The last type of hydrogen is green hydrogen. Green hydrogen is made from the electrolysis of water. Around 70 Mt of dedicated hydrogen is produced annually, 76% from steam methane reforming (SMR) and almost all the rest (23%) from coal gasification. This is both grey hydrogen. Electrolysis of water (green hydrogen) only accounts for around 2% of the total production.

Electrolysis of water

Electrolysis of water has been too expensive in the past, but due to higher efficiency, lower electricity cost, and lower CAPEX for electrolyzers, electrolysis of water is estimated to gain a larger market share in the future (Agency-IEA (2019)). Table 3.1 summarizes the most commonly used electrolyzer technologies: alkaline electrolyzer, polymer emitting membrane (PEM) electrolyzer, and solid oxide electrolyzer (SOEC). LHV is short for lower heating value.

The three electrolyzer technologies are based on the same components, a cathode, an anode, and a membrane separating the anode from the cathode. The membrane in the alkaline electrolyzer transports OH^- ions from the cathode to the anode, in the PEM electrolyzer, H^+ ions are transported, and in the SOEC electrolyzer, O_2^- ions are transported.

| | Alkaline | | | PEM | | | SOEC | | |
|-------------------------------|----------|---------|-----------|-----------|----------|-----------|-----------|----------|-----------|
| | Today | 2030 | Long term | Today | 2030 | Long term | Today | 2030 | Long term |
| Electrical efficiency (% LHV) | 63-70 | 65-71 | 70-80 | 56-60 | 67-74 | 74-81 | 74-81 | 77-84 | 77-90 |
| CAPEX (USD/kW) | 500-1400 | 400-850 | 200-700 | 1100-1800 | 650-1500 | 200-900 | 2800-5600 | 800-2800 | 500-100 |

Table 3.1: Electrolyser technology evolution, now vs. 2030 vs. long term. (Agency-IEA, 2019).

Properties: hydrogen

Hydrogen has high gravimetric energy density (kWh/kg) but low volumetric energy (kWh/m³). This is due to the low density of hydrogen. Hydrogen has a density of 0.09kg/m³ at 1 atm pressure, and 70.1kg/m³ in liquid form. The low density of hydrogen is the factor setting the limitation of storage capacity on ships (see Figure 3.1).

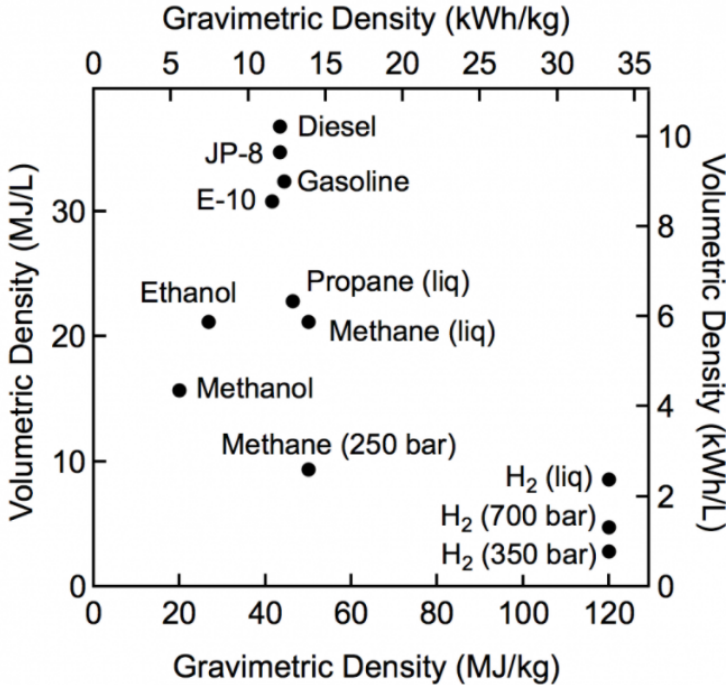


Figure 3.1: The energy density of fuels. (Energy.gov)

Price prediction: hydrogen and ammonia

Today, the most ammonia is produced by the Harber-Bosch process. Hydrogen- and nitrogen gas react under pressure. In this process, the electrolysis of water accounts for almost 93% of the total energy demand. The production cost of ammonia is therefore highly related to the production cost of hydrogen.

Along with the introduction of more renewable energy, the price of green ammonia and hydrogen is predicted to fall drastically. Recent studies from

BNEF estimate the price of green hydrogen to fall under \$2/kg H₂ by 2030 and \$1/kg H₂ by 2050 (FuelCellsWorks, 2021). Another prediction is made by the International Renewable Energy Agency (IREA), and the forecast falls into the same price range. Based on an electrolyzer cost of \$650/MW and an electricity price of \$130/MWh, they estimate hydrogen may be produced at \$1/kg H₂ (The International Renewable Energy Agency (2021)).

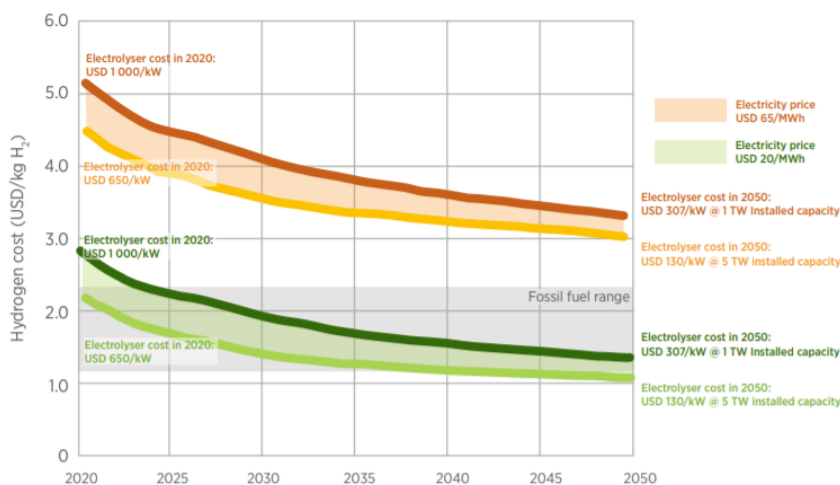


Figure 3.2: Hydrogen price prediction. Courtesy of The International Renewable Energy Agency (2021)

3.1.2 Fuel cell technology

The most used fuel cell technology in the market today is Alkaline fuel cell (AFC), Polymer electrolyte fuel cell (PEMFC) and high-temperature PEMFC (HT-PEMFC), phosphoric acid fuel cell (PAFC), molten carbonate fuel cell (MCFC), and solid oxide fuel cell (SOFC) (Winter and Brodd, 2004). Each of these has its advantages and disadvantages. Table 3.2 shows a summary of the peak electrical efficiency and the working temperature of the fuel cell technology mentioned.

| | Operating Temperature | Electric Efficiency (LHV) | Overall efficiency |
|----------|-----------------------|---------------------------|--------------------|
| PEMFC | <120°C | 60% | - |
| HT-PEMFC | 160-220 | 60% | 80% |
| AFC | <100°C | 60% | - |
| SOFC | 500 - 1000°C | 60% | 85% |
| MCFC | 600 - 700°C | 50% | 85% |
| PAFC | 150 - 200°C | 40% | 80% |

Table 3.2: Fuel cell summary table (Winter and Brodd, 2004)

Ballards FCwave is by DNV, the first type-approved fuel cell for maritime applications worldwide (Hydrogen24, 2022). FCwave is a PEMFC, readily modularized and combined in parallel to provide the power needed. Each fuel cell module delivers 200kW and can be configured in parallel to deliver up to 1MW. The cells have been tested for more than 30,000 hours without reparations or rebuilding of the stack with success. For larger vessels, building blocks of 1 to 3MW are expected to reach the market (Mace, 2019).

The fuel cell technology varies in working temperature and efficiency. Taking power capacity and efficiency into regard, PEMFC/HT-PEMFC, SOFC, and MCFC are the most promising technologies for marine applications (Xing et al., 2021). SOFC and MCFC are very flexible to fuel and may run on LNG (liquefied natural gas), methanol, diesel, etc. The cost, however, is higher than for PEMFC, and concerning low- and zero-emission perspectives, these features are less relevant. Nevertheless, a flexible system may be of interest in the transmission phase from fossil fuel to green solutions.

In Chapter 4, more technical information, such as efficiency, weight and volume of fuel cells are presented.

3.2 Battery energy storage systems

A Battery Energy Storage Systems (BESS) is utilized in a hybrid-electric propulsion system for two reasons: i) keeping the prime movers running at the optimal condition and ii) supplying power at rapidly varying loads. Both conventional machinery and fuel cells have varying efficiencies under different operating conditions. Therefore, the BESS charges when the loads are below the optimal threshold; when loads are above the threshold, the BESS supplies power.

3.2.1 Battery technology

The fast dynamics of batteries are utilized in varying load conditions. When the vessel experiences a rapid increase in load, the battery supplies the residual power until the prime mover catches up with the load. This is especially convenient in a hybrid-electric propulsion system with a fuel cell as the prime mover. Fuel cells have slow dynamics and need time to catch up with rapidly varying loads. Contrary to hydrogen, batteries have a high volumetric energy density but a low specific energy density. To enlighten the issue, the 40 ft. "Flex 40-1100" BESS container of ABB has a capacity of 1100 kWh. This BESS container has a total weight of 26,250 kg and dimensions: 12x2.450x2.900 m, which is 85.26 m³ (Tammema, 2021). The same weight of hydrogen equals 870,125 kWh, but also a total volume of 375 m³. From this, we get an indication of the pros and cons of batteries and hydrogen.

3.2.2 Battery energy storage systems for marine applications

There are a variety of battery concepts in the industry, each with its advantages and disadvantages. Below, some state-of-the-art battery concepts are explained, along with their advantages and disadvantages.

Lithium-ion battery

Rechargeable lithium-ion batteries (LIBs) are well known in the industry due to their high energy density, low self-discharge rate, and low demand for maintenance. In addition, lithium metal is considered to be a good anode (negative electrode) due to its high specific capacity (3860 mAh/g) and low electrochemical potential (Loganathan et al., 2019). If LIBs are operated within manufacturer-recommended limits, the failure rate is estimated to be 1 in 40 million (Doughty and Roth, 2012). However, LIBs are sensitive to mechanical abuse (e.g., crush), electric abuse (e.g., overcharge), and thermal abuse (e.g., overheating), which can cause internal short circuits and thermal runaway, leading to fire and explosion (Wang et al., 2019).

Nickel-metal hydride battery

Nickel-metal hydride (NiMH) battery consists of a positive cathode made of nickel hydroxide, a negative anode made of several metal alloys which store hydrogen atoms, and an electrolyte solution made of potassium hydroxide (BatteryPlus, 2021). NiMH cells are advantageous for high-current-drain

applications, primarily due to their lower internal resistance. Compared to Li-ion batteries, NiMH has a lower gravimetric energy density and lower expected life cycles, but the cost is also significantly lower.

Graphene battery

Graphene batteries are based on graphene in both the cathode and the anode. Graphene has an ultra-high surface area of $2630 \text{ m}^2/\text{g}$ and high electron mobility, providing high-power density, which is better than conventional LIBs (Loganathan et al., 2019; Ji et al., 2016). Pure graphene batteries are still in an early development phase, but the technology has shown to be promising.

Metal-air battery

Metal-air battery is a family of batteries with a metal anode and air cathode. Due to the high theoretical potential of this technology, metal-air batteries are under intense research for reaching commercialization. Because of their high potential, they are frequently discussed as a candidate for next-generation batteries (Li and Lu, 2017). Among metal-air batteries, the aluminum-air battery is considered to be the most promising due to its high theoretical voltage (2.7V) and high specific capacity of 2980 mAh/g (Loganathan et al., 2019), which is significantly higher than for conventional LIBs. However, the downside of using aluminum-based batteries is the high rate of self corrosion, both under open-circuit and discharge conditions. Byproducts such as Al_2O_3 and $\text{Al}(\text{OH})_3$ accumulate at the cathode and anode and prevent the battery from full recovery after recharging. Finding a proper electrolyte for preventing this is under development (Mori, 2019).

Solid-state rechargeable lithium battery

Solid-state battery systems have a solid electrolyte instead of liquid or polymer gel electrolytes. This is of great interest due to its potential for higher volumetric energy density, wider operational temperature range, and robustness to internal short circuits. Because of the many advantages of solid-state batteries, many automotive firms have invested billions of dollars in R&D on solid-state technology (Loganathan et al., 2019).

Battery summary

Table 3.3 shows a summary of the battery technology mentioned. For the metal-air battery, the values in the table are for an aluminum-air battery.

The label "*" indicates not commercialized technology, and the values in the table is based on theoretical calculations.

| Component | Li-ion | Graphene* | Metal-air* | NiMH |
|-----------------------------|---------|-----------|---------------------|-------|
| Gravimetric density [Wh/kg] | 110-190 | 225-600 | 5780 | 60-80 |
| Cell voltage (max) [V] | 3.6 | 4.3 | 2.7 | 2.25 |
| Self discharge [%/month] | 10 | - | 80 (self corrosion) | 30 |
| Mature | Yes | No | No | Yes |

Table 3.3: Summary: Battery technology

3.2.3 Battery for high-speed passenger ferries

There exist several suppliers of industrial batteries in the industry today. Li-ion batteries are the most commercially widespread in the maritime industry due to their high energy density, low discharge rate, and low demand for maintenance. Table 3.4 shows some of the batteries suitable for maritime applications.

| Component | Corvus Dolphin (E P) | AKASOL | SEANERGY (E P) | Fictional average |
|-------------------------------|----------------------|-----------|-------------------|-------------------|
| Q_{nom} [kWh] | 77*n 54*n | 98*n | 53*n 52*n | 67*n |
| $C-rate_{charge}(C/P)$ [C] | 0.4/1.0 1.6/2.0 | 0.81/1.53 | 2.0/2.0 0.5/0.5 | 1.06 / 1.4 |
| $C-rate_{discharge}(C/P)$ [C] | 0.5/1.1 2.2/4.4 | 1.0/1.53 | 4.0/4.0 2.2/2.2 | 1.98 / 2.65 |
| Nominal voltage [V] | 805 805 | 662 | 647 880 | 760 |
| Weight [kg] | 436*n 436*n | 593*n | 560*n 560*n | 517*n |
| Volume [m^3] | 0.77*n 0.78*n | 0.36*n | 0.51*n 0.51*n | 0.48*n |

Table 3.4: Battery technology overview

Here, E is energy, and P is Power. These are two versions of the same battery, one with high energy density and the other with high power density. C is short for continuous load, and P is short for peak load. The battery takes damage if loaded with the peak load over a certain time, usually 10 seconds. The "fictional average" is the average of the values of the different batteries presented. Calculations in upcoming chapters are based on the values for this battery.

Chapter 4

Theory

In this chapter, theory relevant for the optimal design problem is presented.

4.1 Hull resistance models

When a new ship is in the design phase, many parameters need to be decided to fulfill the ship's specific demands. These demands are operational demands set by the shipowner, such as service speed, passenger capacity, depth limitations, and minimum range, but also demands from the ship classification society, such as stability restrictions, emission limitations, and the robustness of the hull. Besides these limitations and specifications, the ship should be as energy effective as possible to reduce the environmental footprint and reduce operational costs. This section presents different models for calculating the power and energy of a vessel. By combining existing models, a new model also is suggested.

4.1.1 Total coefficient method

In marine engineering, the towing resistance of a new ship is based on a total coefficient approach (Amdal et al., 2015).

$$\begin{aligned} R_T &= C_T \frac{\rho_w}{2} u^2 S \\ P &= R_T u = C_T \frac{\rho_w}{2} u^3 S \\ W &= Pt \end{aligned} \tag{4.1}$$

Here R_T is the total resistance, C_T is the total resistance coefficient, ρ_w is the density of water, u is the vessel speed, S is the wet surface, P is power, t is duration, and W_T is the energy (work), due to the towing resistance.

The total resistance coefficient is, in general, divided into wave resistance (C_W), wave sloshing resistance (C_S), hull friction (C_f), air drag (C_{air}), and Appendix resistance (C_{app}). These components are calculated from model testing, empirical equations, and mathematical equations.

All resistance components are linearly dependent on the wet surface, except for air resistance, which is linearly dependent on the front area of the vessel over water. By separating C_T in C_{rest} and C_{air} , where $C_{rest} = C_T - C_{air}$, the model may account for different speeds in air and water. This is convenient for real-world applications when calculating the resistance with environmental disturbances, such as wind and currents.

$$R_T = C_{rest} \frac{\rho_w}{2} u_r^2 S + C_{AA} \frac{\rho_{air}}{2} u_{air}^2 A_{air} \quad (4.2)$$

Here, u_{air} is the air speed relative to the vessel, u_r is the vessel speed relative to the water, A_{air} is the front area of the vessel, over water, and ρ_{air} is the air density.

4.1.2 Top-down approach for energy modeling

Another model used in the industry is the top-down approach of Goldsworthy and Goldsworthy (2015). The method is based on a calculation of an average speed ($u_{1,2}$) over a distance ($X_{1,2}$) and a time ($t_{1,2}$). By knowing the maximum power (P_{max}) at maximum speed (u_{max}) and assuming a cubic propagation of energy consumption from zero to maximum speed, the model can calculate the fuel consumption at given a speed.

$$\begin{aligned} u_{1,2} &= X_{1,2}/t_{1,2} \\ LF &= P/P_{max} = (u_{1,2}/u_{max})^3 = f(u_{1,2}/u_{ss})^3 \\ W_{1,2} &= P_{max} LF t_{1,2} \\ E_{1,2} &= E_f W_{1,2} \text{ and } fuel_{1,2} = BSFC W_{1,2} \end{aligned} \quad (4.3)$$

Here, LF is a load factor, P is the actual power, u_{ss} is the service speed f is a relation factor between u_{max} and u_{ss} , E_f is the emission factor, $W_{1,2}$ is the work over the distance, $fuel_{1,2}$ is the fuel consumption over the distance, $E_{1,2}$ is the emission over the distance, and $BSFC$ is the Break Specific Fuel Consumption.

The Goldsworthy and Goldsworthy approach is based on three simplifications of a real-world scenario:

1. Assuming an average speed over a distance.
2. No wind and no current.
3. Resistance is perfectly proportional with the cube of the vessel speed.

These simplifications lower the model's fidelity, and for accurate energy modeling, the method comes short. On the other hand, the model is based on parameters available to the general public. Hence, the model is transparent and utilizable without much vessel-specific data.

4.1.3 Mathematical representation for energy modeling

In more advanced hydrodynamics, the vessel's motions are expressed mathematically by differential equations. In this section, this model will be presented briefly, without details. Marine vessels have six degrees of freedom: Translation and rotation along the x-, y-, and z-axis. For this scope of work, only translation along the x-axis is considered in the model.

$$M_{RB}\dot{u} + M_A\dot{u}_r + Du_r = \tau_{wind} + \tau_{wave} + \tau \quad (4.4)$$

Here, M_{RB} is the rigid body mass, M_A is the added mass, u is the vessel speed in surge relative to an inertial frame, u_r is the velocity relative to the water fluid, D is damping forces equal to the towing resistance, τ_{wind} and τ_{wave} are external wind and wave loads working in longitudinal direction, and τ is the propulsion loads in surge.

The propulsion loads are provided by solving this differential equation with respect to τ . The instantaneous power is given by $P(t) = \tau(t)v(t)$, which leads us to an expression for the energy.

$$P(t) = (M_{RB}\dot{u}(t) + M_A\dot{u}_r(t) + Du_r(t) - \tau_{wind} - \tau_{wave})u(t)$$

$$W = \int_{t_0}^t P(t)dt = \sum_{i=t_0}^t P_i\Delta t \quad (4.5)$$

The last line expresses the energy in continuous and discrete form.

4.1.4 New approach: Energy modeling for practical applications

The three methods mentioned for energy modeling come along with three levels of complexity. The bottom-up and mathematical modeling of the energy consumption demands detailed knowledge and a lot of ship-specific data. On the other hand, the top-down approach may provide inaccurate results due to simplifications. Hence, a combination of the three will be considered. Here, the total coefficient approach in 4.1.1 will be the base function for being modified.

Comparing the Goldsworthy and Goldsworthy (4.1) and the total coefficient approach (4.3), the cubic relation between the speed and the work appears in both equations. Comparison of the two expressions for the energy consumption ($W_{G\&G}$ and W_{t_c}) provides an expression for C_T .

$$\begin{aligned} \eta_m W_{G\&G} = W_{t_c} &= \eta_m P_{max} \left(\frac{u_{1,2}}{u_{max}} \right)^3 t_{1,2} = C_T \frac{\rho_w}{2} u^3 S t \\ &\downarrow \\ C_T &= \frac{2\eta_m P_{max}}{\rho_w S u_{max}^3} \quad u_{1,2} = u, \quad t_{1,2} = t \end{aligned} \tag{4.6}$$

η_m is the machinery efficiency. It is introduced to find the relation between engine power and hull resistance.

This transmits the transparent properties of the Goldsworthy and Goldsworthy into the total coefficient approach.

In high speed operations, the air resistance accounts for up to 7.5% of the total resistance (Amdal et al., 2015), the remaining resistance falls under R_{rest} . Hence, $R_{air} = 0.075R_T$, $R_{rest} = 0.925R_T$. From this along with the assumption of no wind or current, we get an expression for C_{air} and C_{rest} .

$$\begin{aligned} R_{air} &= \frac{1}{2} C_{air} \rho_{air} u^2 A = 0.075 \frac{1}{2} C_T \rho_w u^2 S \\ &\downarrow \\ C_{air} &= 0.0075 \frac{2\eta_m P_{max}}{\rho_{air} A u_{max}^3} \end{aligned} \tag{4.7}$$

$$\begin{aligned}
 R_{rest} &= \frac{1}{2}C_{rest}\rho_w u^2 S = 0.075\frac{1}{2}C_T\rho_w u^2 S \\
 &\quad \downarrow \\
 C_{rest} &= 0.0075\frac{2\eta_m P_{max}}{\rho_w S u_{max}^3}
 \end{aligned} \tag{4.8}$$

From the mathematical representation in 4.1.3, we introduce the contribution from the acceleration and introduce time-dependent speed to the updated energy model. In this thesis, slender catamarans are studied in calm sea. Hence, the contribution of wave loads are small and neglected in the updated model (4.9). Furthermore, the added mass term is also assumed to be small for a slender surface vessel and is therefore also ignored.

$$P_T(t) = \frac{C_{rest}}{2}\rho_w S u_r(t)^3 + \frac{C_{air}}{2}\rho_{air} A u_{air}(t)^3 + M_{RB}\dot{u}(t)u(t) \tag{4.9}$$

From an energy modeling perspective, the contribution of the acceleration of mass becomes almost zero, given the start and stop speeds are equal. The additional power demand during acceleration is canceled out during retardation. This leads to the following expression for the energy modeling,

$$W = \int_0^t P_T(t)dt = \int_0^t \frac{C_{rest}}{2}\rho_w S u_r(t)^3 + \frac{C_{air}}{2}\rho_{air} A u_{air}(t)^3 dt \tag{4.10}$$

4.1.5 Energy modeling with varying mass

From Equation 4.9, It is clear that the energy model depends on the mass of the vessel. An increase in weight leads to an increase in energy consumption, mainly due to the increase in wet surface, S . Finding the relation between the wet surface and the vessel's mass requires new assumptions if the hull shape of the vessel is not known. The first assumption is perfectly vertical hull walls at the water line. This implicates a linear relationship between an increase in mass, Δm , and an increase in draught, ΔD .

$$\Delta m = \Delta D A_w \rho_w \tag{4.11}$$

Here, A_w is the water line area. Further, the increased area of the wet surface is expressed as the circumference of the water line, O_w , times the change of in draught, ΔD .

$$S_{extra} = \Delta D O_w = \frac{\Delta m}{A_w \rho_w} O_w \quad (4.12)$$

The second assumption is that the hull geometry is based on Figure 4.1, a high speed ferry with a modern catamaran hull (Broedrene AA, 40m hull).

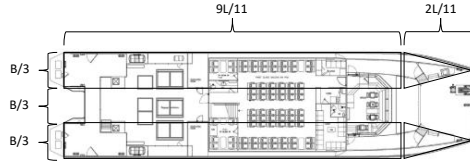


Figure 4.1: Suggestion for simplified waterline area of catamaran hull

From geometrical calculations, expressions for A_w and O_w are expressed with the vessel's length, L , and breadth, B . A minor round-off has been made for the expression of O_w to simplify the fraction.

$$\begin{aligned} A_w &= \frac{22}{33} LB \\ O_w &= \sqrt{\frac{4B^2}{9} + \frac{33L^2}{2}} \end{aligned} \quad (4.13)$$

Earlier, the wet surface of the vessel has been canceled out in the expression of C_{rest} - in the expression for the power (4.9). Because of this, the original wet surface of the vessel is not considered at all. This is an essential characteristic of the energy model in order to have it parameterized by available information of the vessel.

Now, the only known parameter is the increase of wet surface. Based on the results from Cella et al. (2021), who analyzed resistance for multihulls, the increased wave-making resistance is assumed to be small for a high-speed application of slender hull construction. The increase of resistance is then dominated by skin friction. The skin friction coefficient may be estimated by the ITTC-57 formula (International Towing Tank Conference, 1957),

$$C_f = \frac{0.075}{(\log_{10}(R_N) - 2)^2} \quad (4.14)$$

Here, R_N is the Reynolds Number. This number is dependent on the vessel's speed. In this thesis, it is calculated for the service speed,

$$R_N = \frac{u_s L}{\nu} \quad (4.15)$$

ν is the kinematic viscosity of the seawater, and the value is approximately 10^{-6} . The total expression for the updated energy model is then,

$$W = \int_0^t P_T(t) dt = \int_0^t \frac{C_{rest} S + C_{f,extra} S_{extra}}{2} \rho_w S u_r(t)^3 + \frac{C_{air}}{2} \rho_{air} A u_{air}(t)^3 dt \quad (4.16)$$

Summary: Assumptions for energy model

- Calm sea - small waves.
- R_{rest} and R_{air} is proportional with U_r^2 and U_{air}^2 , respectively.
- Constant engine efficiency.
- Added mass is assumed to be small for a slender surface vessel.
- Hull has vertical walls and is based on simple geometry.

4.2 Battery working principle and efficiency

Batteries are built on four main components: an anode, a cathode, a separator, and an electrolyte. As shown in Figure 4.2, the anode and the cathode are the components where electrons and ions are excited/emitted. When charging, electrons and ions (for example, lithium-ions) are forced towards the anode by applying a voltage higher than the difference in electrochemical potential between the anode and cathode. The opposite happens when discharging. The electrolyte is a medium transporting ions, and the separator is present to prevent shorting.

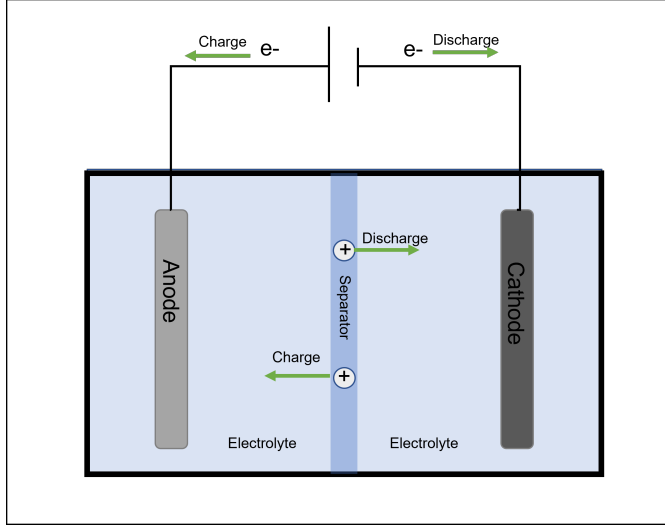


Figure 4.2: Schematic of a battery cell

4.2.1 Battery efficiency

When being charged and discharged, batteries suffer from energy loss due to two types of potential polarization, namely electrochemical polarization and ohmic polarization (Kang et al., 2014). These losses can be calculated as

$$\begin{aligned}
 E_{Loss,\Omega} &= \int_{SoC_0}^{SoC_t} \Delta V_{\Omega} C_b dSoC \\
 E_{Loss,EC} &= \int_{SoC_0}^{SoC_t} \Delta V_{EC} C_b dSoC
 \end{aligned} \tag{4.17}$$

where ΔV_{Ω} and ΔV_{EC} are ohmic and electrochemical polarization, respectively. C_b is the nominal battery capacity, and SoC is the battery state of charge (Kang et al., 2014).

The SoC of the battery is a measure of the remaining energy ($Q_{remaining}$) divided by the total capacity at fully charged (C_b), as shown in (4.18).

$$SoC = \frac{Q_{remaining}}{C_b} \tag{4.18}$$

Further, an expression of the change of SoC with respect to time can be derived from 4.18, where P_{bat} is the instant charging or discharging power

of the battery, and $\eta(P_{bat})$ is the charging or discharging efficiency of the battery.

$$\frac{dSoC}{dt} = \frac{1}{C_b} \frac{dQ_{remaining}}{dt} = \frac{P_{bat}}{\eta(P_{bat})C_b}, \quad \eta = \begin{cases} \eta_{charge} & \text{if } P_{bat} \leq 0 \\ \eta_{discharge} & \text{if } P_{bat} > 0 \end{cases} \quad (4.19)$$

Ghimire et al. (2021) suggests two expressions for the total efficiency of a Li-ion battery when being charged and discharged. The expressions are based on curve fitting from experimental results. Here, x and y represent SoC and C-rate, respectively.

$$\begin{aligned} \eta_{charge} = f(x, y) = & 98.2006 - 0.0102x - 0.8608y \\ & + 0.0140xy - 1.3007y^2 - 0.0036xy^2 + 0.3373y^3 \end{aligned} \quad (4.20)$$

$$\begin{aligned} \eta_{discharge} = f(x, y) = & 96.3034 + 0.0486x - 0.2323y \\ & - 0.0309xy - 1.1432y^2 + 0.0070xy^2 + 0.2499y^3 \end{aligned} \quad (4.21)$$

The C-rate is a measurement of the current a battery is charged or discharged with. C-rate = I/E, where I [A] is the current flowing in or out of the battery, and E [Ah] is the rated energy of the battery. A fully charged battery with rated energy of 10 Ah, being discharged at 1 C, can deliver 10 A for one hour.

Figure 4.3 shows plots of the Equation (4.20, 4.21) with SoC varying from 0-100% and C-rate varying from 0 to 3

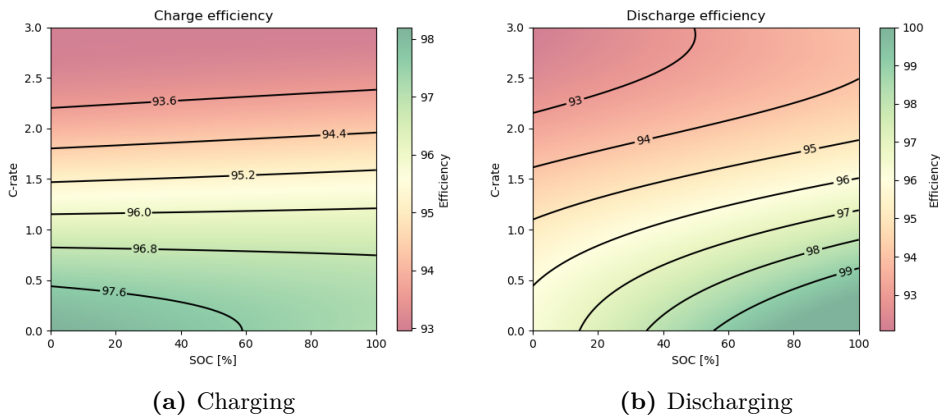


Figure 4.3: Contour plots of the efficiency of a Li-ion battery being charged and discharged

From the plots, it is clear that both charging and discharging efficiency decreases when the C-rate increases. Looking at C-rates above 1.0, the efficiency decreases when the SoC decreases.

The battery capacity and efficiency are also affected by the ambient temperature. Aris and Shabani (2017) investigated the behavior of a Li-ion battery with varying temperature conditions with respect to charging and discharging characteristics. When decreasing the temperature from 25°C , to -15°C the SoC of the battery decreased by 23%. However, in this thesis, it is assumed the batteries are operated at normal conditions, hence this effect is not taken into further considerations.

4.3 Fuel cell working principle

A fuel cell is a device turning chemical energy, from a fuel, directly into electric energy through a chemical reaction with oxygen. The most common fuels for fuel cells are hydrogen and natural gas, but other hydrocarbons may also be applied. In Figure 4.4, the basic principle of a hydrogen fuel cell is illustrated.

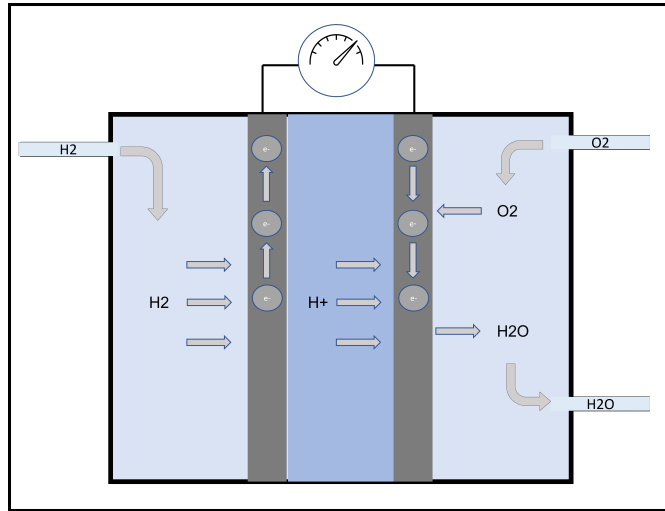


Figure 4.4: Schematic of PEM fuel cell

4.3.1 Fuel cell efficiency

The fuel cell efficiency is defined as the electrical energy produced divided by the chemical energy supplied during the process.

$$\eta_{FC} = \frac{W_{el}}{W_{H_2}} \quad (4.22)$$

The chemical energy supplied to the process is easily calculated as the hydrogen weight multiplied by the gravimetric density. The gravimetric density of a chemical is typically expressed as the lower heating value (LHV), which is the amount of heat released by combusting a quantity and returning the temperature of the products from the combustion to 150°C. Sometimes the higher heating value (HHV) is used as well. The higher heating value includes the energy released, returning the temperature of the products to the initial temperature (25°C). For hydrogen, the LHV is 119.96MJ/kg, and the HHV is 141.88MJ/kg. Using one or the other in the efficiency calculations provides two different answers. $W_{H_2} = m_{H_2}LHV$ (or $W_{H_2} = m_{H_2}HHV$).

The fuel cell efficiency varies based on the technology, as shown in Table 3.2, and the equipment supplier. Figure 4.5 shows the efficiency curve of a fuel cell provided by one of the market leaders in fuel cell technology (provided by mail exchange, the company wanted to remain anonymous). Here, the curve has been scaled up to a fuel cell with rated power of 4000kW.

Zhou et al. (2017) suggests the highest efficiency of the fuel cell takes place between 1/3 and 2/3 of rated power, with the maximum value of 0.6 . This efficiency is based on the lower heating value. Based on the higher heating value, the maximum efficiency would be $0.6LHV/HHV = 0.51$.

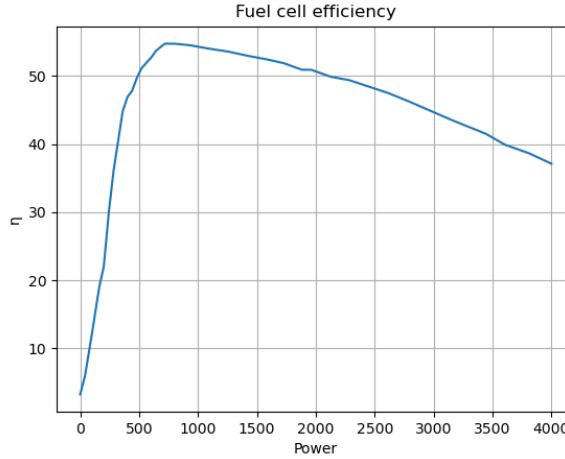


Figure 4.5: Efficiency curve for a PEMFC

Because a fuel cell is not a heat engine, its efficiency is not limited to the Carnot cycle. This leads to high theoretical efficiency of 0.80 (80%) for a low-temperature fuel cell. Nevertheless, the electrochemical kinetic theory says that this ratio is an upper limit only reached at equilibrium when the current is zero (Dell et al., 2014).

Based on the efficiency of a fuel cell, the hydrogen consumption during a period of time, t , may be expressed by rearranging (4.22) and expressing the energy as $W_{el} = P_{FC}(t)dt$, where P_{FC} is the fuel cell power output and dt is a timestep.

$$m_{H_2} = \int_0^t \frac{P_{FC}(t)}{\eta_{FC}(P_{FC}(t))LHV} dt \quad (4.23)$$

Here, $\eta_{FC}(P_{FC}(t))$ is the fuel cell efficiency at a output power $P_{FC}(t)$ at a time instance, t . Further, the fuel consumption rate is expressed as

$$\dot{m}_{H_2} = \frac{P_{FC}(t)}{\eta_{FC}(P_{FC}(t))LHV} \quad (4.24)$$

4.4 ZE-vessel system configuration

For a ZE-vessel, the electric powertrain design is of great interest. The main components of the powertrain are the battery/fuel cell, the DC-DC converters, the switchboard, the DC-AC inverters, and the motor(s). Figure 4.6 shows a simplified single-line diagram of an onboard DC-grid.

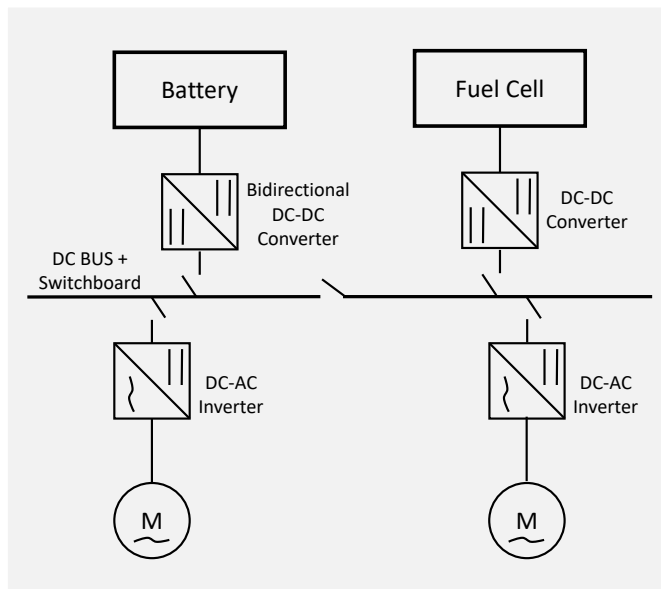


Figure 4.6: Single line diagram of a zero-emission powertrain

4.4.1 System efficiency

In Section 4.2.1 and 4.3.1, the efficiency of the battery and fuel cell was discussed. The efficiency of the remaining components of the powertrain is summarized in Table 4.1.

| Component | Efficiency | Reference |
|---------------------------------------|------------|-----------|
| DC-DC converter | 0.98 | 1 |
| DC-AC inverter | 0.98 | 1 |
| Electric motor | 0.99 | 2 |
| Battery charging | 0.97 | 3 |
| DC bus + Swichboard | 1 | - |
| Battery discharging | 0.96 | 3 |
| Fuel cell | 0.5 | 4 |
| Propulsion | 0.6 | 5 |
| Total efficiency (Battery to thrust) | 0.548 | - |
| Total efficiency (Hydrogen to thrust) | 0.286 | - |

Table 4.1: Efficiency of system components

References in Table 4.1: 1: Zekalabs (2022), 2: RAMME (2022), 3: Section 4.2.1, 4: Section 4.3.1, 5: Servogear (2017)

The battery's efficiency is obtained by evaluating the battery efficiency where SoC is higher than 0.2 and C-rates lower than 1 (see Figure 4.3). The fuel cell efficiency is obtained by assuming the fuel cell is run in its high-efficiency area (see Figure 4.5). The propulsion efficiency is obtained from Figure 2.5. The power loss of the DC bus and switchboard is assumed to be zero.

4.4.2 System weight and volume

In Chapter 5, an iterative process will be discussed, where the goal is to find the optimal structure of a ZE-vessel. The weight and volume of the system play a vital role in the energy modeling. Hence, insight into the component characteristics is essential. The weight and volume of each component are obtained by mail exchanges with market leaders, investigation of online data sheets, and literature studies. Table 4.2 shows component weights and volume for the system. The units vary over the components based on the source of information.

| Component | Weight/- | Volume/- | Reference |
|-----------------------------|---------------|-----------------|-----------|
| DC-DC converter | 30kg/200kW | $1m^3/4896kW$ | 1 |
| DC-AC inverter | 27kg/100kW | $1m^3/2448kW$ | 1 |
| Electric motor | 220kg/100kW | - | 2 |
| Liquid hydrogen (fuel) | 1kg/33kWh | $1m^3/2222kWh$ | 3 |
| Battery (per energy) | 517kg/67kWh | $0.48m^3/67kWh$ | 4 |
| Battery (per nominal power) | 517 kg/133 kW | $0.48m^3/133kW$ | 4 |
| Fuel cell | 1100kg/200kW | $1.95m^3/200kW$ | 5 |
| DC bus + Switchboard | 317kg/1600 A | $0.17m^3/1600A$ | 6 |

Table 4.2: Weight of system components

References in Table 4.2: 1: Zekalabs (2022), 2: TRANSFLUID (2022), 3: 3.1, 4:Table 3.4, 5:Ballard (2022), 6: Schneider-Electric (2010)

Chapter 5

Design: Optimal zero-emission vessel structure

Vessel- and route-specific data are usually confidential and hard to procure. This includes hull resistance, load profiles, speed profiles, and light ship weight. In this chapter, a group of methods is suggested to work around the lack of information to find an optimal design for a ZE high speed passenger ferry. The theory applied in this Chapter is based on Chapter 4. The whole process starts with raw AIS data from one year of operation of a route and ends with measures of optimal component dimensions. The methods presented in this Chapter are programmed in Python 3.9.7, found in attachments of the thesis, and the results are shown in Chapter 7.

5.1 Design overview

Relevant historical data for ferry connections provides valuable information in developing an optimized vessel. An optimal vessel, in this case, is a zero-emission vessel, as cheap as possible, and is still fulfilling the desired operational needs (passenger/car capacity, schedule, comfort, range). The process of finding this vessel is based on several sub-tasks. This includes finding the typical speed profile over the specific ferry connection, deciding the composition of machinery components, calculating the energy demand, and redesigning the structure. After redesigning the structure, the process starts over due to changes in parameters. This iterative process is shown in the flowchart in Figure 5.1.

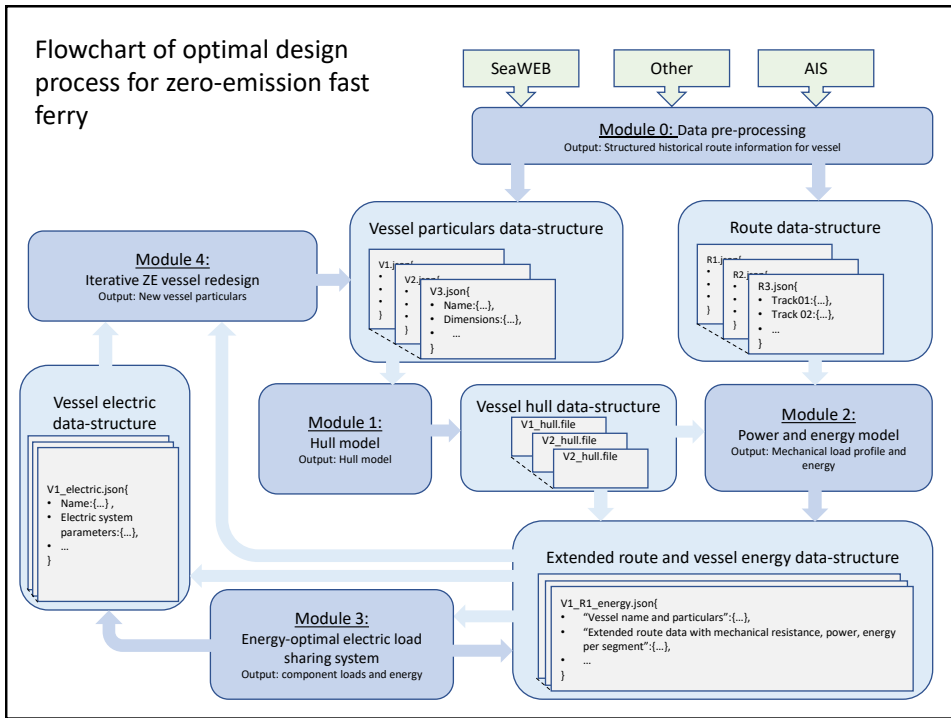


Figure 5.1: Flowchart of the optimal design process for zero-emission fast ferry

In this chapter, Module 0, Module 2, Module 3, and Module 4 will be discussed and explained, as well as the route data structure.

5.2 Module 0: Data pre-processing

As discussed in Section 2.10, AIS data contains a multitude of information. To utilize it to generate route information, latitude-longitude values, sog, cog, heading, and time stamp are of particular interest. In Module 0, raw data is processed, and structured route information is generated. The workflow is shown in Figure 5.2.

5.2.1 Pre-processing of raw AIS-data

In the pre-processing of the data, the raw data is cleaned up and prepared for further utilization. The raw data contains wild-points - such as single data points deviating from the rest of the data set. This is recognized by extreme values in position or sog. Single surveys to other destinations are

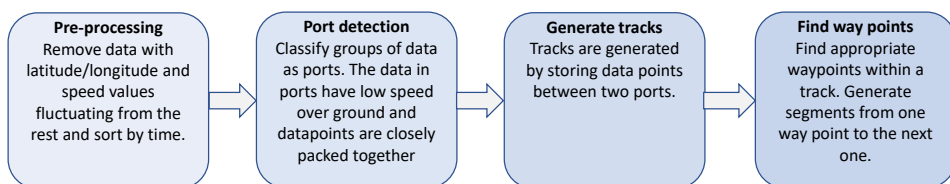


Figure 5.2: Workflow of data processing

also commonly present for an AIS data set of one year. For the scope of this work - to generate route information, single surveys are considered as noise. Both wild points and single surveys are filtered out by a clustering algorithm, respecting sog and position. In this project, the clustering algorithm used is DBSCAN (see Section 2.8.1). DBSCAN allows for clustering of multiple parameters, which provides a good tool for filtering wild-points and single routes (low density of data points). This thesis uses a DBSCAN implementation from the python library *sklearn.cluster*.

The second step of the pre-processing is sorting the data with respect to the time stamp. This is important due to the further data processing, described in 5.2.3.

5.2.2 Port detection

The AIS data contains information on navigation status. This is supposed to provide knowledge of whether the vessel is in transit, at anchor, or moored, among others. From experience, this is not sufficiently accurate for recognizing all the data points located at ports. Instead, ports are detected by evaluating other parameters in the data. First, the data with sog higher than 3 knots are filtered out. This is a rough filtering for reducing the data set to lower the runtime of upcoming processing. Secondly, clusters of the filtered data are generated. Again, this is done using the DBSCAN algorithm, with sog and position as clustering parameters. Data points are closely packed at ports, both in position and in sog. This allows for strict tuning in the distance to neighbors and minimum samples in a cluster. With the proper tuning, the DBSCAN algorithm returns one cluster for one port, regardless of which direction the vessel enters the port. All the data is then labeled with "-1" if the data point is in transit and the cluster-ID if the data point is found in a port cluster. This labeling is further referred to as the cluster-ID.

5.2.3 Track generation

A track is an instance of the whole route, from one port to another. Each track has its characteristics due to local obstacles, traffic at port, and schedule. This results in a unique speed- and load profile for the vessel for each track of the route.

The tracks are generated by evaluating the data from beginning to end. Every time the cluster-ID of the data goes from a port-ID to a transit-ID (-1) to a port-ID, all the data points within this search are stored in a python dictionary. A unique survey from one port to another is from now called a recording. The dictionary's keys are the start/stop index, and under each key, lists of all recordings from start to stop are stored. This dictionary is from now referred to as the track dictionary.

Due to the low quality of the AIS data, there are holes in the timeline with no data. This may result in both generations of tracks that do not exist and holes of data within a recording. These recordings are removed by evaluating the time step between each data point. If the time step is larger than a threshold, the whole recording of the track is removed from the track dictionary. In order to compare the time duration of each recording of a track, the first point of each recording is defined as time 0, and the UTC timestamp of the following data points is substituted with the time duration from the first point.

5.2.4 Waypoint generation

The data in each track recording is further divided into 100 groups. The mean value and the standard deviation, in each group, of the sog, cog, position, time, and heading are then calculated. This is done to compensate for varying lengths of data points in each recording. Then the mean value and standard deviation are calculated for all the recordings of a track, group by group. This results in 100 waypoints containing mean values and standard deviation. These waypoints now represent the expected state of the vessel for some propagation, from 1 to 100, over a track.

Further, the tracks are represented by straight line segments. Each segment has a starting waypoint and an ending waypoint - with mean values of sog, cog, position, heading, and time, a total length - calculated from latitude/longitude values, a duration and length - calculated from starting waypoint to the ending waypoint, and an average sog.

5.3 Route data-structure

The energy modeling problem requires comprehensive information. This includes information regarding the technical characteristics of the vessel, environmental conditions, and route information. The route information of interest is mainly the length of the connection, the speed profile over the tracks, and the time at ports. In Module 0, calculations leading to average values of the route were made. The route data structure stores these values efficiently for further utilization.

To work with all this data efficiently, the data is organized and stored in a nested JSON (JavaScript Object Notation) file, a standard data interchange format. In a nested file, objects are stored within other objects. This is shown in Listing 1.

The data structure is designed to be able to store information on different routes in the first layer. In the example structure in Listing 1, the ferry connection between Trondheim and Kristiansund is appended to the structure along with the two artificial routes, "Route01" and "Route02". In the next layer, the vessel responsible for the AIS data, the ports of the route, and the tracks of the route are stored. The ports and the tracks are further nested. "Tracks" hold the duration and length of each track - calculated by the haversine formula, along with the straight line segments. "Ports" contain information about the place-name of the port, the location, the average duration the vessel is at the port, and battery charging capacity.

```
1  {
2    "Routes":{
3      "Route01":{...},
4      "Route02":{...},
5      "Trondheim_Kristiansund":{
6        "Vessel": "MS Tyrhaug"
7        "Ports":{...},
8        "Tracks":{
9          "T_P1_P2":{...},
10         "T_P2_P3":{...},
11         "T_PX_PY":{
12           "Duration_Transit":3206,
13           "Total_length": 49395
14           "Segments":{
15             "S01":{...},
16             "S02":{...},
17             "S03":{
18               "duration":13,
19               "length":669,
20               "WayPoint_start":{...},
21               "WayPoint_stop":{
22                 "lat":63.3,
23                 "lon":10.1,
24                 "sog":29.95,
25                 "cog":343.6,
26                 "heading":341.69,
27               }
28             }
29           }
30         }
31       }
32     }
33   }
34 }
35 }
```

Listing 1: Route data-structure

5.4 Module 2: Power and energy model

Module 2 takes both the vessel hull data structure and the route data structure as inputs and returns a load profile. The first action of this module is generating a speed profile for each track with a defined resolution. In this thesis, the resolution is allocated to 1 second. From the route data structure, each track is divided into 100 linear segments. Each segment has a duration and a start/stop sog, which is interpolated to create the speed profile.

Further, the desired route to be evaluated is defined by a list of ports. From the route data structure, each port is determined to have charging capacity or not. For the ports with charging capacity, a negative load, the size of the charging capacity is appended to the load profile over the period the vessel is at the port. To avoid steps in the profile while charging, the beginning and the end of the profile are linearly increasing/decreasing before reaching the charging capacity. At transit, the load profile is calculated by the expression for the energy model suggested in Section 4.1.4. This expression takes the speed profile, vessel-specific parameters, and environmental disturbances as inputs and returns a load profile.

The resulting output of Module 2 is a load profile over a whole route with time, in seconds, on the x-axis and load, in kilowatts, on the y axis. The total energy demand over the route is calculated by integrating over the load profile as described in (4.9)

5.5 Module 3: Energy-optimal electric loadsharing system

Parts of the energy-optimal loadsharing system were explored in the pre-project study in Fjelldal (2021), and are here further developed for covering a more comprehensive problem.

Appropriate loadsharing is essential for a ZE-vessel composed of multiple energy sources. This reduces the total energy consumption and reduces wear and tear of the equipment.

For the optimal vessel design problem, the entire load profile of the route is known from Module 2. Obtaining knowledge of the whole environment facilitates a globally optimal solution by using a DP algorithm, as described in Section 2.7.1.

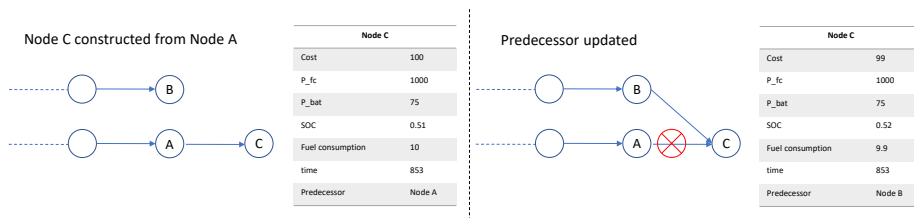


Figure 5.3: Illustration of DP algorithm finding the optimal path

The DP algorithm calculates the optimal energy flow from the fuel cell and the battery for each time step for a particular cost function. Every possible solution at every timestep is stored in a python dictionary. This is an effective structure for checking if a solution has already been added to the list of candidates or not. A candidate is a pair of fuel cell power and battery power. Each candidate has one predecessor, representing from where the candidate was constructed. The predecessor of a candidate is replaced if a path with a lower total cost leads to the same candidate. This is illustrated in Figure 5.3. The cost function to be minimized in the DP implementation of Module 3 is paying attention to the hydrogen consumption (weighting factor: α), the change of power of the fuel cell (weighting factor: γ), the deviation of the SoC from the SoC reference (weighting factor: β), and the battery charge/discharge efficiency (weighting factor Ω).

| Parameter | Description |
|-----------------------|--|
| SOC | State of charge BESS |
| α | Weighting factor for fuel cell efficiency |
| β | Weighting factor for change of SOC from reference |
| γ | Weighting factor for change of power of the fuel cell |
| Ω | Weighting factor for battery charge/discharge efficiency |
| \dot{m}_{H_2} | Fuel consumption rate |
| P_{bat} | Power battery |
| P_{FC} | Power fuel cell |
| \dot{P}_{FC} | Power rate fuel cell |
| \dot{P}_{bat} | Power rate BESS |
| Q_{bat} | BESS capacity |
| LHV_{H_2} | Lower heating value hydrogen |
| $\eta_{FC}(P_{FC})$ | Fuel cell efficiency |
| $\eta_{bat}(P_{bat})$ | Battery efficiency |
| δSOC | SOC - SOC _{ref} |
| J | Cost function |

Table 5.1: Parameters for DP implementation

Cost function:

$$J = \sum_{k=0}^N \alpha \frac{1}{\eta_{FC}(P_{FC})} + \Omega \frac{1}{\eta_{bat}(P_{bat})} + \gamma (\dot{P}_{FC})^2 + \beta (\delta SOC)^2 \quad (5.1)$$

$$\beta = \begin{cases} \text{low penalty} & \text{if } 0.3 < SoC < 0.7 \\ \text{high penalty} & \text{else} \end{cases}$$

The first two factors of the cost function in 7.2 are, for obvious reasons, penalizing running the battery and fuel cell inefficient. The following two factors try to reduce the fuel cell power rate and keep the SoC at a reference, respectively. Reducing the fuel cell power rate leads to less wear and tear on the equipment. Keeping the SoC around a reference value leads to good capacity for charging and discharging. Two beta values are introduced for penalizing SoC values close to the max/min values more. This helps the algorithm to keep the battery SoC away from the thresholds. The objective of the DP algorithm is to minimize the cost function to obtain the optimal power curves for the fuel cell and the battery throughout the route. This is mathematically formulated as:

$$J^* = \min_{\dot{m}_{H_2}, \Delta SOC, \dot{P}_{FC}} J \quad (5.2)$$

The cost function is nonlinear due to the nonlinear efficiency of the fuel cell and battery (shown in Figure 4.3 and 4.5) and the quadratic terms.

Due to the response dynamics of the fuel cell and the battery, and some obvious limitations within the structure, some constraints are taken into account as well:

$$\begin{aligned}
 & \text{low threshold} < SOC < \text{high threshold} \\
 & 0 < P_{FC} < P_{FC,max} \\
 & C - \text{rate}_{max,discharge} C_b < P_{bat} < C - \text{rate}_{max,charge} C_b \\
 & -FC_{max\ rate} < \dot{P}_{FC} < FC_{max\ rate} \\
 & -Bat_{max\ rate} < \dot{P}_{bat} < Bat_{max\ rate} \\
 & P_{bat} + P_{FC} = P_{load}
 \end{aligned} \tag{5.3}$$

The output of the DP algorithm is the optimal power curves for the battery and fuel cell.

5.6 Module 4: Iterative ZE vessel redesign

From the vessel electric data structure and the extended route and vessel energy data structure, Module 4 finds a new onboard system configuration.

5.6.1 Component dimensioning

For a vessel only running on battery, the battery should be dimensioned to have the capacity to operate the whole route, even with one malfunction on a charging station. This capacity is calculated by deactivating the charging opportunity at one port at the time and evaluating the route between the ports with charging capacity with the highest energy demand.

For a hybrid configuration of battery and fuel cell, the system should be dimensioned with more slack due to hydrogen's high gravimetric energy density. The design process should then be an interplay of weight versus volume. Batteries contribute with weight; hydrogen storage contributes with volume.

5.6.2 Iterative process

After finding new equipment dimensions, Module 4 updates the data in the "Vessel particulars data structure". This initiates an iterative process, where heavier equipment leads to an increase of resistance, by the expressions

derived in Section 4.1.4, which leads to new calculations of the optimal load sharing, before reaching Module 4 once again.

This whole process is carried out in Chapter 7.

Chapter 6

Case study

In this thesis, a case study is conducted for the high-speed passenger ferry, MS Tyrhaug. The ferry is chosen to be further examined due to the characteristics of the ferry connection it is operating. The ferry is operating between Trondheim and Kristiansund with a rapid frequency. The connection has a total length of circa 90 nautical miles, a duration of circa 3.5 hours, and the round trip is operated on an average of 3 times per day. This chapter will present the vessel's characteristics and a introduction on the vessel's compliance with zero-emission retrofitting, which will be further discussed in Chapter 7.



Figure 6.1: MS Tyrhaug; Image courtesy of: Maritimt-Magasin (2015)

6.1 Case study: MS Tyrhaug

MS Tyrhaug is a high-speed passenger ferry operating passenger voyages between Trondheim and Kristiansund. The vessel was delivered to Kystekspresen ANS, along with its sister ship - MS Terningen, by Brødrene Aa in 2014. At that time, MS Mørejarl and MS Ladejarl were operating the connection. MS Tyrhaug and MS Terningen are lightweight catamarans of carbon fiber. Compared to their aluminum predecessors, the fuel consumption was lowered by 40% (TU, 2014). The design parameters of MS Tyrhaug are listed in Table 6.1.

| MS Tyrhaug: Vessel specific data | |
|----------------------------------|--------------------------------------|
| Year of build | 2014 |
| Pax capacity | 275 |
| Name | M/S Terningen |
| Operator | Kystekspresen ANS |
| Ferry connection | Trondheim - Kristiansund |
| Materials | Carbon fibre sandwich/ vinylester |
| L/W/GRT | 40.8m/10.8m/492 GRT |
| DWT | 32 T |
| Service speed | 34 knots |
| Main engine | 2x MTU 16V2000 M72 |
| Auxiliary Engines | 2x John Deere Engine Works 4045TFM50 |
| Propulsion | ZF type 4550 / MJP 650 |
| Fuel tank capacity | 6000 l |

Table 6.1: Design parameters of MS Tyrhaug (Maritimt-Magasin, 2015; Sea-web, 2014)

6.1.1 Machinery

MS Tyrhaug is installed with 2 MTU 16V2000 M72 diesel engines, delivering 1440kW each. MTU is owned by Rolls-Royce Group and is one of the world's leaders in large marine diesel and gas engines for commercial marine vessels. Engine specific parameters are listed in Table 6.2.

| MTU 16V2000 M72 | |
|--|--------------------|
| L[mm]xW[mm]xH[mm] | 3240 x 1360 x 1460 |
| Mass, dry [kg] | 4600 |
| Rated power [kW] | 1440 |
| Speed [rpm] | 2250 |
| No. of cylinders | 16 |
| Fuel | DIN EN 590 |
| Fuel consumption [kg/h] at rated power | 299.5 |
| Engine efficiency at rated power | 0.404 |

Table 6.2: Engine specific parameters: MTU 16V200 M72 (MTU, 2020)

The engine efficiency is calculated by using the LHV of the fuel (DIN EN 590), being 11.889kWh/kg.

The engines drive the reduction gears, driving the water jets. Modern reduction gears are typical of high efficiency and low weight. Literature studies show the efficiency varies between 0.98-0.99. The total efficiency of the main engine and the reduction gear at rated power is then 0.396. The efficiency of the water jets varies over the vessel speed, the ratio between the water speed at the inlet and the outlet, and the producer of the equipment. The specific efficiency for the MJP 650 of MS Tyrhaug is hard to find, but different sources suggest modern water jet efficiency is in the range of 0.5-0.7. For the purpose of this case study of finding MS Tyrhaug's compliance to zero-emission retrofit, the same water jet applies for both the diesel configuration and a ZE configuration. Hence, it will not contribute to any conclusion.

The total weight of two engines and a full fuel tank of diesel (density: 850kg/l) is 14300kg. In Section 6.1.3, this mass will be subtracted from the total weight of the vessel when studying the weight of zero-emission configurations.

6.1.2 The ferry connection: Trondheim - Kristiansund

As mentioned above, MS Tyrhaug and MS Terningen operate the ferry connection between Trondheim and Kristiansund an average of 3 times pr day. Table 6.3 shows the timetable route. The table is a reconstruction of the 800 route of Kystekspresen, from Monday to Thursday (Kystekspresen, 2022). Some of the surveys only operate between parts of the route. These are not shown.

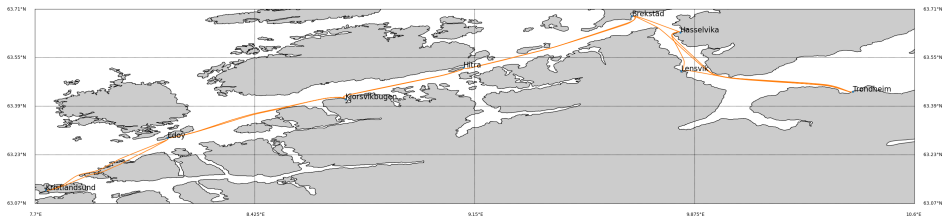


Figure 6.2: Route tracking: MS Tyrhaug (2021)

| | | | | | | | |
|---------------|-------|--------|-------|---------------|-------|-------|-------|
| Trondheim | 08:10 | 12:15 | 16:25 | Kristiansund | 08:00 | 12:00 | 16:30 |
| Lensvik | | | 16:55 | Edøy | 08:40 | 12:40 | 17:10 |
| Hasselvika | 08:55 | | 17:20 | Kjørsvikbugen | 09:20 | 13:20 | 17:50 |
| Brekstad | 09:10 | 13:10 | 17:35 | Hitra | 09:50 | 13:50 | 18:20 |
| Hitra | 09:50 | 13:50A | 18:15 | Brekstad | 10:35 | 14:30 | 19:00 |
| Kjørsvikbugen | 10:20 | 14:20 | 18:45 | Hasselvika | | 14:40 | 19:10 |
| Edøy | 11:00 | 15:00 | 19:25 | Lensvik | | 14:55 | |
| Kristiansund | 11:40 | 15:40 | 20:00 | Trondheim | 11:25 | 15:35 | 20:00 |

Table 6.3: Timetable: Trondheim - Kristiansund

In Chapter 5, a method for processing AIS data has been developed. This method is executed on AIS data for MS Tyrhaug from 2021, and route information is obtained. The data is provided by the Norwegian Coastal Administration. The route information obtained from this data includes information on ports, all single tracks, speed profiles, and other information. The results from this process will be further examined in Chapter 7. Figure 6.2 shows the route of MS Tyrhaug, based on an average of surveys over a year.

From Figure 6.2, it is clear that the vessel either goes directly from Trondheim to Brekstad, Trondheim to Hasselvika, or through all the ports. This coincides with the information in the timetable.

6.1.3 Retrofit of MS Tyrhaug

Several shipowners have retrofitted their vessels to low- or zero-emission configurations during the last years. In this section, a brief discussion of retrofitting MS Tyrhaug will occur.

Capacity: Diesel configuration

From the fuel tank to the actual thrust of MS Tyrhaug, the efficiency, at rated power, is 0.198 (assuming the efficiency of the water jet is 0.5). At the rated power of the two main engines delivering 1440kW each, the vessel travels at 34 knots. This means the towing resistance of MS Tyrhaug, at 34 knots, equals $2 \times 1440 \times 0.198 = 540$ kW. Table 6.2 shows the fuel consumption of each engine at rated power is 299.5 kg/h. Hence, on a full fuel tank, of 6000 l, the vessel can run for a little less than 10 hours and travel 340 nautical miles (629 km), at service speed. This equals approximately 3.5 times the sailing distance from Trondheim to Kristiansund (through all ports of the route).

Corresponding capacity: ZE configuration

In Section 4.4, technical specifications of zero-emission concepts were presented. Table 4.1 shows that the efficiency from the battery to thrust power is 0.548, and from the LHV of hydrogen to the thrust power, the efficiency is 0.286. The diesel configuration of MS Tyrhaug has a total capacity of 5400 kWh. This measure the sailing capacity at rated power/service speed and is calculated from the towing resistance times the operational hours of a full fuel tank. For a pure battery configuration, the battery capacity required for delivering the same capacity is $5400 \text{ kWh} / 0.548 = 9854$ kWh. To match the power capacity of the diesel-mechanic configuration, the electric motor should have a capacity of 2880 kW. Hence, the battery should have a discharge C-rate of at least 0.1 C to provide the needed power. This is a low C-rate, and the battery used for further calculations has a nominal discharge C-rate of 1.98 C. This is based on the fictional average battery in Table 3.4. For a pure fuel cell solution, the fuel cell capacity required for delivering the same capacity is $5400 \text{ kWh} / 0.286 = 18881$ kWh.

System weights and volume

Assuming the only weight of the fuel tank and the engine is replaced by a pure battery configuration or a pure fuel cell configuration, the differences in weight are summarized in Table 6.4. The mass of the equipment is based on Table 4.2 and Table 6.2.

| Component\Configuration | Diesel machinery | Battery | Fuel cell |
|-----------------------------------|------------------|-----------|-----------|
| Engine (+ Fuel cell) | 9200 kg | 6300kg | 22500kg |
| Fuel/battery | 5100kg | 76000kg | 570kg |
| Auxilliary equipment | - | 2800kg | 2800kg |
| Total weight | 14300kg | 85100kg | 25870kg |
| Percentage of DWT [%] | 15.9 | 238 | 52 |
| Difference (Diesel-Configuration) | - | -70800 kg | -11570kg |

Table 6.4: Weight of system configurations

Both the fuel cell configuration and the battery configuration come out heavier than the diesel-mechanic configuration. The increase in weight also leads to an increase in towing resistance, leading to heavier equipment, etc. This will be further explored in Chapter 7. The increased weight of the battery exceeds MS Tyrhaug's DWT by 238%. The fuel cell configuration represents only 52% of the DWT. These calculations are based on the total weight of the system configuration relative to the DWT of MS Tyrhaug, where the weight of the diesel engine is subtracted from the weight of the ZE configurations.

As mentioned above, the diesel-mechanic configuration of MS Tyrhaug has a capacity of 3.5 times the distance from Trondheim to Kristiansund. Assuming a battery configuration where the battery may be fully charged in either Trondheim or Kristiansund, the battery capacity may be decreased 3.5 times. The total weight of the battery configuration is then 30800 kg, and the difference is 21600 kg compared to the diesel-mechanic design (mass of diesel machinery is subtracted). This is 68% of the DWT of MS Tyrhaug. Sundvor et al. (2021) suggests an upper limit of the battery weight to be 80% of DWT for retrofit of old vessels. Both the fuel cell configuration and the battery configuration, with shrunken capacity, are below this limit. This simplistic analysis leaves out essential aspects of the dimensioning problem. In Chapter 7, a more extensive analysis of this design problem will be presented. This analysis will consider malfunctions of charging stations and an iterative process where the weight of the vessel increases, resistance increases, equipment weight increases, etc.

Results

The following results are based on the theory from Chapter 4, the methods from Chapter 5, and the case vessel from Chapter 6. The results will follow the modules of Figure 5.2, from the evaluation of the AIS data to complete load profiles, optimal load sharing, and optimal design of the case vessel. The AIS data used in this thesis is data for MS Tyrhaug from 2021 and is directly obtained from the Norwegian Coastal Administration.

The results concerning positional data are plotted with the Basemap library in python to visualize the data better. Complete codes are attached to the thesis.

7.1 Module 0: Data processing

7.1.1 Pre-processing

Data evaluation

The AIS data contains data points fluctuating from the rest of the data set, especially in position and sog. Figure 7.1 and Figure 7.2, show AIS data for MS Tyrhaug. Here, orange dots represent wild points in position, and blue dots represent data points within the ferry connection. The wild points are obtained by a rough clustering process, where extreme latitude and longitude values are filtered out.

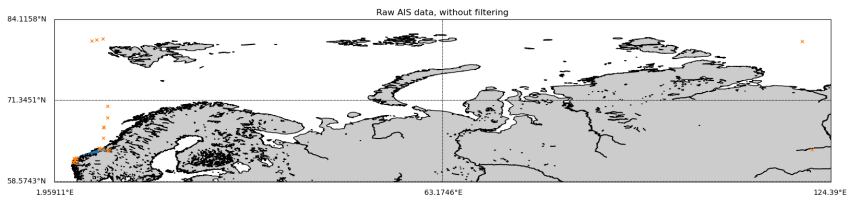


Figure 7.1: Raw data with wild points

Some of the wild points are most likely measurement errors, such as the one data point in the mainland of Russia and the one in the East Siberian Sea (East/right), shown in Figure 7.1. Other data considered as noise are more likely single trips for maintenance/service purposes. One example of this is shown in Figure 7.2, which is a track of orange data towards Florø (West/left).

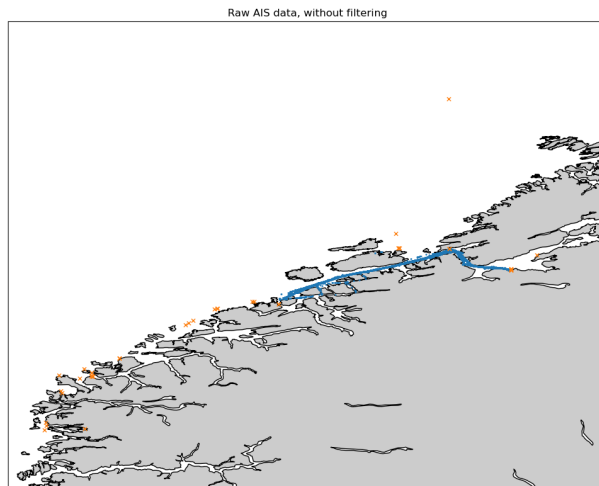


Figure 7.2: Raw data with wild points zoomed in

AIS transponders are programmed to send data every 2 to 10 seconds in transit and every 3 minutes while anchored (from Section 2.10). Figure 7.3,

shows that this is not certain in the real data.

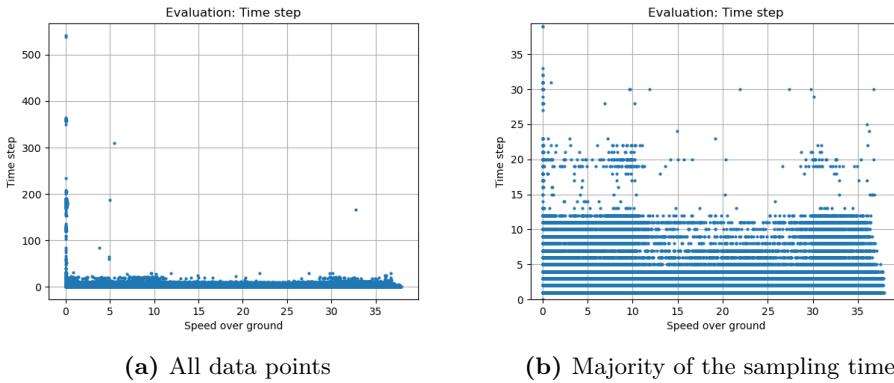


Figure 7.3: Data evaluation: Sampling time vs. sog

Figure 7.3 shows the time step versus the sog. Figure a) shows the highest sampling time to be over 500 s, at 0 kts, and several data points with sampling time at circa 350 s. This contradicts the settings of the AIS transponder and is evaluated as time gaps. Figure b) shows that most data have a sampling time lower than 10 s. It also becomes clear that most data appears around service speed or at a slower speed than 10 kts.

7.1.2 Port detection

Figure 7.4 shows all the data points after the filtering of wild points. The colored dots over the route are the result of a clustering process, identifying the ports. The ports were successfully detected by only considering data with sog lower than 5kts, then clustering the data concerning position and speed.

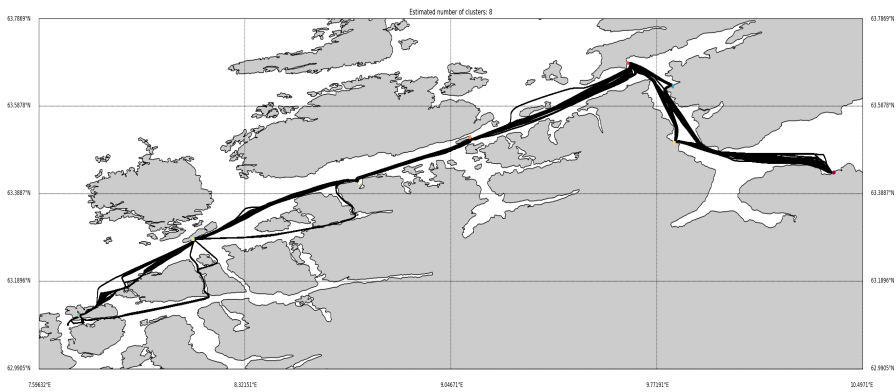


Figure 7.4: Result from clustering process of ports

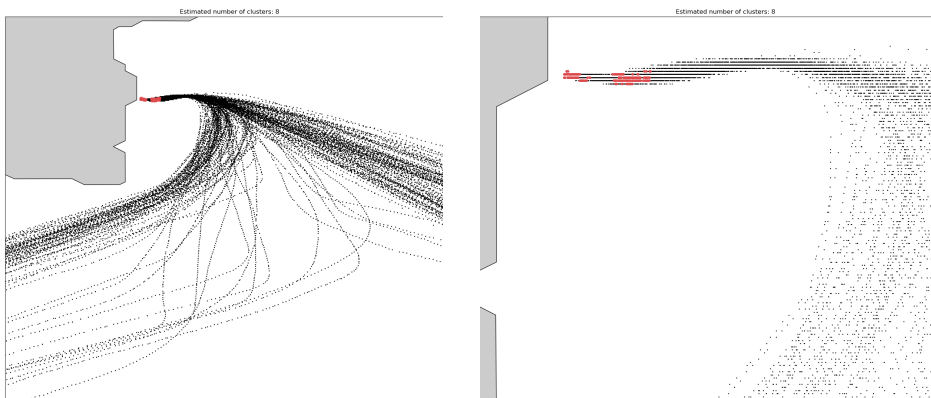


Figure 7.5: Data points in a port cluster

In Figure 7.5, it can be seen that the clustering algorithm has gathered data in the same cluster with a space between some of the data points within. This can be explained by different approach speeds as the vessel enters the port or different ports as the vessel approaches the port from one direction or the other.

7.1.3 Track detection

Figure 7.6 - 7.14 shows each track recording of the route and the corresponding speed profiles for each recording.

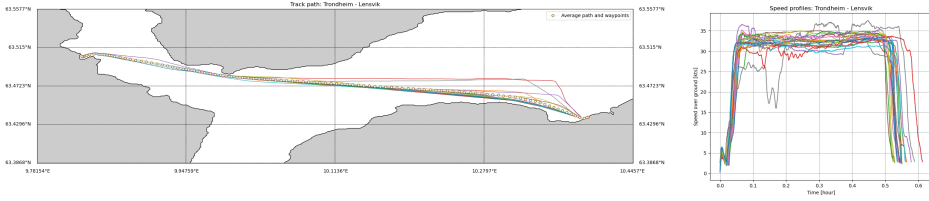


Figure 7.6: Trondheim - Lensvik: Track path and speed profile

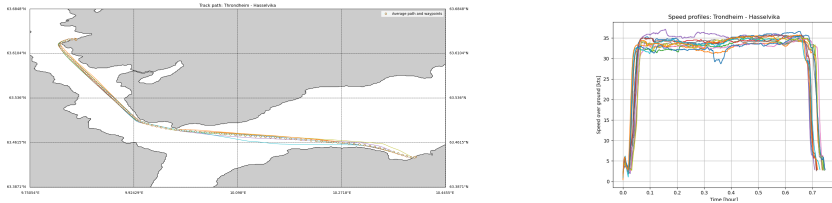


Figure 7.7: Trondheim - Hasselvika: Track path and speed profile

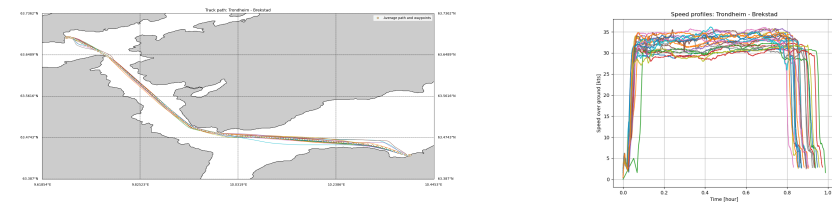


Figure 7.8: Trondheim - Brekstad: Track path and speed profile

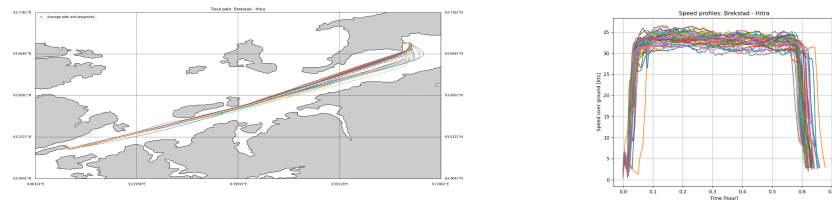
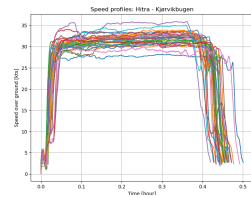
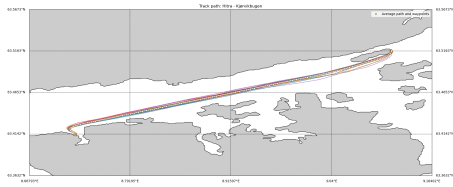


Figure 7.9: Brekstad - Hitra: Track path and speed profile



(a) Majority of the sampling time

Figure 7.10: Hitra - Kjørvikbugen: Track path and speed profile

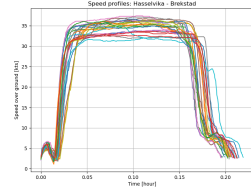
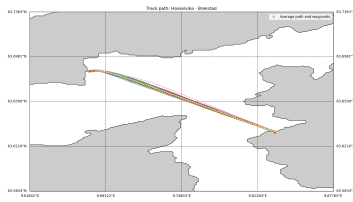


Figure 7.11: Hasselvika - Brekstad: Track path and speed profile

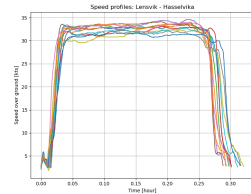
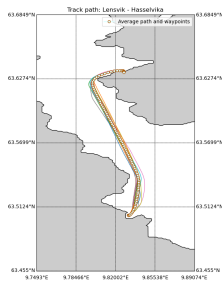


Figure 7.12: Lensvik - Hasselvika: Track path and speed profile

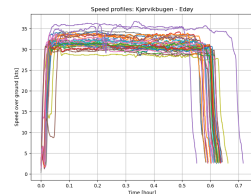
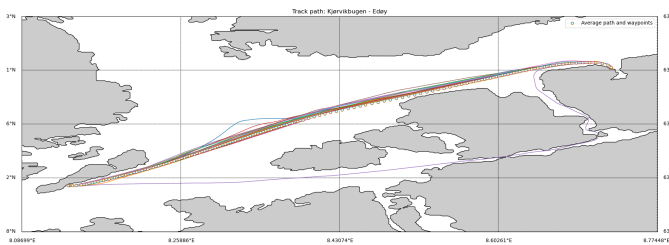


Figure 7.13: Kjørvikbugen - Edøy: Track path and speed profile

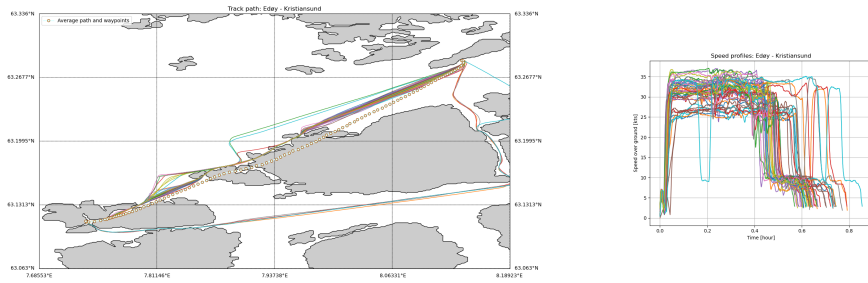


Figure 7.14: Edøy - Kristiansund: Track path and speed profile

From the speed profiles, it comes clear that the duration of each recording varies over the different surveys. Figure 7.14 shows that the fastest survey of the route from Edøy to Kristiansund took circa 0.55 hours (33 min), and the slowest took circa 0.9 hours (54 min). This difference in duration makes sense when studying the different paths of the track. Most likely due to harsh sea conditions, MS Tyrhaug sails inshore sometimes. From the plot of the average path from Edøy to Kristiansund, in Figure 7.14, it comes clear that this path can not be used for path guidance purposes. The path runs over the mainland due to the average calculation of some offshore surveys and some inshore surveys.

The main scope of the data processing is to find the average speed profile to use for energy modeling. Figure 7.15 shows the average speed profile over the track from Edøy to Kristiansund in thick blue line (to the right). Here all the speed profiles are normalized to the average profile. The average duration is circa 0.66 hours (40 min)

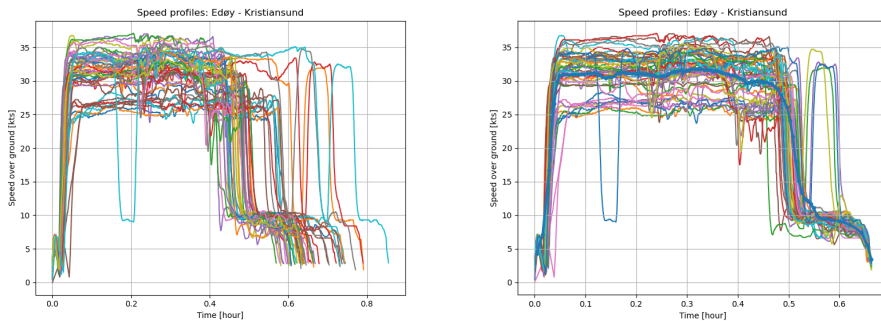


Figure 7.15: Edøy - Kristiansund: Average speed profile

7.1.4 Route data-structure

The average values from the route recordings are stored in the route data structure. The route data structure comes as an attachment to this thesis, named `Route_data_structure.json`. Figure 7.16 and Figure 7.17 show the speed profile from Trondheim to Kristiansund and all the route tracks, respectively. These figures are directly plotted from `Route_data_structure.json`.

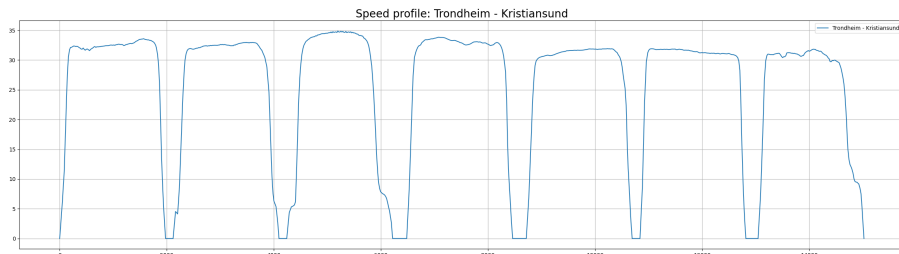


Figure 7.16: Speed profile: Trondheim - Kristiansund

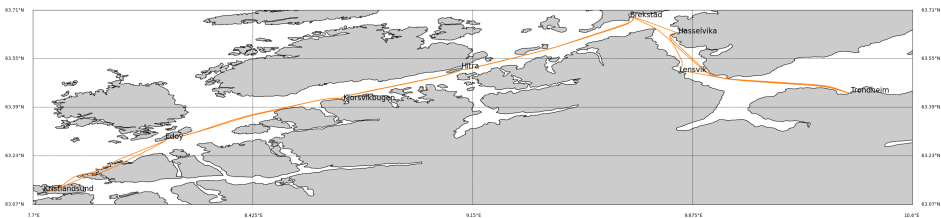


Figure 7.17: Route tracking: MS Tyrhaug

7.1.5 AIS data versus timetable

Figure 7.18 and 7.19 compares the average route generated from the AIS data with the timetable of Kystverket (from 6.3).



Figure 7.18: AIS vs Timetable: Trondheim - Kristiansund

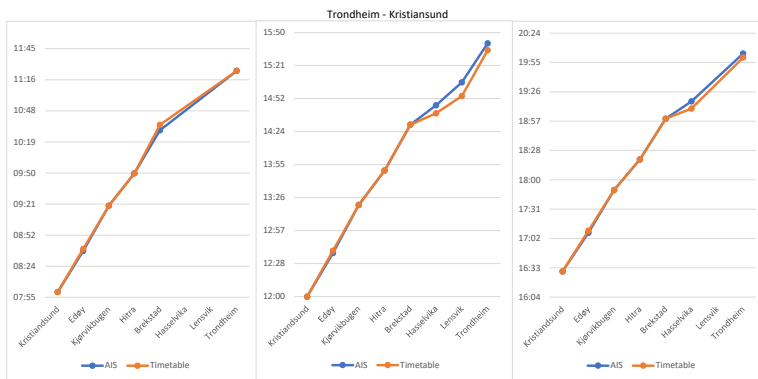


Figure 7.19: AIS vs Timetable: Kristiansund - Trondheim

The generated schedule from the AIS data and the timetable coincides nicely. This is a good verification of how good the performance of the average route generation is.

7.1.6 Summary of route characteristics

| Track | Distance [m] | Duration [min] | Average speed [m/s] |
|------------------------|--------------|----------------|---------------------|
| Trondheim -Lensvik | 29659 | 32.8 | 15.08 |
| Trondheim - Hasselvika | 41905 | 43.3 | 16.13 |
| Trondheim - Brekstad | 49395 | 53.4 | 15.41 |
| Lensvik -Hasselvika | 15703.00 | 18.3 | 14.34 |
| Hasselvika -Brekstad | 9970.00 | 12.5 | 13.26 |
| Brekstad - Hitra | 35108.00 | 37.8 | 15.48 |
| Hitra - Kjørvikbugen | 23714.00 | 27.2 | 14.55 |
| Kjørvikbugen - Edøy | 33520.00 | 37.2 | 15.02 |
| Edøy - Kristiansund | 28471.00 | 40 | 11.96 |

Table 7.1: Summary: Track information

| Average time at port | |
|----------------------|----|
| Trondheim | 53 |
| Lensvik | 2 |
| Hasselvika | 2 |
| Brekstad | 5 |
| Hitra | 4 |
| Kjørvikbugen | 2 |
| Edøy | 4 |
| Kristiansund | 30 |

Table 7.2: Summary: Port information

7.2 Module 2: Energy modeling

7.2.1 Energy modeling

In Section 4.1, four different energy models were presented. Figure 7.20 shows engine power- and energy curve of the Goldsworthy and Goldsworthy approach from 4.1.2, the Total coefficient approach from 4.1.1, and the New approach from 4.1.4. Elements of the last model, the mathematical representation, is included in the new approach. The methods are carried out on a speed profile from Edøy to Kristiansund.

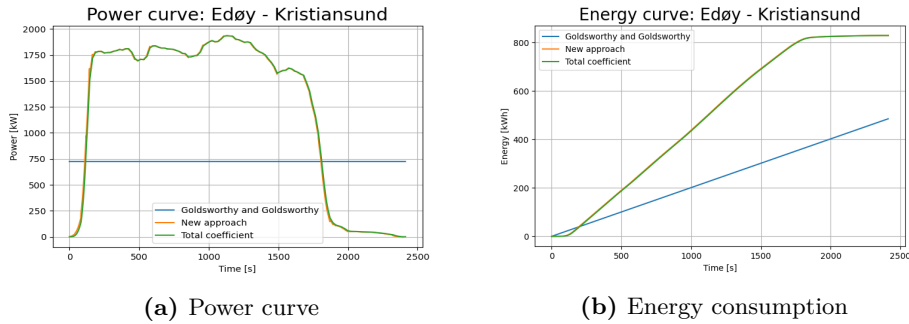


Figure 7.20: Energy modeling: Edøy - Kristiansund

From (a), it is clear that the calculation from the Goldsworthy and Goldsworthy method results in a constant power over the distance, while the Total coefficient and the New approach method vary with speed over ground. The calculation of the energy consumption of the Goldsworthy and Goldsworthy approach results in a total of 60% of the two other approaches. This is as expected due to the cubic terms in the energy calculations, where the average speed assumption of Goldsworthy and Goldsworthy results in lower speed, and lower energy consumption. The difference in the expressions of the New approach and the Total coefficient is due to the contribution from the acceleration of the mass. The mass of MS Tyrhaug is put to 80 tonne in this simulation. This is an estimate based on the LSW of similar vessels. In (a), the New approach models more power during acceleration and less during deceleration. This contribution is low due to low accelerations. From (b), it can be seen that this contribution cancels out in the energy consumption calculations. For the power modeling, the New approach is assumed to be the most precise and the preferred model in further analyses.

Figure 7.20 shows the power and energy of the diesel engine of MS Tyrhaug with constant mass. Figure 7.21 shows the load in (a) and the resulting energy consumption, in (b), of a fuel cell configuration, a battery configuration, a diesel engine, and the hull towing resistance. The energy is a measure of hydrogen energy, diesel energy, battery energy, and work on the ship due to towing resistance. Figure 7.22 shows the hull resistance and resulting energy consumption of different DWT load conditions.

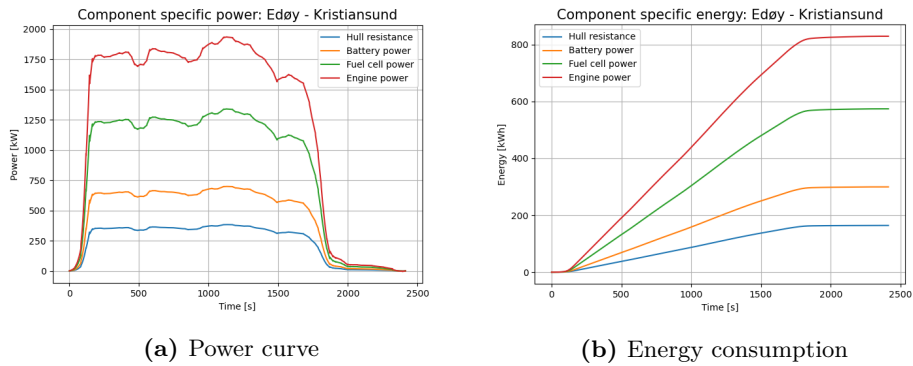


Figure 7.21: Component loads: Edøy - Kristiansund

The curves in Figure 7.21 are based on constant component efficiency from Table 4.1 and 6.2.

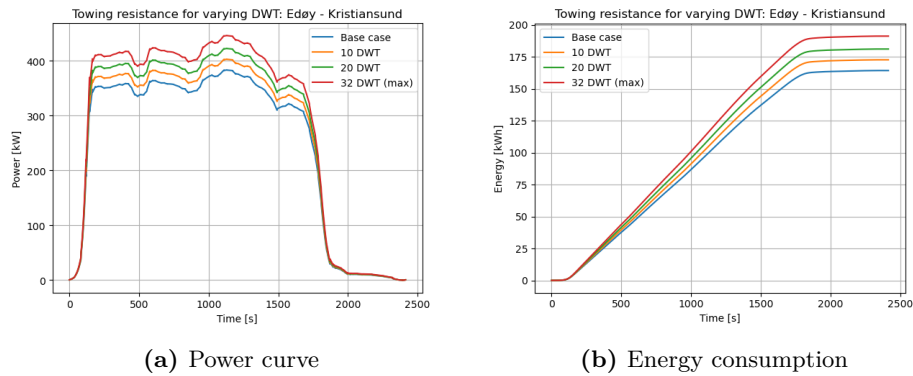


Figure 7.22: Energy modeling with varying mass: Edøy - Kristiansund

Figure 7.22 shows the increase of resistance with the increase in weight of the vessel. Due to towing resistance, the work increases from 165 kWh in the base case to 190 kWh at the maximum weight (32 DWT). This enlightens the issue of increased weight in relation to retrofitting, which will be further discussed in Section 7.4.1.

7.2.2 Total load profile

Figure 7.23 shows the component-specific load profile over the route from Trondheim to Kristiansund, including the system weight of pure configura-

tions of each component. The diesel configuration DWT is put to 5400 kg (full tank of diesel), the battery and fuel cell configuration DWT is set to 31000 kg and 21000 kg (from Section 6.1.3), respectively, and the towing resistance is modeled with 0 DWT.

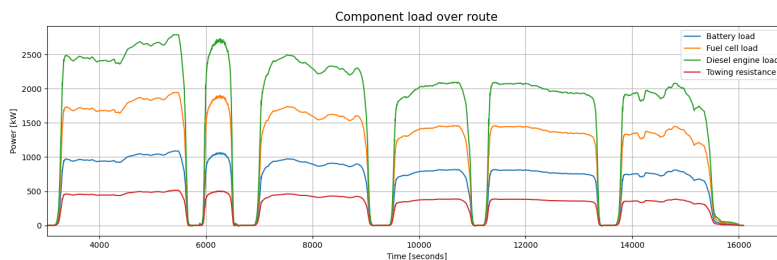


Figure 7.23: Total load profile of components: Trondheim - Kristiansund

7.3 Module 3: Energy-optimal electric load sharing system

A DP algorithm is implemented for the optimal load sharing problem, as explained in Section 5.5. A verification of the optimal solution of the algorithm is found in Appendix B

The DP algorithm finds the optimal load sharing between a fuel cell and a battery. From Figure 7.23, it can be seen a pure fuel cell configuration is run on an average of circa 1300kW (with stops). We want to run the fuel cell in its high-efficiency region to keep the hydrogen consumption low. From Figure 4.5, this is found to be between 12.5% and 50% of rated power. To keep the weight as low as possible, the fuel cell in the hybrid configuration has a rated power of 2600kW, weighing 14300kg. In order to serve the same maximum power as the diesel machinery of MS Tyrhaug, the battery nominal discharge power is put to 200kW. To simplify the problem, it is assumed the charging and discharging C-rate is both 2C; thus, the nominal charging power is 200kW, nominal energy is 100kWh, and the weight of the battery is 777kg. The weight of the hydrogen is relatively low and not taken into account in the modeling of the load profile.

To make the simulations more interesting, charging capacity is added to some ports. This is easily defined in the Route data structure.

7.3.1 Parameters for the dynamic programming algorithm

The parameters are defined based on battery information in Table 3.4 and the dimensioning from above.

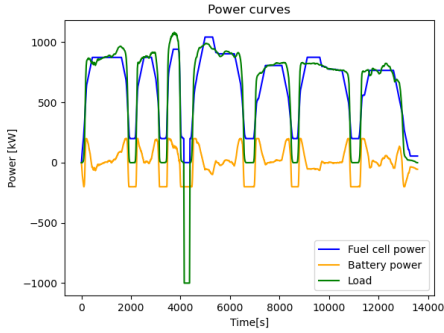
$$\begin{aligned}
 0.2 &< SOC < 0.8 \\
 0 &< P_{FC} < 2600 \\
 -200 &< P_{bat} < 200 \\
 -20 &< \dot{P}_{FC} < 20 \\
 -200 &< \dot{P}_{bat} < 200 \\
 P_{bat} + P_{FC} &= P_{load} \\
 SOC_{ref} &= 0.5
 \end{aligned} \tag{7.1}$$

The cost function to be minimized is (recap for the sake of the reader):

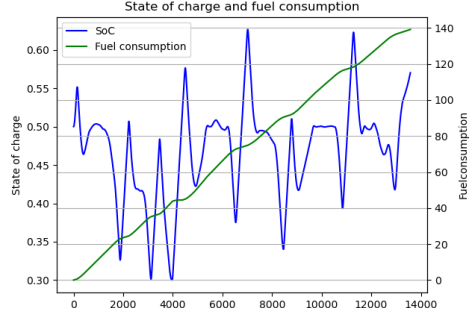
$$\begin{aligned}
 J &= \sum_{k=0}^N \alpha \frac{1}{\eta_{FC}(P_{FC})} + \Omega \frac{1}{\eta_{bat}(P_{bat})} + \gamma (\dot{P}_{FC})^2 + \beta (\delta SOC)^2 \\
 \beta &= \begin{cases} \text{low penalty} & \text{if } 0.3 < SoC < 0.7 \\ \text{high penalty} & \text{else} \end{cases}
 \end{aligned} \tag{7.2}$$

7.3.2 Load sharing: Trondheim - Kristiansund (all ports)

Figure 7.24 shows the result of the DP algorithm on the route from Trondheim to Kristiansund, concerning all parameters. $\alpha = 110$, $\Omega = 110$, $\beta_{low} = 180$, $\beta_{high} = 300$, and $\gamma = 1$ (fuel consumption, battery efficiency, stabilization of fuel cell, and SoC around 50%). The port of Brekstad has been allocated charging capacity. This is shown as a negative power in Figure 7.24 (a). The DP algorithm knows the whole load profile in beforehand. This is an important property of a global optimal solution. From Figure 7.24 (a), it can be seen the fuel cell starts to lower its values before the load starts to decrease. This is due to low throttle response of the fuel cell, and knowing the battery will be charged in the future. This is only possible when the algorithm "knows" the future.



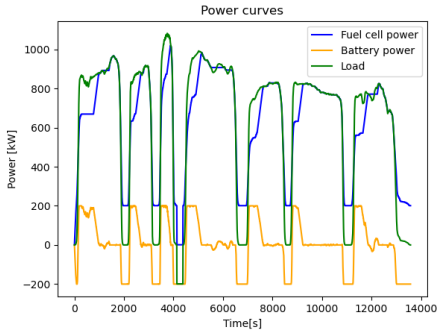
(a) Power curves



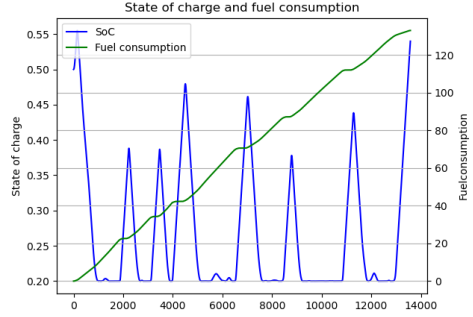
(b) Fuel consumption [kg] and SoC propagation

Figure 7.24: Optimal loadsharing concerning all parameters

Figure 7.25 shows the result of the DP algorithm for the same distance as in Figure 7.24, only concerning the fuel consumption ($\alpha = 1$, others = 0).



(a) Power curves



(b) Fuel consumption [kg] and SoC propagation

Figure 7.25: Optimal loadsharing concerning all parameters: Trondheim - Kristiansund

The two simulations show the fuel consumption was lowered by 10 kg of hydrogen when only the fuel consumption was the objective to optimize (Figure 7.25 (b)). In this simulation, the SoC of the battery was most of the time at 0.2 (20%), which is the lower limit. In a hybrid-electric propulsion system, the battery is supposed to be able to take on a sudden increase in load. This is not possible if the battery is run empty.

7.3.3 Load sharing: Trondheim - Kristiansund (round trip)

Figure 7.26 shows the result of the DP algorithm on a round trip of Trondheim - Kristiansund, concerning all parameters as in 7.3.2. Here, charging capacity is added to the port of Brekstad and Kristiansund.

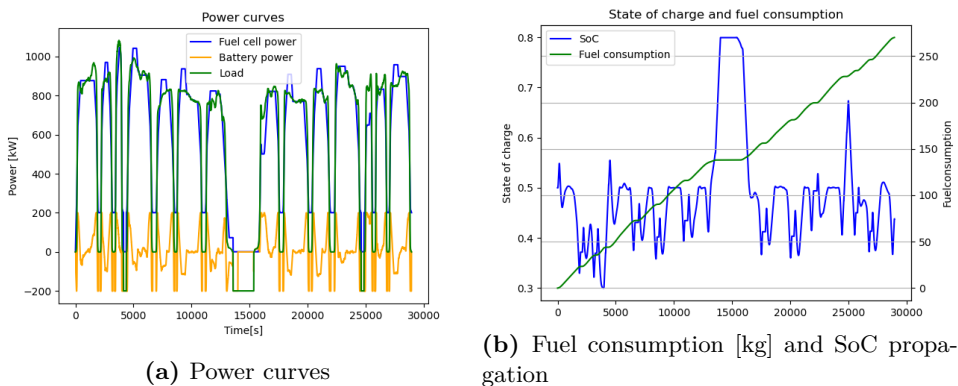


Figure 7.26: Optimal loadsharing concerning all parameters

Figure 7.27 shows the result of the DP algorithm for the same distance, only concerning the fuel consumption ($\alpha = 1$, others = 0)

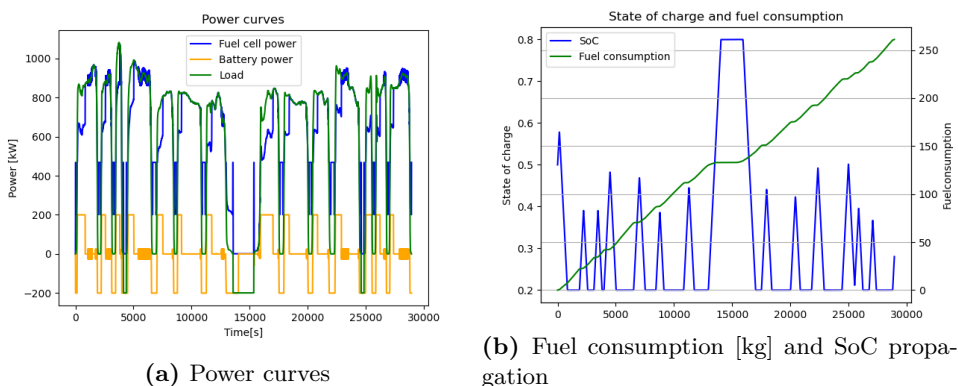


Figure 7.27: Optimal loadsharing concerning all fuel consumption

The two simulations over the round trip from Trondheim to Kristiansund show the same results as for the simulation from Trondheim to Kristiansund in Figure 7.24 and 7.25. The fuel consumption was lowered by ca. 10kg,

and the SoC of the battery was most of the time at the lower limit. At some time steps, the power curves are yo-yoing. This causes more wear and tear on the equipment and is not preferable.

7.3.4 Load sharing: Trondheim - Hitra (with wind)

Figure 7.28 shows the result of the DP algorithm on a survey from Trondheim to Hitra, concerning all parameters as in 7.3.2, with a fluctuating winds component (simple random walk with standard deviation = 2 and mean = 0). Here, it is clear to see the battery power varies with the wind loads, while the fuel cell power remain smooth.

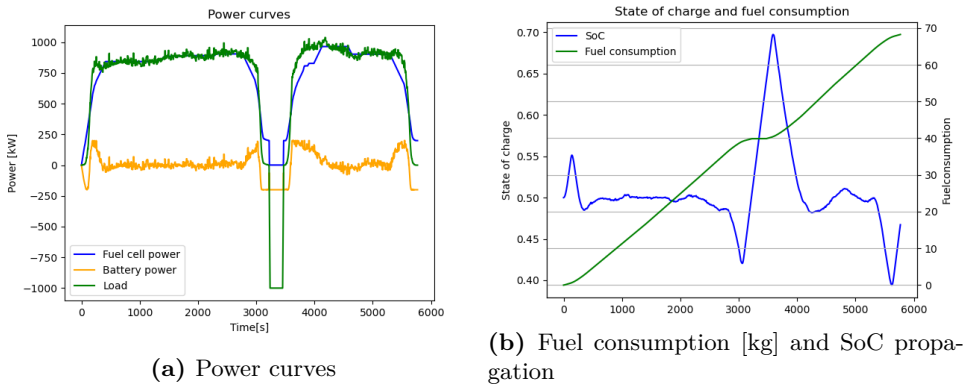


Figure 7.28: Optimal loadsharing concerning all parameters, with fluctuating wind component

7.4 Module 4: Iterative ZE vessel design

This section provides results of the dimensioning of system components. The battery weight is directly related to an increase in deadweight. The case study in Chapter 6 shows the weight of the diesel engine of MS Tyrhaug, and the electric motor and auxiliary equipment (Table 6.4) only differs by 100kg. The difference in component weight for the fuel cell is added to the estimates, which comes clear in the results.

7.4.1 System dimensioning

In Section 5.6.1, the battery's capacity was suggested to be defined by the energy demand over the whole route, with only one port with charging capacity. Figure 7.29 shows the energy, weight, and volume demand for a pure

fuel cell and a pure battery configuration over a round trip for Trondheim - Kristiansund.

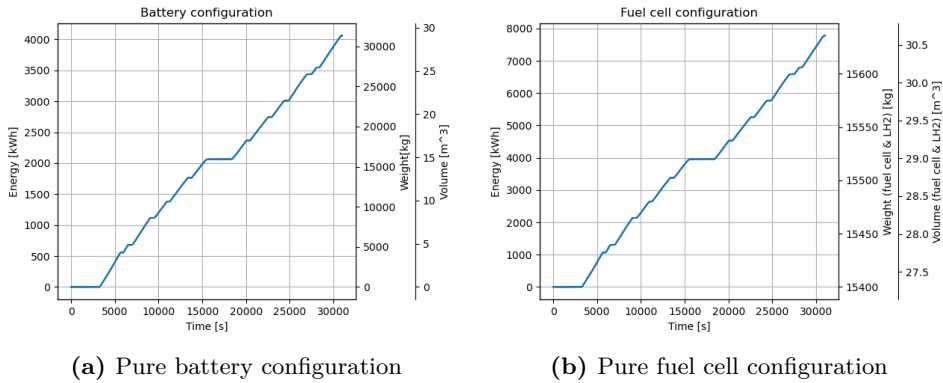


Figure 7.29: Energy, weight, and volume of battery and fuel cell configuration: Trondheim - Kristiansund - Trondheim

The weight and volume axis of the fuel cell configuration starts at 15400kg and $27.3m^3$, respectively, due to the difference in weight and volume of the fuel cell configuration and the diesel configuration.

The total energy demand for the round trip of the battery configuration is approximately half of the fuel cell configuration. The efficiency of the two configurations explains this. It can be seen that both the weight and the volume of the battery increase much faster than for the fuel cell configuration. When the vessel arrives at Kristiansund (15000 s - circa 18000 s), the weight of the two configurations is approximately the same, and the volume of the battery configuration is circa half of the volume of the fuel cell configuration. When the vessel has returned to Trondheim, the battery volume has matched up with the fuel cell volume, and the weight of the battery has doubled in value.

This weight of the battery is approximately the same as the maximum DTW (32 T) of MS Tyrhaug. This is before taking the new weight of the vessel in regards to the energy modeling. This concludes that the battery is too heavy for operating the whole route without charging on the way.

7.4.2 System dimensioning by the iterative approach

By introducing charging capacity at both end-ports (Trondheim and Kristiansund), the battery's capacity may be significantly lower. Figure 7.30

shows the iterative process of finding the capacity and dimensions, considering that an increase in weight leads to an increase in resistance, leading to an increase in weight, etc.

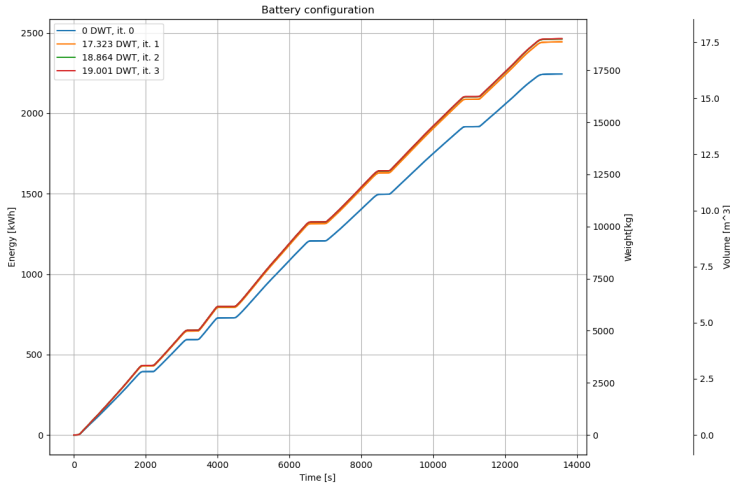


Figure 7.30: The iterative process of finding the total weight, volume, and capacity of a battery

The Figure shows a converging iterative process of 4 iterations. The battery should have a total capacity of at least 2460 kWh with a weight and volume of 19,000 kg and 17.65 m³, respectively, to serve the route from Trondheim to Kristiansund. The steps of the iterations are shown in Table 7.3.

| Iteration no. | Nominal capacity [kWh] | Weight [kg] | Volume [m ³] | Converging error [%] |
|---------------|------------------------|-------------|--------------------------|----------------------|
| 1 | 2245 | 17,323 | 16.1 | - |
| 2 | 2444 | 18864 | 17.51 | 8.75 |
| 3 | 2462 | 19001 | 17.64 | 0.7 |
| 4 | 2464 | 19013 | 17.65 | 0.05 |

Table 7.3: Steps of iteration for finding battery capacity, weight, and volume

Discussion

8.1 AIS data

In this thesis, data have been gathered from two sources for the same case vessel, MS Tyrhaug. The first data investigated was from a local database at The Department of Marine Technology (data for 2018). The second data was directly shared by The Norwegian Coastal Administration (data for 2021). For comparison, the AIS data for MS Terningen, from January to December (2018), contains circa 4,700 data points and circa 6,700,000 data points for the same period of time in the second data set (2021).

The first data set, from 2018, suffered from low data quality with significant time gaps, inconsistent sampling time, and a lot of wild points. This data was studied for a couple of months, and several data mining approaches were explored to provide route information without success. The second data set, from 2021, had few issues with data quality. The methods developed during the work with the first data set provided good results when applying it to the second data set.

8.2 Generation of route-specific data

The results show that the generation of route data from raw AIS data was successfully carried out. Each port was detected by the DSCAN cluster algorithm from the python library "sklearn.cluster". This algorithm was very memory-demanding. Therefore, filtering out data with a higher speed

over ground than a threshold was necessary to avoid memory error for big data applications.

The tracks were generated by iterating from one port to another through the time series. Detecting all, or almost all, data points at the ports revealed its importance when the route generation was carried out. If the clustering algorithm did not detect port data points when the vessel visited a port, a new track was generated without realizing the vessel had visited a port. This was the main issue with the first data set explored (2018 AIS data). The inconsistent sampling time led to the generation of tracks running back and forth of the route several times.

The main target of processing the AIS data was to generate the average speed profile over the route. This was accomplished by separating each track recording in the same amount of waypoints and finding the average value, waypoint by waypoint. The resulting average track path on the other hand showed itself to be of little use when the path from Edøy to Kristiansund went over the mainland.

The method developed for generating route information was programmed in a general way, such that route information for other vessels and routes easily can be obtained. The processing algorithm takes a CSV file of AIS data and returns a route data structure in a JSON file. This provides a valuable tool for gathering route information for more ferry connections and case vessels. However, for large data sets, the program is quite time-demanding. The code compiles in circa one hour for one year of data (6,700,000 data points).

8.3 Energy modeling

A new, transparent model has been suggested for the energy modeling over the route. This model referred to as the "New approach", is a combination of three models found in the literature. The new model can take care of currents, wind, and change of mass in the calculation of the diesel engine power. The key assumptions made in the development of this approach are a cubic relation between speed and energy consumption, vertical hull walls, and a simplified geometric shape of the catamaran hull. The hull resistance was found by assuming a total efficiency of the diesel machinery of 0.198. Further, the energy demand for a pure battery configuration and a pure fuel cell configuration is found by assuming constant system efficiencies of 0.548 and 0.286, respectively.

The results from the energy modeling show the total consumption of energy

is lowest for a battery configuration, a bit higher for the fuel cell configuration, and the highest for the diesel engine configuration. The energy model was also carried out for 4 different weights. The result reveals that the energy consumption increased by 15% when the vessel was loaded to maximum DTW (32 T). This may be an underestimate because resistance components, other than the skin friction, was neglected for increased weight of the vessel.

8.4 Optimal loadsharing

The dynamic programming algorithm for the load sharing problem shows how the tuning of weighting factors affects the total hydrogen consumption, the state of charge of the battery and how much fluctuations the fuel cell power curve has. From the verification in Appendix B it is reasonable to believe the algorithm finds the global optimal solution based on the tuning parameters of the algorithm. However, with that being said, it is hard to prove optimality for sure due to large time series and varying load sharing conditions.

For each time step of the load profile, the power from the fuel cell and the battery can take 400 values (200 values in battery discharge + 200 values in battery charge). This makes the algorithm memory demanding, and the running time is high.

The optimal load sharing solution is the most precise modeling of the energy modeling in this thesis. Here, a defined ZE system configuration with all its constraints and efficiencies is considered. The fuel consumption of the fuel cell and the battery state of charge was calculated for each step, which provides as realistic operational conditions as possible for an optimal survey.

The optimal load sharing may provide a good tool for the guidance of the load sharing in an online EMS. This will provide the EMS knowledge of what will happen in the future, and better load sharing may take place.

8.5 Optimal design problem

The results of the dimensioning problem show how a battery configuration is the most appropriate for shorter surveys, while a fuel cell configuration is better for longer surveys. The limit is shown to be somewhere between 150 nm (distance from Trondheim to Kristiansund) and 290 nm (length of a round trip from Trondheim to Kristiansund)

In the iterative approach in 7.4.1, the method for dimensioning the batteries only considers the energy required for serving the route from Trondheim to Kristiansund. The electric motor used in the case study has a rated power of 2880kW. The battery proposed in the iterative approach would need a discharge C-rate of 1.17 C to run the motor at rated power. This is well below the discharge C-rate of the fictional average battery in Table 3.4. Considering the average time at port, from Table 7.2, the charging C-rate of the battery must be 2 C. This is twice the fictional average battery. With that being said, a charging C-rate of 2 C is not unrealistic, so the results appear feasible.

An in-depth study of the dimensioning of a fuel cell configuration is not conducted due to the high gravimetric density of hydrogen. The weight of the fuel cell stack and the auxiliary equipment dominates the weight of the configuration. Hence, the iteration over increased energy demand is considered redundant.

Conclusion and Further Work

9.1 Conclusion

In this thesis, the field of zero-emission maritime technology has been explored, and an extensive method for finding an optimal design of a zero-emission fast ferry has been carried out. The superior target has been to find an approach for using available information to generate unavailable information in relation to the design process of an optimal zero-emission fast ferry.

For zero-emission operations of shorter fast ferry surveys, batteries and hydrogen fuel cells have shown themselves as the most promising energy sources, both with respect to price estimates and the maturity of technology. Different established and uprisings of technology for both fuel cells and batteries have been discussed, with the conclusion that PEM fuel cells and Li-ion batteries are the most applicable for fast ferry applications.

An energy model has been suggested, inspired by three different energy models found in the literature. The new model is only dependent on available information and can take care of current, wind, and change of vessel mass. This model is based on some assumptions considered reasonable for marine applications.

During this work, AIS data has been verified to be mature for generating valuable route information. In addition, a method for generating route characteristics has been developed. This method provides a good tool for analyzing AIS data.

A case study was conducted for MS Terningen, operating the ferry connection between Trondheim and Kristiansund. The vessel characteristics and AIS data from 2021 sat the ground for evaluating the methods developed in this thesis. The results show that fuel cells are the most suitable for longer ferry connections, while batteries are better for shorter ferry connections. The ferry connection of Trondheim - Kristiansund is somewhere in between these distances, dependent on the charging capacity along the route. After an iterative design process, assuming there is charging capacity in both end ports of the route, the battery configuration will have an increased weight of circa 19000 kg relative to than the diesel configuration. A pure fuel cell configuration will have a total weight of circa 15700 kilos more than the diesel configuration. The weight of both configurations is well below the maximum DWT. Hence, zero-emission operation of the ferry connection between Trondheim and Kristiansund is considered appropriate.

A dynamic programming algorithm was implemented to solve a hybrid-electric configuration's optimal load sharing problem. The results show the power curves, fuel consumption, and the state of charge propagation over the route. Different algorithm tuning parameters showed that circa 10 kg of H₂ was saved on a survey from Trondheim and Kristiansund when only lowering the fuel consumption was the objective. Furthermore, with this tuning, the battery was most of the time at the low threshold. This illustrates the importance of tuning the DP algorithm.

9.2 Recommendations for further work

This thesis has provided some background for further work. Several suggestions have been stated throughout the project. Here, a summary is presented:

- Gather historical weather data for the same period as for the AIS data and find the correlation between speed profiles and weather data.
- Examine the infrastructure along the route to obtain realistic charging opportunities. This provides more realistic load profiles along the route, resulting in a more optimal vessel design.
- Use the method developed in this thesis to study more ferry connections and case vessels. This provides a background for drawing conclusions about the characteristics of routes and vessels suitable for zero-emission operation.

-
- Implement an ML algorithm to predict the load profile based on historical operations and weather forecasts.
 - Implement an online EMS system using the optimal solution from the dynamic programming as guidance

Bibliography

- Agency-IEA, I.E., 2019. The future of hydrogen. *SPE Journal* , 37.
- Amdal, J., Endal, A., Fuglerud, G., Hultgreen, L.R., Steen, S., 2015. TMR4105 - MARIN TEKNIKK GRUNNLAG.
- Andersson, K., Salazar, C.M., 2015. Methanol as a marine fuel report
URL: <https://www.methanol.org/wp-content/uploads/2018/03/FCBI-Methanol-Marine-Fuel-Report-Final-English.pdf>. [Online; accessed 14-December-2021].
- Aris, A.M., Shabani, B., 2017. An experimental study of a lithium ion cell operation at low temperature conditions. *Energy Procedia* 110, 128–135. URL: <https://www.sciencedirect.com/science/article/pii/S1876610217301479>, doi:<https://doi.org/10.1016/j.egypro.2017.03.117>. 1st International Conference on Energy and Power, ICEP2016, 14-16 December 2016, RMIT University, Melbourne, Australia.
- Bahtić, F., 2021a. Maersk’s boxships to feature world’s largest methanol dual-fuel engines. <https://www.offshore-energy.biz/new-maersks-boxships-to-feature-worlds-largest-methanol-dual-fuel-engines/>.
- Bahtić, F., 2021b. Mol to order ammonia-fueled engine for ships. URL: <https://www.offshore-energy.biz/mol-to-order-ammonia-fueled-engine-for-ships/>. [Online; accessed 14-December-2021].
- Ballard, 2022. Fcwave. [Personal communication; Mail exchange 9-May-2022].

-
- BatteryPlus, 2021. Differences between nimh and li-ion rechargeable batteries. URL: <https://www.batteriesplus.com/blog/power/rechargeable-battery-types>. [Online; accessed 25-May-2022].
- Bomberger, N., Rhodes, B., Seibert, M., Waxman, A., 2006. Associative learning of vessel motion patterns for maritime situation awareness, pp. 1–8. doi:10.1109/ICIF.2006.301661.
- Brodrene-Aa, 2019. Aero - the future of fast ferries. URL: <https://www.braa.no/news/aero-design-revealed?fbclid=IwAR3MMmE5sII6Z6BxKihVZtI00eFZ5mYGL-eDsDlkrn9WDzNLpHItnhhwhck>. [Online; accessed 15-december-2021].
- Cella, U., Salvadore, F., Ponzini, R., 2021. Vpp coupling high-fidelity analyses and analytical formulations for multihulls sails and appendages optimization. *Journal of Marine Science and Engineering* 9. doi:10.3390/jmse9060607.
- Chen, Z., Mi, C., Xu, J., Gong, X., You, C., 2014. Energy management for a power-split plug-in hybrid electric vehicle based on dynamic programming and neural networks. *Vehicular Technology, IEEE Transactions on* 63, 1567–1580. doi:10.1109/TVT.2013.2287102.
- ColorLine, . Worlds largest plug-in hybrid ship. URL: <https://www.colorline.no/om-oss/om-color-line/hybrid-skip>.
- Corvus, 2021. Ms medstraum - the world's first zero emission fast ferry. URL: <https://corvusenergy.com/projects/medstraum/>. [Online; accessed 15-december-2021].
- Dell, R.M., Moseley, P.T., Rand, D.A., 2014. Chapter 8 - hydrogen, fuel cells and fuel cell vehicles, in: Dell, R.M., Moseley, P.T., Rand, D.A. (Eds.), *Towards Sustainable Road Transport*. Academic Press, Boston, pp. 260–295. URL: <https://www.sciencedirect.com/science/article/pii/B9780124046160000086>, doi:<https://doi.org/10.1016/B978-0-12-404616-0.00008-6>.
- Demetriou, D., Michailides, C., Papanastasiou, G., Onoufriou, T., 2021. Coastal zone significant wave height prediction by supervised machine learning classification algorithms. *Ocean Engineering* 221, 108592. URL: <https://www.sciencedirect.com/science/article/pii/S0029801821000275>, doi:<https://doi.org/10.1016/j.oceaneng.2021.108592>.
-

-
- Deng, W., Xu, J., Zhao, H., 2019. An improved ant colony optimization algorithm based on hybrid strategies for scheduling problem. *IEEE Access* 7, 20281–20292. doi:10.1109/ACCESS.2019.2897580.
- DNV, . Eexi – energy efficiency existing ship index. URL: <https://www.dnv.com/maritime/insights/topics/eexi/index.html>. [Online; accessed 14-December-2021].
- Doughty, D.H., Roth, E.P., 2012. A general discussion of li ion battery safety. *Electrochemical Society Interface* URL: <https://doi.org/10.1149/2.f03122if>, doi:10.1149/2.f03122if.
- Ellis, J., Ramne, B., Falk, T., et al., 2014 URL: <http://www.dendanskemaritimefond.dk/wp-content/uploads/2016/02/Final-report-SPIRETH-Energy-Transport-20140228.pdf>. [Online; accessed 14-December-2021].
- Energy.gov, . Hydrogen storage. <https://www.energy.gov/eere/fuelcells/hydrogen-storage>. [Online; accessed 04-December-2021].
- Enova, . Raskere fra idè til marked. URL: <https://www.enova.no/pilot-e/>. [Online; accessed 14-December-2021].
- Enova, 2018. 22 statlige millioner til batterifartøy som skal operere i oslofjorden <https://presse.enova.no/news/22-statlige-millioner-til-batterifartoy-som-skal-operere-i-oslofjorden-332859>. [Online; accessed 15-December-2021].
- EU-Commission, . Innovation fund. URL: https://ec.europa.eu/clima/eu-action/funding-climate-action/innovation-fund_en. [Online; accessed 14-December-2021].
- Fjelldal, S., 2021. A pre study on energy modeling and energy optimization for low- and zero-emission high speed passenger ferries .
- FuelCellsWorks, 2021. Green hydrogen in on track to be cheaper than natural gas by 2050: Bnef. <https://fuelcellworks.com/news/green-hydrogen-is-on-track-to-be-cheaper-than-natural-gas-by-2050-bnef/>.
- Fumo, D., 2017. Types of machine learning algorithms you should know. URL: <https://towardsdatascience.com/types-of-machine-learning-algorithms-you-should-know>. [Online; accessed 14-december-2021].
-

-
- Ghimire, P., Zadeh, M., Pedersen, E., Thorstensen, J., 2021. Dynamic efficiency modeling of a marine dc hybrid power system, in: 2021 IEEE Applied Power Electronics Conference and Exposition (APEC), pp. 855–862. doi:10.1109/APEC42165.2021.9487343.
- Goldsworthy, L., Goldsworthy, B., 2015. Modelling of ship engine exhaust emissions in ports and extensive coastal waters based on terrestrial ais data – an australian case study. *Environmental Modelling Software* 63, 45–60. URL: <https://www.sciencedirect.com/science/article/pii/S136481521400262X>, doi:<https://doi.org/10.1016/j.envsoft.2014.09.009>.
- Graziano, M.D., Renga, A., Moccia, A., 2019. Integration of automatic identification system (ais) data and single-channel synthetic aperture radar (sar) images by sar-based ship velocity estimation for maritime situational awareness. *Remote Sensing* 11. URL: <https://www.mdpi.com/2072-4292/11/19/2196>, doi:10.3390/rs11192196.
- Grudin, N., 1998. Reactive power optimization using successive quadratic programming method. *IEEE Transactions on Power Systems* 13, 1219–1225. doi:10.1109/59.736232.
- Han, X., Armenakis, C., Jadidi, M., 2021. Modeling vessel behaviours by clustering ais data using optimized dbscan. *Sustainability* 13, 8162. doi:10.3390/su13158162.
- Heyman-Yachts, 2018. Hull supported vessels. URL: <https://heymanyachts.com/>. [Online; accessed 19-January-2022].
- Hu, W., Xiao, X., Fu, Z., Xie, D., Tan, T., Maybank, S., 2006. A system for learning statistical motion patterns. *IEEE Transactions on Pattern Analysis and Machine Intelligence* 28, 1450–1464. doi:10.1109/TPAMI.2006.176.
- Hydrogen24, 2022. Ballard lanserer verdens første typegodkjente marine brenselcellemodul. URL: <https://hydrogen24.no/2022/04/06/>.
- IEA, 2020. Renewables 2020 - analysis and forecast to 2025. *SPE Journal*, 32.
- IMO, . Initial imo ghg strategy. URL: <https://www.imo.org/en/MediaCentre/HotTopics/Pages/Reducing-greenhouse-gas-emissions-from-ships.aspx>. [Online; accessed 14-December-2021].

-
- IMO, 2015. Revised guidelines for the onboard operational use of shipborne automatic identification systems (ais) URL: [https://wwwcdn.imo.org/localresources/en/OurWork/Safety/Documents/AIS/Resolution%20A.1106\(29\).pdf](https://wwwcdn.imo.org/localresources/en/OurWork/Safety/Documents/AIS/Resolution%20A.1106(29).pdf). [Online; accessed 21-March-2022].
- Ji, L., Meduri, P., Agubra, V., Xiao, X., Alcoutlabi, M., 2016. Graphene-based nanocomposites for energy storage. *Advanced Energy Materials* 6, 1502159. doi:10.1002/aenm.201502159.
- Johannessen, T.M., 2016. Sikkerhetsfokus fra systemintegrator ved overgang til ny teknologi URL: <https://www.sdir.no/globalassets/sjofartsdirektoratet/fartoy-og-sjofolk---dokumenter/ulykker-og-sikkerhet/sjosikkerhetskonferansen>. [Online; accessed 14-December-2021].
- Kang, J., Yan, F., Zhang, P., Du, C., 2014. Comparison of comprehensive properties of ni-mh (nickel-metal hydride) and li-ion (lithium-ion) batteries in terms of energy efficiency. *Energy* 70, 618–625. URL: <https://www.sciencedirect.com/science/article/pii/S0360544214004514>, doi:<https://doi.org/10.1016/j.energy.2014.04.038>.
- Kantor, I., Robineau, J.L., Bütün, H., Maréchal, F., 2020. A mixed-integer linear programming formulation for optimizing multi-scale material and energy integration. *Frontiers in Energy Research* 8, 49. URL: <https://www.frontiersin.org/article/10.3389/fenrg.2020.00049>, doi:10.3389/fenrg.2020.00049.
- Karim, G.A., 1987. *The Dual Fuel Engine*. Springer US, Boston, MA. pp. 83–104. URL: https://doi.org/10.1007/978-1-4757-9348-2_3, doi:10.1007/978-1-4757-9348-2_3. [Online; accessed 30-November-2021].
- Kleven Godø, J.M., Vinje Kramer, J., 2019. Batteridrift på alle hurtigbåtruter i Trøndelag. Trondheim Fylkeskommune.
- Kystekspresen, 2022. Timetable: route 800-805. URL: <https://atb.no/trondheimsområdet/>.
- Kystverket, 2022. Access to ais data. URL: <https://www.kystverket.no/en/navigation-and-monitoring/ais/access-to-ais-data/>. [Online; accessed 21-March-2022].
-

-
- Lane, R., Copsey, K., 2012. Track anomaly detection with rhythm of life and bulk activity modeling, pp. 24–31.
- Li, Y., Lu, J., 2017. Metal–air batteries: Will they be the future electrochemical energy storage device of choice? *ACS Energy Letters* 2, 1370–1377. URL: <https://doi.org/10.1021/acsenergylett.7b00119>, doi:10.1021/acsenergylett.7b00119, arXiv:<https://doi.org/10.1021/acsenergylett.7b00119>.
- Lin, H., Cui, J., Bai, X., 2021. Feature extraction of marine water pollution based on data mining. *Symmetry* 13, 355. doi:10.3390/sym13020355.
- Lindstrand, N., . Unlocking ammonia’s potential for shipping. URL: <https://www.man-es.com/discover/two-stroke-ammonia-engine>. [Online; accessed 5-December-2021].
- Loganathan, M.K., Ming Tan, C., Mishra, B., Msagati, T.A.M., Snyman, L.W., 2019. Review and selection of advanced battery technologies for post 2020 era electric vehicles, in: 2019 IEEE Transportation Electrification Conference (ITEC-India), pp. 1–5. doi:10.1109/ITEC-India48457.2019.ITECINDIA2019-254.
- Mace, A., 2019. Fuel cell applications for marine vessels [Online; accessed 6-december-2021].
- Marine-Clean-Tech, . Zeff - zero emission fast ferry. URL: <https://maritimecleantech.no/project/zeff-zero-emission-fast-ferry/>. [Online; accessed 14-December-2021].
- Maritimt-Magasin, 2015. Tyrhaug (01/2015). URL: <https://maritimt.com/nb/batomtaler/tyrhaug-012015>. [Online; accessed 20-May-2022].
- Marta, M., Ireneusz, C., 2021. K-means clustering for sat-ais data analysis doi:<https://doi.org/10.1007/s13437-021-00241-3>.
- Mascaro, S., Nicholso, A.E., Korb, K.B., 2014. Anomaly detection in vessel tracks using bayesian networks. *International Journal of Approximate Reasoning* 55, 84–98. URL: <https://www.sciencedirect.com/science/article/pii/S0888613X13000728>, doi:<https://doi.org/10.1016/j.ijar.2013.03.012>. applications of Bayesian Networks.
- Mitsubishi, 2021. Press release: Mitsubishi power commences development of world’s first ammonia-fired 40mw class gas turbine system. URL: <https://power.mhi.com/news/20210301.html>. [Online; accessed 14-December-2021].
-

-
- Mori, R., 2019. All solid state rechargeable aluminum–air battery with deep eutectic solvent based electrolyte and suppression of byproducts formation. *RSC Adv.* 9, 22220–22226. URL: <http://dx.doi.org/10.1039/C9RA04567H>, doi:10.1039/C9RA04567H.
- MTU, 2020. Diesel engines 12v/16v 2000 m72. [Online; accessed 22-May-2022].
- Pallotta, G., Vespe, M., Bryan, K., 2013. Vessel pattern knowledge discovery from ais data: A framework for anomaly detection and route prediction. *Entropy* 15, 2218–2245. URL: <https://www.mdpi.com/1099-4300/15/6/2218>, doi:10.3390/e15062218.
- Puchalski, S., 2015. All-electric car ferry URL: <https://corvusenergy.com/all-electric-car-ferry/>. [Online; accessed 15-December-2021].
- R. Praveen, Jain, E.F.B., Adil, R., 2022. Unsupervised clustering of marine vessel trajectories in historical ais database .
- RAMME, 2022. Pure efficiency with ramme electric machines. URL: <https://www.ramme.de/en/bannerleiste/industry-solutions/shipping>. [Online; accessed 19-May-2022].
- Rhodes, B.J., Bomberger, N.A., Seibert, M., Waxman, A.M., 2005. Maritime situation monitoring and awareness using learning mechanisms. *MILCOM 2005 - 2005 IEEE Military Communications Conference* , 646–652 Vol. 1.
- Rong, H., Teixeira, A., Guedes Soares, C., 2020. Data mining approach to shipping route characterization and anomaly detection based on ais data. *Ocean Engineering* 198, 106936. URL: <https://www.sciencedirect.com/science/article/pii/S0029801820300202>, doi:<https://doi.org/10.1016/j.oceaneng.2020.106936>.
- Schneider-Electric, 2010. Estimated switchboard shipping weights. URL: <https://www.se.com/us/en/download/document/2742DB0201/>. [Online; accessed 23-May-2022].
- Scordia, J., Desbois-Renaudin, M., Trigui, R., Jeanneret, B., Badin, F., Plasse, C., 2005. Global optimisation of energy management laws in hybrid vehicles using dynamic programming. *International journal of vehicle design* 39, 349–367.

-
- Sea-web, 2014. Tyrhaug. URL: <https://maritime.ihs.com/Ships/Details/Index/9693850>. [Online; accessed 21-May-2022].
- Servogear, 2017. Propulsion efficiency - beyond belief URL: <http://resources.servogear.no/controllable-pitch-propeller-concept-brochure-tp?submissionGuid=05368aa3-1149-4109-bd7e-5714ae1e891b>. [Online; accessed 14-December-2021].
- Shin, H., Hou, T., Park, K., Park, C.K., Choi, S., 2013. Prediction of movement direction in crude oil prices based on semi-supervised learning. *Decision Support Systems* 55, 348–358. URL: <https://www.sciencedirect.com/science/article/pii/S0167923612003417>, doi:<https://doi.org/10.1016/j.dss.2012.11.009>.
- Ship-Technology, . Francisco papa high-speed ferry. URL: <https://www.ship-technology.com/projects/francisco-high-speed-ferry/>. [Online; accessed 14-December-2021].
- Sivanagaraju, S., Rao, J.V., Raju, P.S., 2008. Discrete particle swarm optimization to network reconfiguration for loss reduction and load balancing. *Electric power components and systems* 36, 513–524.
- Skipsrevyen, 2014. Ship of the year - m/s ampere. URL: <https://www.skipsrevyen.no/batomtaler/m-s-ampere/>. [Online; accessed 14-december-2021].
- Skipsrevyen, 2020. Ms bard. URL: <https://www.skipsrevyen.no/batomtaler/bard/>. [Online; accessed 15-december-2021].
- Skipsrevyen, 2021. Ship of the year - m/s hydra. URL: <https://www.skipsrevyen.no/article/ship-of-the-year-2021-mf-hydra-1/>. [Online; accessed 14-december-2021].
- Soni, D.K., Gupta, R., 2016. Numerical investigation of emission reduction techniques applied on methanol blended diesel engine. *Alexandria Engineering Journal* 55, 1867–1879. URL: <https://www.sciencedirect.com/science/article/pii/S1110016816000727>, doi:<https://doi.org/10.1016/j.aej.2016.02.019>.
- Strømgren, T., Aa, .A., Aa, O.A., 2019. Brodrene aa and the fjords pioneering with 'future of the fjords' – offering zero emission fjord cruise URL:

-
- <https://corvusenergy.com/all-electric-car-ferry/>. [Online; accessed 15-December-2021].
- Sundvor, I., Thorne, R.J., Danebergs, J., Aarskog, F., Weber, C., 2021. Estimating the replacement potential of norwegian high-speed passenger vessels with zero-emission solutions. *Transportation Research Part D: Transport and Environment* 99, 103019. URL: <https://www.sciencedirect.com/science/article/pii/S1361920921003175>, doi:<https://doi.org/10.1016/j.trd.2021.103019>.
- Swarnkar, A., Swarnkar, A., 2020. Artificial intelligence based optimization techniques: A review, in: Kalam, A., Niazi, K.R., Soni, A., Siddiqui, S.A., Mundra, A. (Eds.), *Intelligent Computing Techniques for Smart Energy Systems*, Springer Singapore. pp. 95–103.
- Tammemae, T., 2021. Abb estorage flex 40 - fully integrated energy storage system. <https://library.e.abb.com/public/d82c1037f88b414d897ad856c5c6435a/Containerized%20energy%20storage%20brochure.pdf>. [Online; accessed 6-december-2021].
- Tenfen, D., Finardi, E.C., 2015. A mixed integer linear programming model for the energy management problem of microgrids. *Electric Power Systems Research* 122, 19–28. URL: <https://www.sciencedirect.com/science/article/pii/S0378779614004659>, doi:<https://doi.org/10.1016/j.epsr.2014.12.019>.
- The-Explorer, 2019. Hydrogen fast ferry for zero-emission passenger transport. URL: <https://www.theexplorer.no/solutions/hydrogen-fast-ferry-for-zero-emission-passenger-transport/>. [Online; accessed 15-december-2021].
- The International Renewable Energy Agency, I., 2021. Green hydrogen cost reduction: Scaling up electroly. *SPE Journal* , 11.
- Thorat, L., Skjetne, R., Osen, O.L., 2021. Genset Scheduling in a Redundant Electric Power System for an Offshore Vessel Using Mixed Integer Linear Programming. *Journal of Offshore Mechanics and Arctic Engineering* 143. URL: <https://doi.org/10.1115/1.4050643>, doi:10.1115/1.4050643.
- TRANSFLUID, 2022. Electric propulsion system – marine – eps. URL: <https://www.transfluid.eu/product/eps-marine-system/>. [Online; accessed 19-May-2022].
-

-
- TU, 2014. Karbonbåter kutter 40 prosent av utslippene. URL: <https://www.tu.no/artikler/karbonbater-kutter-40-prosent-av-utslippene/232404>. [Online; accessed 21-May-2022].
- TU, 2015. Fjordbanen: – båtene bør bygges i karbon, ikke aluminium. URL: <https://www.tu.no/artikler/fjordbanen-batene-bor-bygges-i-karbon-ikke-aluminium/275634>. [Online; accessed 16-December-2021].
- UNFCCC, 2015. Paris agreement .
- Vicente-Cera, I., Acevedo-Merino, A., Nebot, E., López-Ramírez, J.A., 2020. Analyzing cruise ship itineraries patterns and vessels diversity in ports of the european maritime region: A hierarchical clustering approach. *Journal of Transport Geography* 85, 102731. URL: <https://www.sciencedirect.com/science/article/pii/S096669231931049X>, doi:<https://doi.org/10.1016/j.jtrangeo.2020.102731>.
- Wang, Q., Mao, B., Stoliarov, S.I., Sun, J., 2019. A review of lithium ion battery failure mechanisms and fire prevention strategies. *Progress in Energy and Combustion Science* 73, 95–131. URL: <https://www.sciencedirect.com/science/article/pii/S0360128518301801>, doi:<https://doi.org/10.1016/j.pecs.2019.03.002>.
- Wang, Z., Hong, T., Piette, M.A., 2020. Building thermal load prediction through shallow machine learning and deep learning. *Applied Energy* 263, 114683. URL: <https://www.sciencedirect.com/science/article/pii/S0306261920301951>, doi:<https://doi.org/10.1016/j.apenergy.2020.114683>.
- Wavecraft, 2018. Air-cushion principle. URL: <https://www.wavecraft.no/technology/air-cushion-principle/>. [Online; accessed 19-January-2022].
- Wikipedia contributors, 2021a. Hydrogen production — Wikipedia, the free encyclopedia. URL: https://en.wikipedia.org/w/index.php?title=Hydrogen_production&oldid=1052075955. [Online; accessed 2-November-2021].
- Wikipedia contributors, 2021b. Quadratic programming — Wikipedia, the free encyclopedia. <https://en.wikipedia.org/w/index.php?title=>
-

-
- Quadratic_programming&oldid=1054581513. [Online; accessed 15-November-2021].
- Winter, M., Brodd, R.J., 2004. What are batteries, fuel cells, and supercapacitors? [Online; accessed 5-december-2021].
- Wu, B., Neilsen, T.B., 2021. Identifying the optimal k-mean clustering for ship noise spectrograms. *The Journal of the Acoustical Society of America* 150, A197–A197. URL: <https://doi.org/10.1121/10.0008110>, doi:10.1121/10.0008110.
- Wärtsilä, . World’s first full scale ammonia engine test - an important step towards carbon free shipping. URL: <https://www.wartsila.com/>. [Online; accessed 10-December-2021].
- Wärtsilä, 2017. Wärtsilä 20df. URL: <https://www.wartsila.com/marine/products/engines-and-generating-sets/dual-fuel-engines/wartsila-20df>. [Online; accessed 10-December-2021].
- Wärtsilä, 2021. Jet powered efficiency and reliability URL: <https://www.wartsila.com/docs/default-source/product-files/gears-propulsors/waterjets/brochure-o-p-waterjets.pdf>. [Online; accessed 14-December-2021].
- Xing, H., Stuart, C., Spence, S., Chen, H., 2021. Fuel cell power systems for maritime applications: Progress and perspectives .
- Yan, W., Wen, R., Zhang, A.N., Yang, D., 2016. Vessel movement analysis and pattern discovery using density-based clustering approach, in: 2016 IEEE International Conference on Big Data (Big Data), pp. 3798–3806. doi:10.1109/BigData.2016.7841051.
- Yun, L., Bliault, A., 2012. High performance marine vessels. New York:Springer.
- Zekalabs, 2022. Redprime dc-dc converter 200kw, 1200v. URL: zekalabs.com/products/non-isolated-high-power-converters/dc-dc-converter-200kw-1200v. [Online; accessed 19-May-2022].
- Zhang, S., Xiong, R., 2015. Adaptive energy management of a plug-in hybrid electric vehicle based on driving pattern recognition and dynamic programming. *Applied Energy* 155, 68–78.

Zhou, D., Al-Durra, A., Gao, F., Ravey, A., Matraji, I., Godoy Simões, M., 2017. Online energy management strategy of fuel cell hybrid electric vehicles based on data fusion approach. *Journal of Power Sources* 366, 278–291. URL: <https://www.sciencedirect.com/science/article/pii/S0378775317311400>, doi:<https://doi.org/10.1016/j.jpowsour.2017.08.107>.

Appendix **A**

High-Speed Vessels

A.1 Relevant high-speed vessels (from SeaWeb)

| Name | GT | Year | Loa | Draught | Width | Passengers | Total power[kw] | Ship builder |
|-----------------------|-----|------|--------|---------|-------|------------|-------------------------|--------------|
| Admiralen | 402 | 2010 | 33.45 | 1.6 | 10.6 | 280 | 3236 | |
| BARONEN | 330 | 2009 | 32.3 | 0.95 | 10.8 | 250 | 2160 | |
| BARONESSEN | 228 | 2009 | 27 | 0.95 | 8.8 | 180 | 1498 | |
| BORTIND | 289 | 2020 | 28.175 | 1.483 | 9 | 147 | 2880 | |
| EKSPRESSEN | 416 | 2008 | 32.5 | 1.6 | 10.6 | 296 | 3236 | |
| ELSA LAULA RENBERG | 583 | 2019 | 44.363 | 1.392 | 10.8 | 220 | 3600 | |
| FIORD VIKING | 105 | 2005 | 18.6 | | 7.2 | 97 | 1100 | |
| FIORDBRIS | 416 | 2014 | 36.7 | 1.25 | 10.7 | 230 | 3600 | |
| FIORDDRONNINGEN | 428 | 2019 | 39.09 | | 10.6 | 296 | 2880 | |
| FIORDDROTT | 226 | 2007 | 27 | 0.95 | 8.8 | 180 | 1498 | |
| FIORDFART | 226 | 2007 | 27 | 0.95 | 8.8 | 180 | 1498 | |
| FIORDGLIMT | 179 | 2009 | 24.5 | 0.95 | 8 | 147 | 1618 B aa | |
| FIORDJARL | 428 | 2020 | 39.1 | | 10.6 | 296 | 2880 Oma Baatdyggeri AS | |
| FIORDKATT | 226 | 2006 | 27 | 0.95 | 8.8 | 180 | 1498 Brodrene AA AS | |
| FIORDLYN | 192 | 2009 | 24.46 | 1.4 | 9 | 125 | 1498 Oma Baatdyggeri AS | |
| FIORDLYS | 251 | 2014 | 27.8 | 1 | 8.8 | 180 | 1800 Brodrene AA AS | |
| FIORDPRINSEN | 428 | 2019 | 39.09 | 1.376 | 10.6 | 296 | 2880 Oma Baatdyggeri AS | |
| FLOYFJELL | 332 | 2011 | 35.3 | 1.455 | 10.5 | 250 | 2160 | |
| FREDRIKKE TONDER-OLSE | 583 | 2021 | 44.6 | 1.38 | 10.8 | 193 | 3600 Brodrene AA AS | |
| FROYA | 388 | 2012 | 34.5 | 1.6 | 10.6 | 190 | 3600 Oma Baatdyggeri AS | |
| KISTEFJELL | 332 | 2011 | 35.3 | 1.455 | 10.5 | 250 | 2160 | |
| LADEJARL | 490 | 2002 | 37.6 | 1.68 | 10.1 | 276 | 4640 Fjellstrand AS | |
| TERNINGEN | 492 | 2014 | 40 | 1.077 | 11 | 275 | 2800 Brodrene AA AS | |
| TYRHAUG | 492 | 2014 | 40 | 1.077 | 11 | 275 | 2800 Brodrene AA AS | |

| Engine | Propulsion | Service speed [kts] | Max speed [kts] |
|---|----------------|---------------------|-----------------|
| 4 x oil engine Engine Builder: MAN Nutzfahrzeuge AG | 4 x water jet | | 34 |
| 2 x oil engine MTU Friedrichshafen GmbH - Friedrichshafen | 2 CP propeller | | 30 |
| 2 x oil engine MTU Friedrichshafen GmbH - Friedrichshafen | 2 CP propeller | | 30 |
| 4 x oil engine MTU Friedrichshafen GmbH - Friedrichshafen | 4 x vannjet | | 32 |
| 4 x oil engine MAN Nutzfahrzeuge AG - Nuernberg | 4 x vannjet | | 34 |
| 4 x oil engine MTU Friedrichshafen GmbH - Friedrichshafen | 4 x vannjet | | 32 |
| 2 x oil engine Scania AB - Sweden | 2 x Propeller | | 32 |
| 4 x oil engine MTU Friedrichshafen GmbH - Friedrichshafen | 2 CP propeller | | 35 |
| 4 x oil engine MTU Friedrichshafen GmbH - Friedrichshafen | 4 x vannjet | | 35 |
| 2 x oil engine MTU Friedrichshafen GmbH - Friedrichshafen | 2 x Propeller | | 30 |
| 2 x oil engine MTU Friedrichshafen GmbH - Friedrichshafen | 2 x Propeller | | 30 |
| 2 x oil engine MTU Friedrichshafen GmbH - Friedrichshafen | 2 CP propeller | | 30 |
| 2 x oil engine MAN Nutzfahrzeuge AG - Nuernberg | 2 CP propeller | | 30 |
| 4 x oil engine MTU Friedrichshafen GmbH - Friedrichshafen | 4 x vannjet | | 35 |
| 2 x oil engine MTU Friedrichshafen GmbH - Friedrichshafen | 2 x Propeller | | 30 |
| 2 x oil engine MAN Nutzfahrzeuge AG - Nuernberg | 2 x vannjet | | 30 |
| 2 x oil engine MTU Friedrichshafen GmbH - Friedrichshafen | 2 CP propeller | | 30 |
| 4 x oil engine MTU Friedrichshafen GmbH - Friedrichshafen | 4 x vannjet | | 35 |
| 2 x oil engine | 2 CP propeller | | 33 |
| 4 x oil engine MTU Friedrichshafen GmbH - Friedrichshafen | 4 x vannjet | | 32 |
| 4 x oil engine MTU Friedrichshafen GmbH - Friedrichshafen | 4 x vannjet | | 34 |
| 2 x oil engine | 2 CP propeller | | 33 |
| 2 x oil engine MTU Friedrichshafen GmbH - Friedrichshafen | 2 x vannjet | | 32 |
| 2 x oil engine MTU Friedrichshafen GmbH - Friedrichshafen | 2 x vannjet | | 33.5 |
| 2 x oil engine MTU Friedrichshafen GmbH - Friedrichshafen | 2 x vannjet | | 33.5 |

36

Appendix B

DP algorithm verification

B.1 Respect to alpha (fuel)

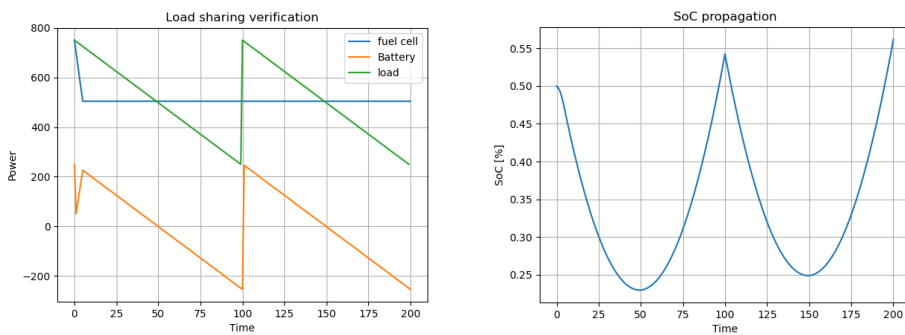


Figure B.2: Optimizing the fuel consumption

The fuel cell is loaded at its highest efficiency

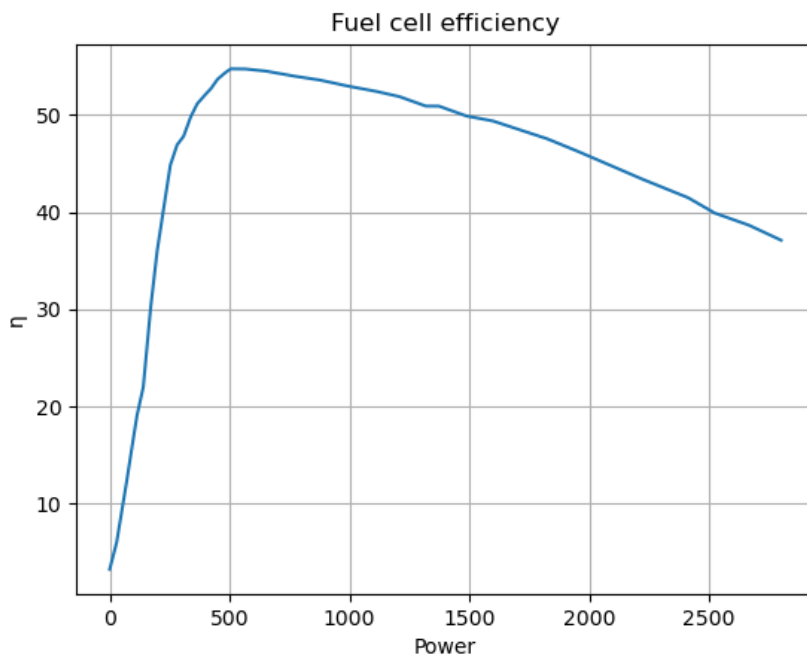


Figure B.1: Fuel cell efficiency for verification

B.2 Respect to beta (stable SOC)

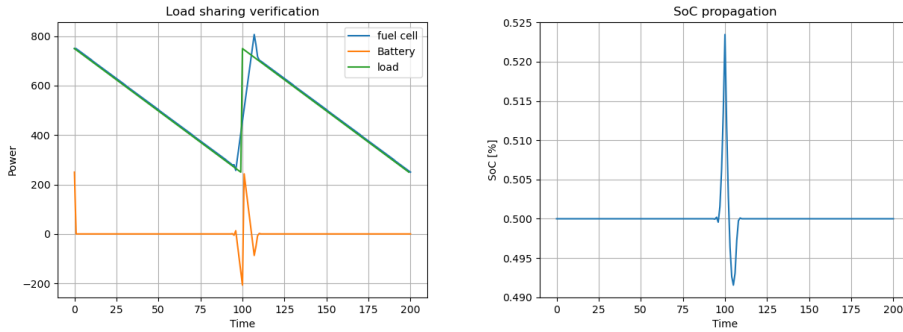


Figure B.3: Optimizing the stable SOC

The SOC is kept almost constant

B.3 Respect to gamma (low variation of fuel cell power)

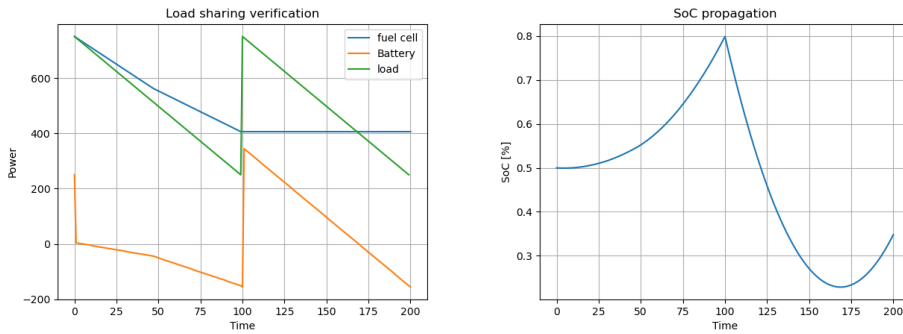


Figure B.4: Optimizing the stable fuel cell power

